Numerical Studies of Nuclear Containment Spray Process by Stochastic Field Method and CGCFD approach

Zur Erlangung des akademischen Grades
Doktor der Ingenieurwissenschaften (Dr.-Ing.)

von der KIT-Fakultät für Maschinenbau des
Karlsruher Instituts für Technologie (KIT)
angenommene

Dissertation

von

M. Sc. Fujiang Yu

Tag der mündlichen Prüfung: 24.07.2020
Hauptreferent: apl.Prof. Dr.-Ing. Andreas Class
Korreferent: Prof. Dr.-Ing. Xu Cheng

Vorwort

Die vorliegende Dissertation entstand während meiner Tätigkeit am Institut für Kern- und Energietechnik (IKET) unter Leitung von Herrn Prof. Dr.-Ing. Andreas Class des Karlsruher Instituts für Technologie (KIT). Die Arbeit wurde von Herrn Prof. Dr.-Ing. Andreas Class betreut. Bei der Anfertigung dieser Arbeit wurde ich von vielen Personen unterstützt, denen ich an dieser Stelle danken möchte.

Herrn Prof. Dr.-Ing. Andreas Class möchte ich besonders für die Betreuung der Promotion sowie die Übernahme des Hauptreferates danken. Bei Herrn Prof. Dr.-Ing. Xu Cheng, Leiter des Institutes für Angewandte Thermofluidik (IATF) am KIT, möchte ich mich für die Übernahme des Korreferates bedanken.

Außerdem gilt mein Dank Herrn Dr.-Ing. Thomas Jordan, Leiter der Gruppe Wasserstoffverteilungs und Verbrennungsanalysen (H2), für die organisatorische sowie wissenschaftliche Unterstützung. Allen Kollegen des IKET, besonders Herrn Dr. Jianjun Xiao, Herrn Dr. Han Zhang, Herrn Dr.-Ing. Abdalla Batta, Herrn Dr.-Ing. Karsten Litfin, Herrn Dr.-Ing. Martin Raquet und Herrn Viktor Klüber, sowie allen Beteiligten meiner Arbeit bin ich sehr dankbar für die gute und zahlreiche Unterstützung sowie die konstruktive und angenehme Zusammenarbeit.

Harbin, im Februar 2020 Fujiang Yu

Abstract

Nuclear energy is one of the basic technologies to satisfy the world's electricity needs. Due to the low CO2 emissions, nuclear energy represents one of the most important options in the eyes of the advocates in the new century. Nuclear safety is the crucial issue in the operation of nuclear reactors and in the development of the future reactor design, since the decay products of the nuclear fission reaction have a high level of radiotoxicity. The prediction accuracy of nuclear safety analysis remains as one of the most important issues among all topics of nuclear safety research.

There have been three major nuclear accidents, which have caused enormous damage in the past 60 years. It affected not only the lives of individuals but also the cohesion of the whole society. The recent Fukushima Daiichi nuclear disaster has firmly shown the evidence that the hydrogen explosion occurred in the containment was the cause of the eventual radioactivity release into the environment. During serious accidents, the nuclear containment represents the last protective barrier of the nuclear power plant from the environment. This containment is subject to long-term heating and high pressures. To prevent the containment from failing during a nuclear accident, spray systems are used to cool the atmosphere in the containment. For this reason, this doctoral thesis presents the topic of spray cooling modeling to contain the consequences of serious nuclear accidents.

When analyzing the processes during an accident, the extensive spatial dimension of a nuclear power plant and its containment alone presents the scientists with challenges. Traditionally, an experimental approach is used when spray processes in containment are examined. However, the high costs of building suitable test on facilities and carrying out the following measurements considerably drive up the total project costs of new nuclear power plants. On the other hand, with the increasing performance of computers, numerical simulation using Computational Fluid Dynamics (CFD) is becoming increasingly popular in the design process. However, the lack of sufficiently reliable physical spray models and the efficiency in predicting large-scale problems limit the use of CFD in spray cooling studies, which used to mitigate the consequences of accidents in severe nuclear accidents.

In this work, the analysis of spray cooling in the nuclear reactor containment is considered with special consideration of two aspects: reliability and speed. For the "Reliability" mission, a suitable modeling approach for spray cooling is derived, which can also be applied to spatially extensive problems. In addition, it is discussed how the turbulence-droplet interactions can be described. The Lagrangian approach, the mixing approach and the Euler approach on modeling the discrete liquid droplets are discussed and compared, in order to make a suitable model choice. The modeling of exchange terms for mass, momentum and energy is presented and discussed. Appropriate thermophysical modeling, including a new gas film-based evaporation model, is presented. After the most suitable modeling approach for the spraying process has been derived, the handling of the nonlinear properties of the turbulent transport of spray droplets is discussed further. The PDF method is presented in detail. For large-scale spray cooling problems, the application of its Eulerian implementation, the Stochastic Field Method, is discussed in detail. Particular attention is paid to the handling of mass and heat transfer.

A recently developed Coarse Grid CFD method is presented and discussed for the speed mission.

This can be used to efficiently predict problems by making good use of previous detailed simulation data, in particular to derive coarse grid models for the flow terms in the equations. A new physically-based flow correction method is introduced and compared to the original geometric-based flow correction approach. Some techniques for dealing with singular problems in Coarse Grid CFD simulation are also discussed.

In the case study section, the THAI benchmark is first used to validate the spray modeling approach. In addition, a dryer case is considered, with similar geometric and physical properties compared with nuclear reactor containment. In this case, the Stochastic Field Method for the consideration of turbulent interactions with spray droplets is evaluated. Finally, the Coarse Grid CFD is validated using a physically-based flow correction approach. A nuclear prototype fuel bundle with a wire spiral spacer is considered as a nuclear application. In the outlook, the dryer case is examined again in order to test the combination of all the approaches for spray cooling simulation discussed above, with typical operating parameters. In summary, it can be stated that the work demonstrates, on the one hand, the practicability of an Eulerian approach in the form of the stochastic field method for providing reliable simulation results, and on the other hand shows the suitability of the Coarse Grid CFD for fast predictions in the case of large-scale problems.

Kurzfassung

Die Kernenergie ist eine der grundlegenden Technologien zur Deckung des weltweiten Stromversorgungsbedarfs. Aufgrund des geringen CO2-Ausstoßes, welcher durch Kernenergie verursacht wird, stellt die Kernenergie in den Augen der Befürworter eine der bedeutendsten Optionen im neuen Jahrhundert dar. Die nukleare Sicherheit ist das entscheidende Thema beim Betrieb von Kernreaktoren und bei der (Weiter-) Entwicklung von Reaktorkonzepten, da die Zerfallsprodukte der Kernspaltungsreaktion eine hohe Radiotoxizität aufweisen. Unter allen Fragestellungen der nuklearen Sicherheitsforschung bleibt die Vorhersagegenauigkeit von nuklearen Sicherheitsanalysen eines der wichtigsten Themen.

In den letzten 60 Jahren ereigneten sich drei schwere nukleare Unfälle, die enormen Schaden verursacht haben. Betroffen war nicht nur das Leben einzelner, sondern der Zusammenhalt der ganzen Gesellschaft. Bei der jüngsten nuklearen Katastrophe von Fukushima Daiichi wird fest davon ausgegangen, dass die im Sicherheitsbehälter aufgetretene Wasserstoffexplosion der ursächliche Auslöser für die schlussendliche Freisetzung von Radioaktivität an die Umgebung war. Im Falle schwerer Störfälle stellt das nukleare Containment die letzte Schutzbarriere des Kernkraftwerks gegenüber der Umgebung dar. Dieses Containment ist einer lang anhaltenden Erwärmung und hohen Drücken ausgesetzt. Um zu verhindern, dass der Sicherheitsbehälter während eines nuklearen Unfalls versagt, werden Sprühsysteme eingesetzt, welche die Atmosphäre im Sicherheitsbehälter kühlen. Aus diesem Grund betrachtet diese vorgelegte Dissertationsschrift den Themenkomplex der Sprühkühlungsmodellierung zur Eindämmung der Folgen schwerer nuklearer Störfälle.

Bei der Analyse der Vorgänge während eines Störfalls stellt schon alleine die ausgedehnte räumliche Dimension eines Kernkraftwerks und dessen Containments den Wissenschaftler vor Herausforderungen. Traditionell wird auf einen experimentellen Ansatz zurückgegriffen, wenn Sprühprozesse im Containment untersucht werden. Allerdings treiben die hohen Kosten, für den Bau geeigneter Versuchsanlagen und die Durchführung von Messkampagnen, die Projektkosten von Kernkraftwerksneubauprojekten erheblich in die Höhe. Andererseits, mit der stetig wachsenden Leistungsfähigkeit von Computern, wird die numerische Berechnung mittels der Computational Fluid Dynamics (CFD) im Konstruktionsprozess immer beliebter. Das Fehlen hinreichend zuverlässiger physikalischer Sprühstrahlmodelle und die nach wie vor unbefriedigende Effizienz bei der Vorhersage von großräumigen Problemen, schränken jedoch die Anwendung von CFD in Sprühkühlungsstudien zur Begrenzung der Unfallfolgen bei schweren nuklearen Störfällen ein.

In dieser Arbeit wird die Analyse von Spühstrahlen im Containment eines Kernreaktors unter besonderer Berücksichtigung zweier Aspekte betrachtet: Zuverlässigkeit und Geschwindigkeit. Für die Mission „Zuverlässigkeit“ wird ein geeigneter Modellierungsansatz für Sprühnebel, welcher auch auf bei räumlich ausgedehnten Problemen anwendbar ist, abgeleitet. Darüber hinaus wird diskutiert wie die Turbulenz-Tröpfchen-Wechselwirkungen beschrieben werden kann. Der Lagrange-Ansatz, der Mischungsansatz und der Euler-Ansatz zur Modellierung der diskreten Flüssigkeitströpfchen werden auf drei verschiedene Arten diskutiert und verglichen, um eine geeignete Modellwahl zu treffen. Die Modellierung von Austauschtermen für Masse-, Impuls- und Energie wird vorgestellt und diskutiert. Eine geeignete thermophysikalische Modellierung,

einschließlich eines neuen Gasfilm-basierten Verdampfungsmodells, wird vorgestellt. Nachdem der geeignetste Modellierungsansatz für den Sprühprozess abgeleitet wurde, wird der Umgang mit den nichtlinearen Eigenschaften des turbulenten Transports von Sprühtröpfchen weiter diskutiert. Die PDF-Methode wird detailliert vorgestellt. Für großskalige Sprühkühlungsprobleme wird die Anwendung einer Euler‘schen Realisierung, der stochastischen Feldmethode, ausführlich diskutiert. Dabei gilt der Handhabung von Stoff- und Wärmeübertragung ein besonderes Augenmerk.

Für die Geschwindigkeitsmission wird eine kürzlich entwickelte Coarse Grid CFD-Methode vorgestellt und diskutiert. Mit dieser lassen sich Probleme effizient vorhersagen, indem vorausgehende detaillierte Simulationsdaten gut genutzt werden, um insbesondere Grobstrukturmodelle für die Flussterme in den Gleichungen abzuleiten. Eine neue physikalisch basierte Flusskorrektur wird eingeführt und mit dem ursprünglichen geometrischen Flusskorrekturansatz verglichen. Einige Techniken zur Behandlung singulärer Probleme in der Coarse Grid CFD-Simulation werden ebenfalls diskutiert.

Im Fallstudienteil wird zunächst der THAI-Benchmark zur Validierung des Sprühmodellierungsansatzes verwendet. Zusätzlich wird ein Trocknergehäuse mit ähnlichen geometrischen und physikalischen Eigenschaften betrachtet. Bewertet wird die stochastische Feldmethode zur Berücksichtigung turbulenter Wechselwirkungen mit Sprühtröpfchen. Zuletzt wird die Coarse Grid CFD mit einem physikalisch basierten Flusskorrekturansatz validiert. Betrachtet wird als kerntechnische Anwendung ein prototypisches Brennelementbündel mit Drahtwendelabstandshalter. Im Ausblick wird der Trocknerfall erneut untersucht, um die Kombination aller oben diskutierter Ansätze für die Sprühstrahlsimulation bei typischen Betriebsparametern zu testen. Zusammenfassend kann festgestellt werden, dass die Arbeit einerseits die Praktikabilität eines Euler‘schen Ansatzes in Form der Stochastischen Feldmethode zur Bereitstellung zuverlässiger Simulationsergebnisse demonstriert und andererseits die Eignung der Coarse Grid CFD für schnelle Vorhersagen bei großen Problemen zeigt.

Publication

This thesis is in part based on the following publications by the author:

1. Class, Andreas G., Yu, Fujiang, and Jordan, Thomas. "An engineering closure for heavily under-resolved coarse-grid CFD in large applications." Bulletin of the American Physical Society 61 (2016). Paper No. KP1.135
2. Yu, Fujiang, Class, Andreas G., Xiao, Jianjun and Jordan, Thomas. Coarse grid CFD methodology: flux corrections for individual mesh cells and application to rod bundles. SE 17th International Topical Meeting on Nuclear Reactor Thermal Hydraulics, Xi'an, Shaanxi, China, Sept. 3-8, 2017. Paper No. 21717
3. Yu, Fujiang., Zhang, Han., Li, Yabing., Xiao, Jianjun., Class, Andreas G., & Jordan, Thomas. "Voxelization-based high-efficiency mesh generation method for parallel CFD code GASFLOW-MPI." Annals of Nuclear Energy 117 (2018): 277-289.
4. Yu, Fujiang., Zhang, Han., Class, Andreas G., Xiao, Jianjun., Travis, Jack. R., & Jordan, Thomas. "Winding number based automatic mesh generation algorithm for hydrogen analysis code GASFLOW-MPI." International Journal of Hydrogen Energy 44.26 (2019): 14070-14084.
5. Yu, Fujiang., Ji, Yu., Zhang, Han., Class, Andreas G., Xiao, Jianjun., & Jordan, Thomas. "Development of reverse meshing technology on geometry reconstruction for CFD code GASFLOW-MPI." Progress in Nuclear Energy 118 (2020): 103124.

Contents

Nomenclature

Symbols

C_p	Specific heat capacity	$[J/(kg \cdot K)]$
d	Diameter of the spray droplet	$[m]$
D_{drag}	*drag force coefficient*	*[–]*
E	*inner energy*	$[J/kg]$
F_T	*Coarse Grid volumetric force*	$[m/s^2]$
f	*momentum interaction between two phases*	$[(kg \cdot m)/s]$
h	*enthalpy*	$[J/kg]$
K	*heat transfer coefficient*	$[W/(kg \cdot K)]$
L	*latent heat*	$[J/kg]$
Le	*Lewis number*	*[–]*
$\dot{m}$	*mass amount of evaporated liquid*	*[kg]*
Nu	*Nusselt number*	*[–]*
p	*pressure*	*[Pa]*
Pr	*Prandtl number*	*[–]*
$\dot{q}$	*energy interaction between two phases*	*[W]*
R	*gas constant*	$[J/(mol \cdot K)]$
Re	*Reynolds number*	*[–]*
Sc	*Schmidt number*	*[–]*
Sh	*Sherwood number*	*[–]*
t	*time*	*[s]*
T	*temperature*	*[K]*
U	*velocity*	$[m/s]$
v_{dr}	*drift velocity*	$[m/s]$
W	*Mole mass weigh*	$[kg/mol]$
X	*possible particle movement trace*	*[m]*
x	*location*	*[m]*
Y	*mass fraction*	*[–]*
α	*Volume fraction in Chapter 2,3;* *Volume porosity in Chapter 6*	*[–]*
β	*surface permeability*	*[–]*
κ	*thermal conductivity*	$[W/(m \cdot K)]$
λ	*mean free path*	*[m]*
μ	*kinetic viscosity*	$[m^2/s]$
ρ	*density*	$[kg/m^3]$
τ	*stress tensor*	*[Pa]*
υ	*dynamic viscosity*	$[Pa \cdot s]$

Indices

B	boiling point
$drag$	drag force
$H2O$	water vapor component
g	gas phase
k	certain realization following a given stochastic process
l	liquid phase
lam	laminar flow
m	mass
mix	gas mixture
$sature$	satured condition
st	stochastic process
sub	sub-grid
tur	turbulent flow

Abbreviations

CEA	Commissariat à l'énergie atomique et aux énergies alternatives
IAEA	International Atomic Energy Agency
KALLA	Karlsruhe Liquid Metal Laboratory
NASA	National Aeronautics and Space Administration
OECD	Organisation for Economic Co-operation and Development
AP600	Advanced Passive PWR 600
AP1000	Advanced Passive PWR 1000
CALIST	Characterization and Application of Large and Industrial Spray Transfer
CFD	Computational Fluid Dynamics
CFL	Courant–Friedrichs–Lewy
CGCFD	Coarse Grid CFD
DNS	Direct numerical simulation
JANAF	Joint Army-Navy-NASA-Air Force
LES	Large Eddy Simulation
MAXSIMA	Methodology, Analysis and eXperiments for the Safety In MYRRHA Assessment
MISTRA	Experimental facility used to study hydrogen risks at the Commissariat à l'énergie atomique et aux énergies alternatives (Mitigation et stratification)
MOM	Method of Moment
MYRRHA	Multi purpose hYbrid Research Reactor for High tech Applications
PANDA	Large-scale, thermal-hydraulics test facility at the Paul Scherrer Institute

PDF	Probability Density Function
RANS	Reynolds-averaged Navier–Stokes
SARNET	Severe Accident Research NETwork of Excellence
SFM	Stochastic Field Method
THAI	Thermal-Hydraulic Aerosol Iodine
TOSQAN	TOnuS Qualification ANalytique
WENRA	Western European Nuclear Regulators Association

1. Introduction

1.1 Importance of nuclear energy

Nuclear energy stays as an important part of world's energy needs. In 2013, nuclear energy contributes to 2477/23234 TWh of the global energy production [1]. Until end of 2017, there are 450 nuclear reactors in total under operation with 393843 MW installed capacity, while 57 nuclear reactors under construction with 58535 MW installed capacity [3]. Based on IAEA's early estimation, there would be a 17% increase of nuclear energy [2].

During the development of nuclear energy, one of the key issues is the concerning of energy security and environment protection. Nuclear energy stands as a potential choice for national energy security, which calls for the uninterrupted availability of energy sources with an affordable price [4]. With the advantage of high energy density in nuclear fuel, the users can share sustainable national energy supply by stockpiling only small amount of uranium. Therefore, all the fossil fuel price volatility suffering from economic and political accidents can be avoided. Nuclear energy can also be a good solution for environmental protection. Based on early statistics, around 80% of the world energy consumption relies on fossil fuel [5], which releases large amount of CO_2. Due to the study, the greenhouse gas effect has been shown as one key reason of climate system perturbation and global warming [6]. Without nuclear energy supply in the global electricity market, additional 2.5 billion ton CO_2 emission [7] will be produced. At the same time, nearly no airborne pollutants will be produced in nuclear power plant compared with traditional coal power plant, which offers a better way to eliminate air pollution.

Nuclear energy can also be a source of renewable energy study, like solar energy and hydrogen energy. Studies [8] have shown the possibility of using waste heat from the nuclear power plant to supply the solar chemical power plant, as way to increase the efficiency of solar energy. There are also studies [9] on hydrogen production by nuclear energy. The hybrid nuclear-renewable energy system [10] is also is discussed. Therefore, except the ability of providing cheap and clean power solution, the development of nuclear energy plays as a strong support for further renewable energy study.

1.2 Nuclear safety in nuclear power plant

In the past 60 years of nuclear power plant development, there were three severe accidents: The Three Mile Island disaster, Chernobyl disaster and Fukushima Daiichi nuclear disaster. The history of nuclear accident has shown the catastrophic consequence brought by nuclear accident, like permanent pollution of the land, masses of radiative dust and million tons of radioactive water. Until now, the only strategy against nuclear accident is to seal the damaged reactor and isolate the whole power plant from the public. Therefore, the delay and defense of nuclear accident stays as a vital issue in nuclear power technology development.

Nuclear safety targets on protecting persons, property, society and the environment from harmful

effects of ionizing radiation [11]. To realize the commission of nuclear safety, modern commercial nuclear power plants are designed with the concept of “Defense in depth”. Five independent and subsequent layers are built aiming at the plant safety, which ensure the former layer’s failure can be mitigated and delayed by the later layers.

Table 1 Five levels of defense against nuclear accident

Level	Function and target [12]
1st	Prevent abnormal operation and failures. By implementing high quality of the reactor circuit, ensuring low probability of accidents
2nd	Control abnormal operation and detect failures. By setting up specific systems, design features and operating procedures, try to prevent normal operation developing into accidents
3rd	Control accidents within the design basis. Assuming all the safety actions failed in the former two levels, the design itself shall be able to limit the accident effects within an acceptable level, so that the core structure integrity will be maintained and the release to the environment is controlled
4th	Control severe nuclear power plant accidents. Facing the highly improbable problems like core meltdown, all kinds of efforts will be done to prevent accident progression and mitigate the severe consequences, saving time for further manipulations. Therefore, containment is quite necessary in modern nuclear power plant
5th	Mitigate radiological consequences of significant off-site releases of radioactive materials. Under the condition that all former four levels failed, emergency measures will be taken into action, as way to protect the public and the environment from the drastic radiative dose.

In practice, four barriers are set up to block the fission products from releasing to the environment. From the fuel matrix to the containment, all the following barrier shall be able to contain the radiative materials from the former one.

After the iteration of Generation I, II, III, the Generation IV of nuclear power plant is the mainstream of modern study. Among all the six Generation IV potential reactor types, safety improvement is one of the most important criteria of the reactor, which again stress that multiple failure events and core melt accidents should be considered [13]. The new designed reactor shall be able to resist natural hazards and keep the integrity of the containment. Additional attention will be paid on safety/security interface, as part of the new safety management system. Under the new design of Generation IV reactor, the nuclear power plant will give a better performance on safety and reliability, keep a low frequency and degree of core damage and get rid of offsite emergency response [14].

1.3 Nuclear containment safety

Nuclear containment is the fourth and the last barrier in the “Defense in Depth” system of nuclear power plant, which provides the radiation protection for the public. As shown in the WENRA safety objectives, the containment integrity is vital to the safety of nuclear power plant.

Before the Fukushima Daiichi nuclear disaster [15][16], the world's fourth ever largest observed tsunami-earthquake came on March 11, 2011. Under consisted staking attack, the structural design of the power plant is able to resist the damage. However, emergency generators are disabled owing to the tsunami sea water into the plant, which leads to the gap of power support in the cooling system pump. Because of the insufficient cooling, the decay heat from the reactor core kept on heating the coolant of the primary loop. At last, the high temperature and high-pressure atmosphere finally broke down the integrity of the containment and released radiative materials into the outer environment, as shown in **Figure 1**. The lesson from Fukushima Daiichi nuclear disaster [17] has strongly highlighted the importance of nuclear containment safety, especially the ability of the emergency cooling under severe accident condition.

In the modern Generation III reactor technology, the safety issues on containment has again been stressed. As the Generation III Pressurized Water Reactor technology designed by Westinghouse Electric Company, AP1000 [18] was born with the idea of less equipment but stronger safety characteristics. Compared with traditional AP600 technology, AP1000 has 35% fewer pumps, 45% less seismic building volume, 50% fewer safety-related valves, 80% less safety-related piping, 85% less control cable, but still keeps controlling the core damage frequency under 5.09×10^{-7} per plant per year. The key design of AP1000 is the Passive Core Cooling System, which implement a water tank on top of the containment, as shown in **Figure 2**. By gravity and natural circulation effect, the atmosphere in containment can be cooled down and depressurized in a passive way, in order to absorb the radioactive decay heat from the reactor. By the passive cooling on containment, the dependence of power plant operator control can be partly reduced.

Figure 1 Fukushima accident[19]

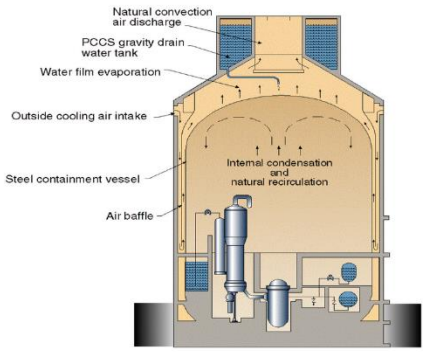

Figure 2 AP1000 containment[20]

1.4 Nuclear containment spray study

Spray is one of the most important safety devices in nuclear containment, which will be active during accident condition, in order to maintain the completeness of containment. During accident condition, the heat released from the reactor core can't be removed smoothly, which will result in a consistency pressure increasing. With no safety devices enabled, the closure of primary loop will finally be broken, owing to the consisting over-pressure. With the failure of all the three former barriers, the fission materials will be release from the fuel rod claddings and escape into the containment, following the high temperature and high-pressure vapor vaporized from the primary loop coolant. By implementing the spray system, the cold water droplets will be released from the top of the containment, absorbing the heat of the atmosphere and washing out the radiative productions. Furthermore, the stratified distribution of hydrogen will also be disturbed by the

spray, which ensures the hydrogen safety of the containment. The integrity of the nuclear containment depends on the performance of the spray system.

The early studies on nuclear containment spray can be back to the time of 1970s. A series of work [21][22][23][24] have been done in Oak Ridge National Lab on the design considerations of the containment spray system. Tanaka, Mitsugu [25] has done a work on comparison of the rigid droplet model and the complete mixing droplet model on spray droplet heat transfer in containment, which shows the importance of fall distance. Chung, J. N., and P. S. Ayyaswamy [26] have done a work comparing three droplet models, which shows the importance of internal circulation effect in spray heat transfer. Griess, J. C., and A. L. Bacarella [27] have given a study of material corrosion in containment spray. Nishio, Gunji, et al [28] have given a study of radioiodine removal model in containment spray. Hashimoto, Kazuichiro, et al [29] and Nishio, Gunji & Mitsugu Tanaka [30] have done work on spray Iodine removal in BWR and PWR. Nagasaka, H & T. Kagawa [31] and Tanaka, Mitsugu, et al [32] have done a general study on heat removal characteristics of spray in nuclear containment.

By the literature study of the past works, three main drawbacks of the early nuclear containment spray characteristics research can be concluded:

(1) The studies always focused on basic mechanism of spray droplets or spray performance in some certain kind of commercial reactor types, which leaves the model and result hard to compare and shared between different reactor technologies.

(2) The studies are largely from experimental side, while the numerical side is not frequently visited. Among the rare numerical studies of the containment spray, the works are heavily based on some self-coded in-house programs, which leave the validation and wide-spread application further difficulties.

(3) The study of spray in nuclear academic community was shared and discussed in a small circle constituted by national labs and a few college institutes. The theory, model and methods are still dependent on early 1960s studies, without absorbing the new advancements and ideas of the spray study in automotive industry, safety industry and chemical industry.

1.4.1 Benchmarks of containment spray study

International society has found the deficits of non-organized independent studies on nuclear safety issues. Therefore, SARNET (Severe Accident Research NETwork of Excellence) was set up in 2004, as way to fix the fragmentation and gap between the research programmes from different countries and companies. The network was started by EU, but also included non-European members like Canada, Korea, India, etc.

SARNET was coupled into the FP6 framework of European Commission [33], which targeted on severe accident studies of nuclear power plant, covering core melt, plant damage, radiation dispersal, etc. The aim of SARNET is to accumulate severe accident knowledge, provide the link among different research communities and preserve research data for further study. The topics of SARNET includes: In-vessel corium & debris coolability, Ex-vessel corium interactions & coolability, Containment behavior, Source term, severe accidents linkage to environmental impact & emergency management and severe accident scenarios.

Containment spray performance is an important area in severe accident analysis. To well study and validate spray models in nuclear containment, SARNET provides several spray benchmarks in a

small-scale simple structured containment experimental facility. A comprehensive review work has been done by Malet, J., et al [38], which provides a summary of the past 20 years' work on containment spray modeling. An overall introduction of the existing experimental facilities and simulation codes are listed in this section.

1.4.1.1 TOSQAN

TOSQAN (TOnuS Qualification ANalytique) facility was set up by IRSN to study nuclear power plant severe accidents, as shown in **Figure 3**. The experimental facility got a volume of round $7m^3$, with height of 4m and internal diameter of 1.5m. The vessel was made by stainless steel, with double walls providing channels for coolant oil to circulate. By controlling the flow rate, the wall temperature can be kept between 60°C and 160°C. The whole facility got over 150 thermocouples, 54 mass spectrometry sample points and 14 overpressure resistant viewing windows for optical measurements. The sketch of the TOSQAN design is shown in **Figure 4**.

The spray system was installed in the facility to produce full-cone water spray, with a single nozzle installed on the top of the vessel at the vertical axis. At the bottom of the facility, a sump was set to collect and remove the unevaporated spray water, in order to prevent further evaporation from water accumulation. Two categories of test are performed in TOSQAN spray program: TOSQAN test 101 series and TOSQAN test 113 series. TOSQAN test 101 series mainly cover the single gas-spray interaction phenomenon with heat and mass transfer on spray droplets and containment wall, by injecting cold water spray into the pre-heated air atmosphere. TOSQAN test 113 series mainly covers the gas droplet momentum interaction, by injecting cold water spray into a stratified mixture of air and helium in the containment.

Figure 3 TOSQAN facility[39]

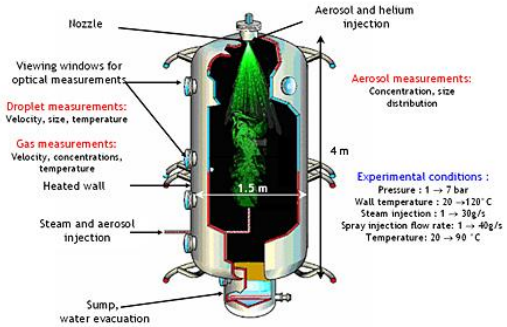

Figure 4 The design of TOSQAN[39]

A lot of studies have been done based on TOSQAN benchmark. Emmanuel Porcheron et al [45] have done an experimental study of heat and mass transfer during spray process based on TOSQAN. Later a work [48] about its influence on spray mass flow rate. S. Mimouni et al [46] introduces a wall evaporation model of spray into nuclear containment analysis code NEPTUNE_CFD, and validate it on the benchmark of TOSQAN 113 test. Porcheron, Emmanuel, et al [47] have done a study of aerosol removal by both experimental and numerical methods based on TOSQAN. Several other validation work of analysis codes were also done on TOSQAN. Malet, J. et al [81] have done a study of water evaporation around the sump of TOSQAN by both CFD code, TONUS-CFD and LP code, ASTEC. Malet, J., and R. Laissac. [88] have done a numerical study of gas stratification in TOSQAN.

1.4.1.2 MISTRA

MISTRA facility was set up by CEA, which tries to study the condensation effect on the wall and the spray droplet in a larger geometry compared with TOSQAN, as shown in **Figure 5**. The experimental facility got an internal volume of 99.5m^3, with height of 7.4m and internal diameter of 4.25m. The wall of MISTRA was designed to be thermally insulated, without controlling of wall temperature. The whole facility has coupled with measure instrumentations including pressure, temperature, gas concentration and laser Doppler velocity detector.
The experiment was performed with well-defined initial condition of quiescent atmosphere. The spray system was processed with constant boundary conditions and last less than two hours.

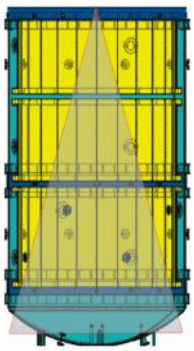

Figure 5 MISTRA facility[82]

Povilaitis, Mantas et al [82] have done a validation work of lumped-parameter injection modelling based MISTRA. Ravva, Srinivasa Rao, et al [83] have conducted a numerical study of air-helium test on MISTRA. Abe, Satoshi, et al [84] have done a study of stratification breakup based on MISTRA. Hoyes, J. R., and M. J. Ivings. [85] have done a work on hydrogen stratification modelling based on MISTRA. Povilaitis, Mantas, et al. [86] have done a sensibility and uncertainty study on atmosphere stratification modelling in MISTRA. A similar work can be found in [87].

1.4.1.3 THAI

THAI (thermal-hydraulic aerosol iodine) is a facility performance by Becker Technologies GmbH in Eschborn, Germany [34], which provides for 3D full containment computer simulation, as shown in **Figure 6**. THAI facility got a cylinder vessel with volume of 60m^3. 3D innovative measurement instrumentation is installed as way to measure local atmosphere temperature distributions, concentrations and velocities. The experiment design is shown in **Figure 7** and a detailed description can be found in [43].
THAI was involved in multiple international benchmarks like OECD ISP-47, OECD ISP-49, OECD THAI HM-2, etc. THAI covers most of the containment physical phenomenon like containment thermal-hydraulics, hydrogen distribution, aerosol removal and Iodine transport. Recently a second vessel part PAD (parallel attachable drum) was coupled to the original facility forming a new generic 2-room experimental facility THAI+ [35]. New test like TH-27 based on

THAI+ provides better performance of the 2-room behavior in sub-compartment rooms of real nuclear power plant containment.

Figure 6 THAI facility[43]

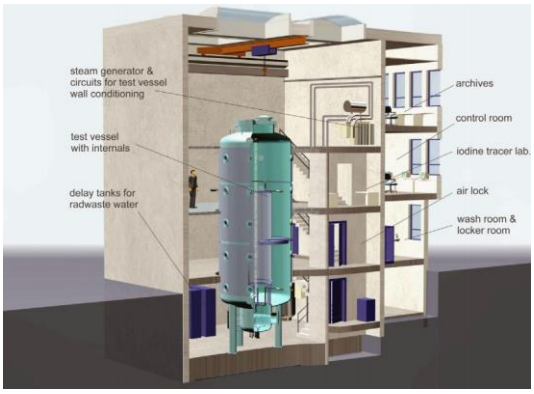

Figure 7 The design of THAI[43]

Kaltenbach, C., and E. Laurien have done works on aerosol particle removal [36] and spray cooling [37] based on THAI. And later on, a numerical error analysis on THAI+ [38]. Freitag, M., et al [40] and Li, Yabing, et al. [41] have also done works on the natural convection benchmark of THAI [42]. Gupta, S., et al. [43] have done a work of hydrogen and fission product behavior based on THAI. Funke, F., et al. [44] have a study of Iodine oxides in THAI.

1.4.1.4 PANDA

PANDA was a large-scale containment experimental facility built at PSI (Paul Scherrer Institute) in Switzerland, as shown in **Figure 8**. The facility got a two-compartment design, with total inner volume of 200m^3. Each of the two vessels got a height of 3.96m and inner diameter of 0.928m. PANDA was involved in the OECD/SETH II project, providing experimental data for containment safety code analysis. The overall design and geometric characteristics have been shown in **Figure 9**. More detailed information about PANDA facility can be found in [60].

PANDA facility is mainly used to study topics like wall condensation and atmosphere stratification break-up phenomena.

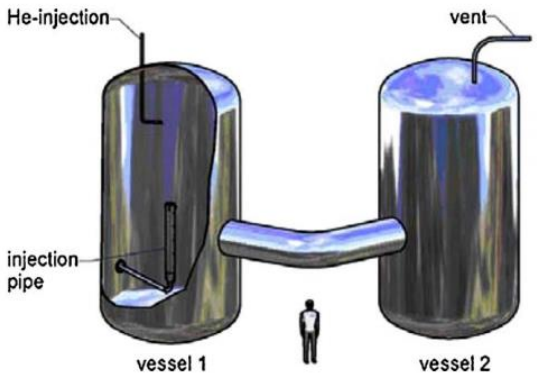

Figure 8 The PANDA facility[60]

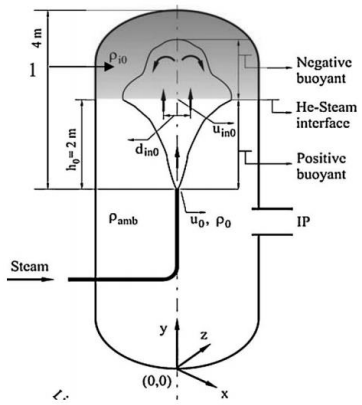

Figure 9 The design of PANDA[60]

Erkan, Nejdet, et al. [50] have done an experimental study on gas stratification in interconnected structure containment like PANDA. A similar work has been done by Kapulla, Ralf et al [51] on the cooler performance in PANDA. Filippov, A., et al. [91] have done a numerical study of spray on PANDA benchmark with the Eulerian mixture (drift flux) model. Paladino, Domenico, et al.

[52] have done an experimental study of light gas effect based on PANDA. Yang, Jun, et al. [56] have done a counterpart experimental study on PANDA. Kim, Jungwoo et al. [57] have done a numerical study of hydrogen dispersion from leakage in PANDA. Bandurski, Th, et al. [58] have done an experimental study on distribution of noncondensibles based on PANDA. Auban, O. et al. [59] have done a work on gas mixing and stratification in PANDA. Ritterath, Martin, et al. [60] have done an experimental study on gas concentration in PANDA.

1.4.1.5 CALIST

CALIST (Characterization and Application of Large and Industrial Spray Transfer) facility was carried out by IRSN, as shown in **Figure 10**. The benchmark is trying to study the characteristics of spray droplet in real large size space. CALIST got a room with volume of 160m^3, while 7m, 6m and 3.5m for each direction. Two nozzles are installed on the roof following the design French 900-MW PWR. A 5m^3 pool was set at the bottom to collect the droplets. With the help of PDI (phase-Doppler interferometry), the droplet size distribution, poly-dispersion and collisions are studied. The concept draw of CALIST design has been shown in **Figure 11**.

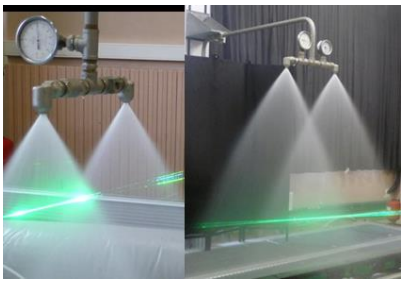

Figure 10 The CALIST facility[68]

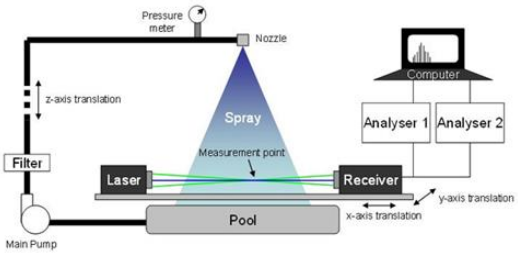

Figure 11 The design of CALIST[68]

A summary of CALIST benchmark simulation results by multiple containment analysis code is given in [68], in which droplet size, droplet velocity and gas velocity are deeply studied and compared. Foissac, Arnaud, et al. [62] have done a work extending droplet collision model based on CALIST benchmark.

Table 2 Summary of nuclear containment test facilities

Name	Size	Experiment types
TOSQAN	7m^3	Small-scale facility, mainly covering basic spray characteristics study
THAI	60m^3	Medium-scale facility, covering diverse kinds of physical phenomenon including spray, hydrogen distribution, aerosol removal and Iodine transport
MISTRA	99.5m^3	Large-scale facility, testing macro spray performance in a real containment size
CALIST	160m^3	Large-scale facility without any containment structure, mainly used to study basic mechanisms of spray process
PANDA	200m^3	Large-scale facility, mainly testing the performance of spray in the type of containment with counterpart structure

1.4.2 CFD codes in containment analysis area

Thermal-hydraulics analysis is an important part of containment safety study. Owing to the high expense of experimental study, computer code simulation always plays as the toolkit for real engineering problem. Because of the large-scale characteristics of nuclear containment, the numerical study always relied on LP (lumped-parameter) code, owing to the fast simulation speed and low memory requirement. Such kind of code can found like ASTEC [53], COCOSYS [54] and MELCOR [55]. Though able to get macro change of physical variables in the containment, the LP codes can hardly predict the spatial distribution at the same time, which put limits on the further safety analysis of the containment. Recently, since the development of hardware performance and software technology, CFD (Computational Fluid Dynamics) becomes a stronger tool on containment safety study, by numerically solving 3D Navier-Stokes Equations. In containment analysis area, the widely used codes are TONUS-CFD, NEPTUNE_CFD, GASFLOW and CFX.

1.4.2.1 TONUS-CFD

TONUS-CFD was developed together by The French Atomic Energy Commission (CEA) and the Institute for Radiological Protection and Nuclear Safety (IRSN), aiming to provide a hydrogen safety analysis toolkit and applied in the real plants like EPR.

TONUS-CFD implements a typical Two-fluid model with N species. A low Mach number model is used to consider the weak compressibility in containment thermal-hydraulic flows, while a separated Riemann-type high speed solver for detonation simulation. A mix-length turbulence model and a k-epsilon turbulence model are used to deal with the turbulent effect in the flow. Chilton-Colburn model is used on condensation effect.

Kudriakov, S., et al. [93] have done an overall validation work of physical models and numerical schemes in TONUS-CFD based the benchmarks of TOSQAN, MISTRA and THAI. Malet, J., et al [81] have done a numerical study by TONUS-CFD and experiment on wall condensation based on TOSQAN.

1.4.2.2 NEPTUNE_CFD

NEPTUNE_CFD was developed under a joint research project by CEA, EDF, FRAMATOME and IRSN, as a way to provide a multiphase flow solver on overall thermal-hydraulics problems in nuclear power plant, including the nuclear containment.

To deal with two-phase problem in nuclear reactor, NEPTUNE_CFD implements a two-fluid Eulerian framework. Unstructured mesh is supported in NEPTUNE_CFD as way to describe complex geometry. The flow is assumed to be incompressible and solved by pressure-based solution routine. To consider turbulence, both RANS model and LES model are used. Except all the above, there’re also porous medium model, cavitation model and boiling model.

Guelfi, Antoine, et al. [61] have given a comprehensive summary of models, methods and characteristics in NEPTUNE_CFD. Foissac, Arnaud, et al. [62] have done a work extending

droplet collision model by NEPTUNE_CFD. Validation work of two-phase Pressurized Thermal Shocks in NEPTUNE_CFD could be found by Coste, P., et al. [63] and Mérigoux, N., et al. [64]. Laviéville, Jérôme, et al. [65] have done a numerical study of bubbly flow by NEPTUNE_CFD. A similar work could be found in [66]. Prošek, Andrej, Boštjan Končar, and Matjaž Leskovar. [67] have done an uncertainty analysis by NEPTUNE_CFD.

1.4.2.3 GASFLOW

GASFLOW is a 3D CFD code maintained by Karlsruhe Institute of Technology, which was born in Los Alamos National Lab [72]. GASFLOW was designed to analyze physical processes like spray, aerosol, combustion, etc in containment, which later on also extended to hydrogen energy area.

GASFLOW implements ICE'd-ALE numerical methodology to deal with the flow problem in containment, and also a full-speed scheme covering low Mach number to high Mach number condition. Recently a new Parallel Computing module [94] was added to promote the efficiency of simulation. GASFLOW implements both RANS model and LES model for turbulent flow simulation. Multiple flames are also added as way to enhance the performance of hydrogen combustion, while also other engineering models like water film model used in containment accident analysis.

Xiao, Jianjun, et al. [94] have given a summary of the containment analysis code GASFLOW. Ding, Peng, et al. [74] have done a comparison work of Eulerian homogeneous method and Euler-Lagrangian method on TOSQAN 101 and 113 benchmarks using GASFLOW. Also a following study [75] on real size containment study in AP600 PCCS. Kim, Jongtae, et al. [92] have done a numerical study of real-size APR1400 containment BY GASFLOW. Li, Yabing, et al. [76] have done a study of natural convection in containment based on GASFLOW. Zhang, Han, et al [77] have done a study of Large Eddy Simulation model with GASFLOW. Xiao, Jianjun, Jack Travis, and Maurizio Bottoni. [78] have given a work of dynamic water film model development in GASFLOW. Ma, Zhenhui, et al. [79] have done a work of hydrogen risk of PWR by GASFLOW.

1.4.2.4 CFX

CFX is a component in the ANSYS software [69], which is widely used in industrial CFD studies. By modeling spray process, CFX provides both Eulerian approach and Lagrangian approach. With the solid support from ANSYS platform, CFX provides well consistence to other ANSYS imulation products during the general interface. As a commercial software, CFX provides much more friendly user interface compared with others. However, the general function oriented strategy of ANSYS makes CFX not well fit for specified problems in nuclear engineering, which may require for self-modification in practice.

Babić, Miroslav et al [70][71] have done a numerical study of TOSQAN 101 and 113 tests by Euler-Lagrangian method using CFX. Kljenak, Ivo, et al. [90] have done a CFD study of atmosphere mixing and stratification by CFX on TOSQAN benchmark. Houkema, M., et al. [95] have given a validation work of CFX on containment thermal-hydraulics based on the benchmark

of PANDA.

1.4.2.4 OpenFOAM

OpenFOAM (Open Source Field Operation and Manipulation) [96] is an open-source package on CFD analysis, which tries to bring into modern software development and management technologies on CFD code maintaining. By C++ coding and object-oriented design, OpenFOAM shows its strong advantage on simple coding style on writing and easy implementation on new module extension. Together with the support and contribution from the open source community, OpenFOAM now shows a trend of popularity in scientific research area.

The numerical study in nuclear engineering area by OpenFOAM is not rare. Ishigaki, Masahiro, et al [97] have done a work on mesh non-orthogonality in buoyant jet flow. Patel, G., V. Tanskanen, and R. Kyrki-Rajamäki [98] have done a work on condensation in suppression pool. Corzo, Santiago F., et al. [99] have done a work on Thermal hydraulics simulation of steam generator. Wu, Hsingtzu [100] has done a work on coupling between neutronics and thermal–hydraulics. Alali, Abdullah, et al. [101] have done a work on subcooled boiling models. Sugrue, Rosemary, et al. [102] have done a work on bubble flow.

As a CFD package oriented on solving general flow problems, the application of OpenFOAM into the specified nuclear containment area is not much. Hasslberger, Josef, et al. [103] have done a work on APR1400 containment analysis by OpenFOAM. Though some physical models are still not available in the modern OpenFOAM package, the flexibility on fast extension makes it a potential platform for nuclear containment study.

The overall comparison of all the CFD codes for nuclear containment study can be found in Table 3. Though well studied models and well-developed code system can be found in TONUS-CFD, NEPTUNE_CFD, GASFLOW and CFX. Owing to the strong advantage of extension flexibility in self-development, OpenFOAM will be used as the platform on the issues in this work.

Table 3 Summary of nuclear containment analysis codes

Name	Modeling	Parallelization	Mesh	Open-source
TONUS-CFD	Eulerian	No	Structured	No
NEPTUNE_CFD	Eulerian	Yes	Unstructured	No
GASFLOW	Mixture	Yes	Structured	No
CFX	Lagrangian	Yes	Unstructured	No
OpenFOAM	Eulerian Lagrangian	Yes	Unstructured	Yes

1.5 Thesis Objectives

As shown in most of the previous studies, one of the biggest challenges in nuclear power plant simulation is the huge scale range among different physical phenomenon. The smallest scale can be down to nanometer level during the neutron transportation process, while the largest one can be up to kilometer level when comes to the system performance analysis. As shown in **Figure 12**,

from the nuclei movement to power plant system level, the scale has increased more than 10 billion times.

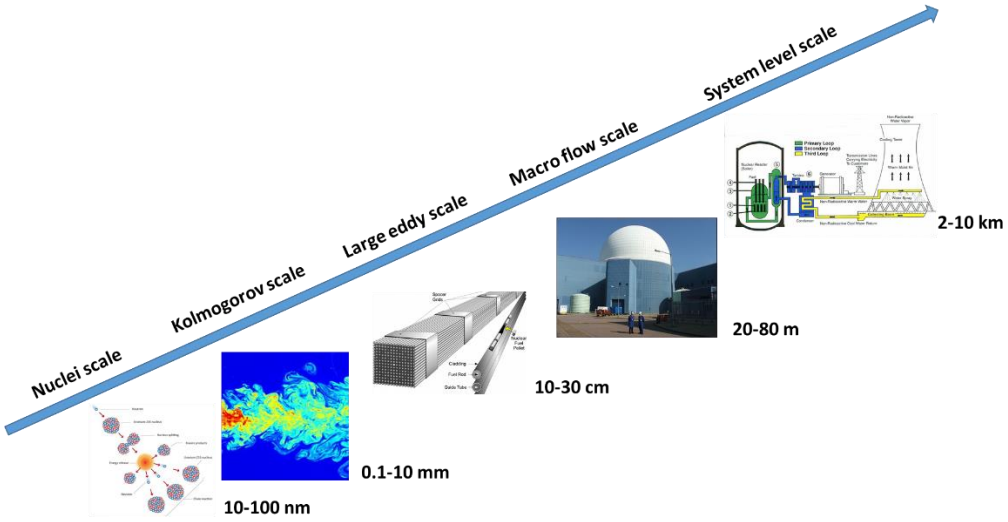

Figure 12 Huge range of scales in nuclear power plant

Such a wide-spanning scale phenomenon can also be found in nuclear containment study, as shown in **Figure 13**. During the spray process in containment cooling, multiple physical processes happen in the meantime. The cavitation and turbulent fluctuation of the flow in the spray nozzle will result in atomization of the liquid sheet into spray droplets. The big droplets will split into small ones owing to the secondary breakup. The final spray droplets will go through mass, momentum and energy exchange with the atmosphere. Meanwhile, the gas phase movement will also be under turbulent condition and carries different size of eddies according to the structural components in the containment. The wall surface of the containment will also suffer from the thermal stress from the heat transfer with atmosphere. Compared with the large geometric physical process in the containment, the droplet only got a size of around 10-100 μm.

From engineering viewpoint, two targets are set up for nuclear containment study, reliability and speed.

Reliability: the numerical simulation should provide a prediction with reasonable matching with the real physical process.

Speed: the numerical simulation should provide a fast prediction, which allows quick modification and low time cost in design process.

In the scope of nuclear containment spray study, the mission of reliability sets further requirement on spray CFD study. Spray cooling process turns out as a complicated process with coupling among multiple physical effects, including multi-phase, multi-component, mass transfer, heat transfer, turbulence and phase change. Even neglecting some tiny-scale effect like atomization in numerical simulation, the modeling of spray process in nuclear containment is a big challenge. Therefore, the modeling of spray cooling process demands deep study. Moreover, turbulence is a chaos process, which still stays as one of the giant difficulties in physical community. The non-linear property of fluid mechanics makes the turbulence bring in high fluctuation and closure problem in traditional statistics-based modeling. Therefore, the study of the turbulent effect on spray cooling requires further study on modeling.

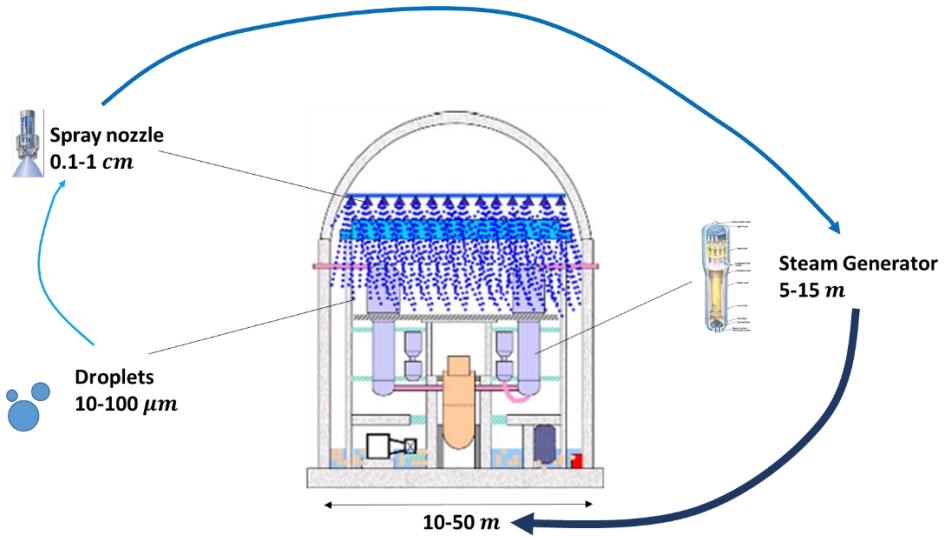

Figure 13 Multi-scale problem in nuclear containment spray

The mission of speed also produces new challenges on traditional numerical study. A detailed simulation by CFD (Computational Fluid Dynamics) with fine mesh always calls for large calculation amount. Even by a rough simulation with a scale similar to nuclear containment, a 0.1 – 1 million cell mesh with tiny time step is still the typical configuration for numerical simulation. Parallel running on 4 – 8 cores with time cost from 3 days to 1 week is common on spray cooling simulation, which however heavily delaying the engineering design process. Therefore, the way to accelerate the simulation in large-scale industrial application like nuclear containment is worth further research.

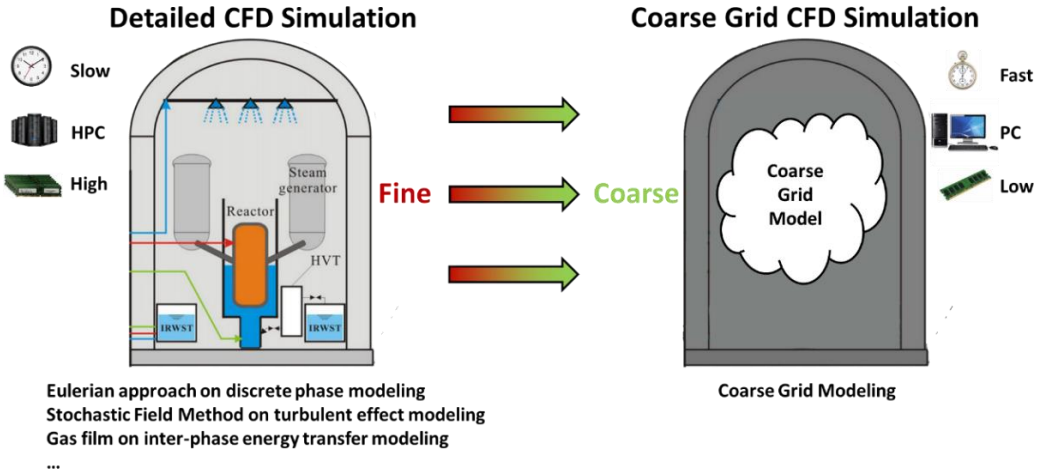

Figure 14 Technical solution routine for nuclear containment spray modeling

In this thesis, an exploration targeting on the two missions is given:

Target 1: Concerning the sophisticated physical processes during spray evaporation cooling process in nuclear containment, a detailed CFD simulation with well-established spray modeling should be discussed and validated by the typical nuclear containment benchmarks, as shown in the left part in **Figure 14**. In addition, the turbulent effect on droplet evaporation, which is the key factor in containment cooling, should be discussed, modelled and validated by common-used benchmarks.

Target 2: For the requirement of speed in nuclear containment study, the fast prediction approach

should be derived, as shown in the right part in **Figure 14**. The method will be extended to fit the problem in the large industrial scale problem in nuclear engineering, which well take advantage of the detailed CFD simulation data done in the past.

1.6 Thesis Outline

The thesis is organized as following:

In Chapter 2, the detailed physical modeling of spray process will be listed, compared and discussed. The three kinds of discrete phase modeling, Lagrangian, mixture and Eulerian, will be introduced and compared. In the following section, the different kinds of turbulence modeling for momentum equation will be discussed. Then, the modeling of turbulent influence on scalar transport will be shortly introduced and further discussed in the next chapter. Next, the modeling of mass, momentum and energy interaction between two phases will be discussed, as well as the thermodynamic model. At last, the algorithm of numerically solving Eulerian two-phase flow system will be discussed. By detailed comparison and summarization, the proper modeling combination on nuclear containment spray is derived. With the theoretical study in this chapter, a solid fundamental step has been set on providing fine simulation for nuclear containment spray in a stable atmosphere.

In Chapter 3, the turbulent transport of the passive scalar will be discussed. The three different kinds of PDF family methods, original PDF, MOM and Stochastic Field Method will be introduced. A discussion of the models will be given, in order to pick up the right method for spray modeling. In addition, a deep theoretical discussion of modeling droplets' transport under turbulence will be given, which is different from traditional way in original Stochastic Field Method. At last, a 1D plug-flow chemical reactor case will be studied by Stochastic Field Method and compared with the theoretical solution, as validation of the performance. With the theoretical study in this chapter, a further effort has been made on providing theoretical support for nuclear containment spray under turbulent atmosphere.

In Chapter 4, a practical work on the validation of the spray physical models in a stable atmosphere evaporation cooling case will be presented. The international severe accident experimental facility, THAI is used as the benchmark. A Eulerian-based numerical simulation of spray process is proceeded and compared with the experiment data. With the contribution in this chapter, the spray modeling solution discussed in the previous chapter has been already validated, which can be used on detailed containment spray CFD study and data generation for coarse simulation.

In Chapter 5, a practical work will be presented, on the validation of turbulent droplet transport in a turbulent status atmosphere. Owing to the rare experiments done in nuclear containment benchmarks on this topic. The dryer facility with turbulent hot air flow is used instead, which got similar geometric characteristics, material properties and boundary conditions to the containment. Stochastic Field Method has been implemented on modeling the process, and further compared with the naive Eulerian approach and the experiment data. With the contribution in this chapter, the validation on the turbulent spray modeling discussed in the previous chapter will be done, which provides guideline for CFD simulation of spray cooling when the atmosphere in the containment is under turbulent status.

In Chapter 6, the discussion on acceleration of the prediction on large-scale problem in nuclear

facilities will be given. The data-driven method, Coarse Grid CFD will be introduced. In this work, a further flux correction method by physical-based approach will be derived and compared with the former geometric-based approach. Furthermore, the new way on treating the inconsistence between coarse mesh and CAD will be discussed in detail. At last, the liquid metal flow experiment of 19-pin wired bundle case done by Karlsruhe Liquid Metal Laboratory (KALLA) is used as the benchmark on validation of CGCFD method with the additional modifications. With the contribution of this chapter, the way to take use of the fine data in fast simulation on coarse mesh is set up.

In Chapter 7, the summary of the whole thesis is given. The final conclusion is derived and discussed. Finally, an outlook of the future work is presented, which including all the previous work on fine simulation with detailed spray cooling model and coarse grid CFD approach. An early exploration of applying fast simulation onto containment cooling study is done, coupled with new artificial intelligence advancements.

2. Physical modeling of spray process

A detailed CFD simulation with proper model on physical process is vital in a reliable prediction of containment cooling ability analysis. The spray cooling is a complicated process mixed with multiple physical effects, including discrete phase modeling, momentum turbulence modeling, inter-phase effect modeling, phase change modeling and physical property modeling. Owing to different working conditions of the two-phase flow, the way of modeling each single process can have diverse options. In order to set up the best solution choice of nuclear containment spray modeling, the physical models of two-phase flow will be introduced and compared, until the proper combination is constructed.

2.1 Discrete phase modeling

In spray process, one of the key questions is the treatment of the liquid phase. Since the gas phase occupies a large volume in the two-phase flow, its continuous property is maintained. However, the liquid phase always stays as droplets in most parts of the spray vessel, which makes it as a discrete phase require further modeling.

In this section, the three methods of discrete phase modeling, Lagrangian approach, Mixture approach and Eulerian approach, will be introduced and compared. At last, the proper choice of liquid phase modeling in nuclear containment spray will be set up.

2.1.1 Lagrangian approach

Lagrangian approach treats the gas phase as a single continuous phase, while setting up another independent tracking system of the liquid droplet movement. The early use of Lagrangian framework can be back to the work by FH Harlow [104], which solves the incompressible flow by a particle-in-cell method. Later on, it was extended to two-phase flow simulation [105] [106].

Concerning the rare fraction of liquid in a spray process, large part of the calculation domain is filled with the two-phase mixture nearly 100% contributed by gas. With low volume fraction, the existence of the water droplet has nearly no direct influence on controlling equation, but only as a source term. Therefore, in Euler-Lagrangian approach, the liquid phase is directly modelled like the single phase in a continuous way, as

$$\frac{\partial \rho_g U_{gi}}{\partial t} + \frac{\partial \rho_g U_{g,i} U_{g,j}}{\partial x_j} = -\frac{\partial p}{\partial x_i} + \tau_{g,ij} - f_{gl,i}, \tag{2.1}$$

$$\frac{\partial \rho_g E_g}{\partial t} + \frac{\partial \rho_g E_g U_{g,j}}{\partial x_j} = -\frac{\partial}{\partial x_j}\left[U_{g,j}\left(p\delta_{ij}\right) - \tau_{g,ij}\right] + \dot{q}, \tag{2.2}$$

where ρ_g is the density of gas phase, U_g is the velocity of gas phase, E_g is the inner energy of gas phase, p is the pressure, τ_g is the stress tensor, f_{gl} is the momentum interaction between gas phase and liquid phase, and $\dot{q}$ is the energy interaction between gas phase and liquid phase.

In terms of liquid phase, Lagrangian approach tries to track the path of each liquid droplet. Therefore, a Lagrangian approach can be concluded as

$$\frac{d}{dt}(\boldsymbol{x_p}) = \boldsymbol{u_p}, \tag{2.3}$$

$$m_p \frac{d}{dt}(\boldsymbol{u_p}) = \boldsymbol{f_{gl}}, \tag{2.4}$$

$$C_p m_p \frac{d}{dt}(T_p) = \dot{q}, \tag{2.5}$$

where $\boldsymbol{x_p}$ stands for the location of the droplet, $\boldsymbol{u_p}$ stands for the velocity of the droplet, T_p stands for the temperature of the droplet. m_p and C_p stand for the droplet's mass and heat capacity. $\boldsymbol{f_{gl}}$ and $\dot{q}$ stand for the momentum and energy exchange between the droplet and the surrounding atmosphere. The whole process of Lagrangian approach is shown in **Figure 15**.

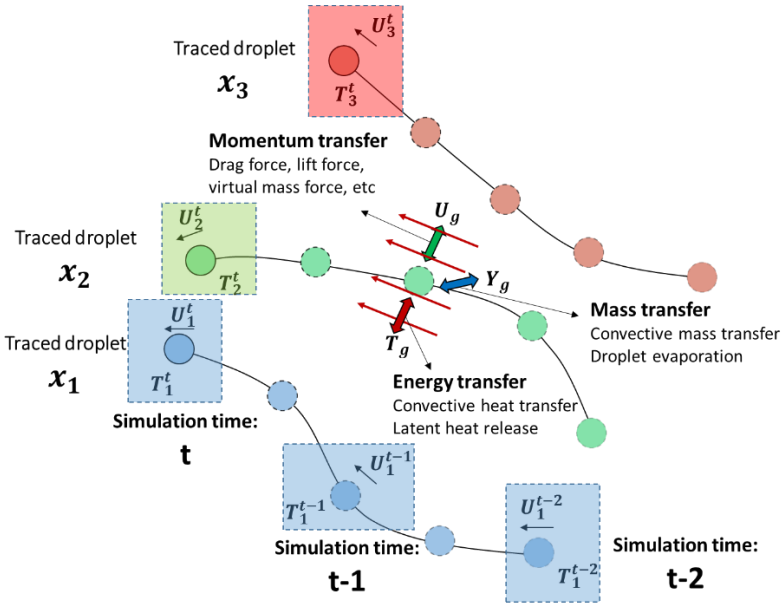

Figure 15 Discrete phase modeling by Lagrangian approach

By modeling liquid droplets as a particle system approach, Lagrangian approach provided a way much closer to the real physical process, which principally results in a better simulation performance. However, for a spray process simulation at the engineering level, its computing resource requirement is normally not affordable. Large amount of liquid will be injected from the nozzle during the spray process, which finally result in millions of droplets distributed widespread in the space. Independent tracing of each single droplet will call for large-scale parallel computing. Furthermore, the situation will become even tougher when comes to the nuclear containment study, concerning its large volume. In addition, nuclear containment safety always requires long period analysis to ensure the performance under accident, which further increases the total calculation amount.

Some studies try to decrease the droplet number by bringing in the concept of parcel [107], which use one chosen "particle" standing for a cloud of particles sharing similar shape, momentum and energy characteristics. Though partly mitigates the burden of computing capacity, the implementation of parcel obeys the principle of real-time tracing in Lagrangian method and partly lose the precision advantage to Eulerian approach.

Lagrangian simulation of droplets also requires an independent system of particle tracing to code, which is not naturally consisting with the former CFD coding structure. In addition, the numerical

schemes and stability analysis criterions may as well call for new theoretical backgrounds [108], which waste the previous experience learned in CFD studies. As a result, a further development of Lagrangian modeling based on existing code will face certain difficulty. Therefore, Lagrangian approach may be better fit for small-scale short-term spray problem.

2.1.2 Mixture approach

Mixture approach tries to implant the reactive flow modeling approach into two-phase flow problem. In mixture approach [109], phases are assumed to be "volume" components like chemical components in reactive flow, where the discrete phase is uniformly distributed in certain location and reach the momentum equilibrium status with the carrier phase. Since the two phases share one common velocity, this model is also named homogenous model, as shown in **Figure 16**. To further model the volume occupation of the discrete phase in the mixture, one additional volume fraction is coupled with Eulerian mixture equations. Since the volume fraction equation describes the movement of discrete phase following the continuous flow, this modeling approach is called drift flux model. The influence of discrete phase on the continuous phase momentum will be further prescribed to a certain value achieved by an experiment-based model.

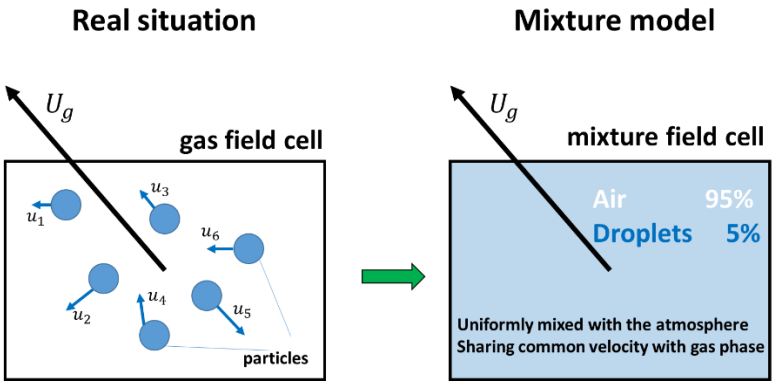

Figure 16 Discrete phase modeling by mixture approach

The mixture model can be briefly summarized as

$$\frac{\partial(\rho_m)}{\partial t}+\frac{\partial(\rho_m U_i)}{\partial x_j}=0, \tag{2.6}$$

$$\frac{\partial(\rho_l\alpha_l)}{\partial t}+\frac{\partial}{\partial x_i}(\rho_l\alpha_l U_i)=-\frac{\partial}{\partial x_i}\left(\rho_l\alpha_l v_{dr,i}\right)+\dot{m}, \tag{2.7}$$

$$\frac{\partial(\rho_m U_i)}{\partial t}+\frac{\partial\left(\rho_m U_i U_j\right)}{\partial x_j}=-\frac{\partial p}{\partial x_i}+\tau_{g,ij}+\frac{\partial\left(\rho_l\alpha_l v_{dr,i}v_{dr,j}\right)}{\partial x_j}, \tag{2.8}$$

$$\rho_m=\rho_g(1-\alpha_l)+\rho_l\alpha_l, \tag{2.9}$$

$$v_{dr,i}=\frac{\tau_p}{D_{drag}}\frac{\rho_l-\rho_m}{\rho_l}\left(-U_i\frac{\partial}{\partial x_j}U_j\right), \tag{2.10}$$

where ρ_m, ρ_g and ρ_l stand for the density of gas-liquid mixture, gas phase and liquid phase. U_i stands for the gas phase's velocity. α_l stands for the volume fraction of liquid phase. $\dot{m}$ is the mass transfer between two phases. $v_{dr,i}$ is the drift velocity with τ_p as the droplet time and D_{drag} as the drag force coefficient.

Mixture approach is well fit for cavitation or boiling problem, but less qualified for spray problem. In cavitation or boiling problem, liquid phase stays as the carrier phase. Bubbles' movement will

always follow the large amount of liquid around them, since the density of the gas phase is much less compared with liquid phase. Therefore, owing to the weak inertial property compared with liquid phase, bubbles will easily reach momentum equilibrium with the liquid flow. On the contrary, since the gas phase occupies most of the space in spray problem, the liquid droplets plays as discrete phase instead. Owing to its strong inert, the liquid droplet is able to better resist the fast velocity change. Therefore, Mixture approach is not well fit for spray modeling, which is a problem with heavy discrete phase and light continuous phase.

2.1.3 Eulerian approach

Eulerian approach [110] is an updated version of Mixture approach. By treating both gas phase and liquid phase as two separated Eulerian field systems with independent velocity and temperature, Eulerian approach succeeds in fixing the deficit of Mixture approach. With independent momentum and energy systems for both gas and liquid phase, Eulerian approach solves two single phase problems coupled by the volume fraction equation, as shown in **Figure 17**. That's why it's also called two-fluid model.

The Eulerian approach can be briefly summarized as

$$\frac{\partial\left(\rho_g\alpha_g+\rho_l\alpha_l\right)}{\partial t}+\frac{\partial\left(\rho_g\alpha_g U_{g,i}+\rho_l\alpha_l U_{l,i}\right)}{\partial x_i}=0, \tag{2.11}$$

$$\frac{\partial(\rho_l\alpha_l)}{\partial t}+\frac{\partial}{\partial x_i}(\rho_l\alpha_l U_i)=\dot{m}, \tag{2.12}$$

$$\frac{\partial\rho_g\alpha_g U_{g,i}}{\partial t}+\frac{\partial\rho_g\alpha_g U_{g,i}U_{g,j}}{\partial x_j}=-\frac{\partial\alpha_g p}{\partial x_i}+\tau_{g,ij}-f_{gl}, \tag{2.13}$$

$$\frac{\partial\rho_l\alpha_l U_{l,i}}{\partial t}+\frac{\partial\rho_l\alpha_l U_{l,i}U_{l,j}}{\partial x_j}=-\frac{\partial\alpha_l p}{\partial x_i}+\tau_{l,ij}+f_{gl}, \tag{2.14}$$

$$\frac{\partial\rho_g\alpha_g E_g}{\partial t}+\frac{\partial\rho_g\alpha_g E_g U_{g,j}}{\partial x_j}=-\frac{\partial}{\partial x_j}\left[U_{g,j}\left(\alpha_g p\delta_{ij}\right)-\tau_{g,ij}\right]+\dot{q}, \tag{2.15}$$

$$\frac{\partial\rho_l\alpha_l E_l}{\partial t}+\frac{\partial\rho_l\alpha_l E_l U_{l,j}}{\partial x_j}=-\frac{\partial}{\partial x_j}\left[U_{l,j}\left(\alpha_l p\delta_{ij}\right)-\tau_{l,ij}\right]-\dot{q}, \tag{2.16}$$

where ρ_g and ρ_l, α_g and α_l, $U_{g,i}$ and $U_{l,i}$, E_g and E_l stand for the density, volume fraction, velocity and energy of the gas phase and liquid phase. $\dot{m}$ is the inter-phase mass transfer, f_{gl} is the inter-phase momentum transfer and $\dot{q}$ is the inter-phase energy transfer.

Since there are totally 6 equations in the model, the model is also called 6-Equation model. Considering the continuous phase is also modelled from the Eulerian viewpoint, the two-phase modeling by Eulerian approach is also called Euler-Euler approach.

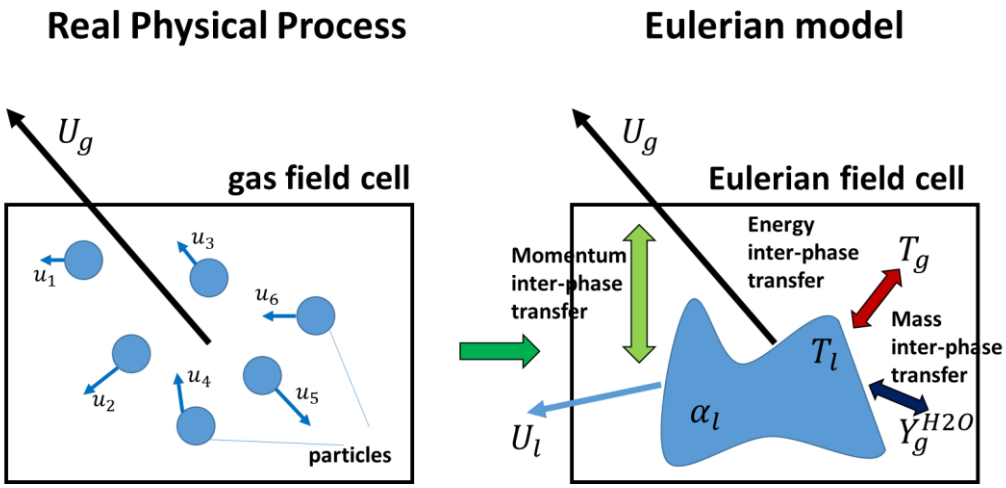

Figure 17 Discrete phase modeling by Eulerian approach

The discrete phase would be further modelled in Eulerian approach, but avoid the heavy burden on single droplet tracking, which keeps the calculation amount at a reasonable level. With two independent Eulerian systems of gas phase and liquid phase, the velocity and temperature can be better predicted over Mixture approach. Therefore, it can provide a better performance when the discrete phase owns a strong inertial characteristic and large heat capacity. The advantage of Eulerian approach is the high efficiency on numerical simulation, owing to the low calculation amount. Only one physical field needs to be solved, instead of tracing multiple droplets in Lagrangian approach. Moreover, the liquid droplet field shares a common mesh with gas phase, which gets rid of the sophisticated interpolation treatments. Lastly, the simulation of liquid droplets on Eulerian mesh will be naturally compatible with existing CFD numerical schemes and convergence criterions.

2.1.4 Discussion of methodology choice in nuclear containment spray

A detailed summary and comparison among the three ways of modeling discrete phase are provided in **Table 4**.

In nuclear containment spray cooling study, the long spray time period and the large volume space result in trillions of droplets wide spreading in the vessel. A specified single-by-single particle tracking will fail on normal computer hardware device, considering the time and memory cost. In addition, owing to the numerical stability requirement, time step needs further reducing to avoid divergence on iteration, which give additional difficulty on fast simulation. However, the simulation speed will be of more importance since the fast design iteration is necessary in nuclear engineering projects.

The physical value in nuclear containment is always smoothly distributed with no abrupt change in space, which makes the assumption of continuous change valid. In addition, the macro-level physical change is of more importance than the tiny changes brought in by one certain droplet behavior, which makes the balanced approach a good choice on modeling. Therefore, the “Field” concept well matches the requirement of nuclear containment modeling.

Considering all the issues discussed above, Eulerian approach well balances precision and calculation amount in this sense and is therefore chosen as the method in the nuclear containment study of this work.

Table 4 Summary of discrete phase modeling approaches

model	Calculation amount	precision	Single particle characteristics	Independent particle system	Numerical scheme Stability criterion
Lagrangian	High	High	Yes	Yes	needs further study
Mixture	Low	Low	No	Yes	Same as usual
Eulerian	Medium	Medium	No	No	Same as usual

2.2 Turbulence modeling

To make spray modeling well work in fine CFD simulation, special treatment on turbulence is necessary. In this section, the mechanism of turbulence will be discussed in details. The way of modeling turbulence will also be introduced and compared to figure out the best option for momentum modeling in containment spray, and also illuminates the way of modeling turbulent scalar transport, which will be discussed further in Chapter 3.

Turbulence process is a chaos process controlled by non-linear equation, Navier-Stokes Equation. Owing to its special property, the real-time simulation of turbulence can only be achieved with time and spatial scale down to the Kolmogorov scale, which puts strong restricts on time step and spatial size. Therefore, the numerical simulation always requires additional treatment.

In this section, the turbulence modeling will be introduced. The strategies on modeling turbulence can be roughly divided into two kinds: statistical-based approach, including RANS, LES, DNS and probability-based approach, including PDF. At last, all the methods will be compared, and the proper choice of the gas phase turbulence modeling will be derived

2.2.1 Chaotic Nature of Navier-Stokes Equation

The nature of Navier-Stokes Equation has been discussed in the book of S.B Pope [111], which is sensible to the small perturbation when the inertial effect is much stronger than the viscous effect in the flow. The chaotic property of Navier-Stokes Equation makes it difficult to model turbulence. Following the previous work, Navier-Stokes Equation was derived following the conservative law. Assuming an infinite small controlling volume in the flow. The mass equation can be constructed based on the continuity of material,

$$\frac{\partial \rho}{\partial t} + \frac{\partial \rho U_i}{\partial x_i} = 0, \tag{2.17}$$

where ρ is the density and U_i is the velocity.

The momentum equation can be constructed based on Newton's Second Law,

$$\frac{\partial \rho U_i}{\partial t} + \frac{\partial \rho U_i U_j}{\partial x_j} = \frac{\partial \tau_{ij}}{\partial x_j}, \tag{2.18}$$

where τ_{ij} is the viscous stress tensor. Assumed the fluid as a Newtonian Fluid, under Stokes' hypothesis, τ_{ij} can be modelled as

$$\tau_{ij} = -p\delta_{ij} + \mu\left(\frac{\partial U_j}{\partial x_i} + \frac{\partial U_i}{\partial x_j} - \frac{2}{3}\frac{\partial U_k}{\partial x_k}\delta_{ij}\right), \tag{2.19}$$

where μ is the kinetic viscosity.

The energy equation can be constructed based energy conservative law,

$$\frac{\partial \rho h}{\partial t} + \frac{\partial \rho U_i h}{\partial x_i} = \frac{\partial}{\partial x_i}\left(\frac{\mu}{Sc}\frac{\partial h}{\partial x_i}\right) + \dot{q}, \tag{2.20}$$

where h is the enthalpy, $\dot{q}$ is the heat source and Sc is the Schmidt number.

Owing to the similar structure of equations in Navier-Stokes Equations, a general form equation can be summarized as

$$\underbrace{\frac{\partial \rho \phi}{\partial t}}_{\substack{\text{Transient term} \\ \text{Linear}}} + \underbrace{\frac{\partial \rho U_i \phi}{\partial x_i}}_{\substack{\text{Convection term} \\ \text{Non-linear}}} = \underbrace{\frac{\partial}{\partial x_i}\left(\Gamma \frac{\partial \phi}{\partial x_i}\right)}_{\substack{\text{Diffusion term} \\ \text{Linear}}} + \underbrace{S(\phi)}_{\substack{\text{source term}}} \tag{2.21}$$

where ϕ can be 1, U_i or h to form the mass, momentum and energy equation.

Assume the flow as an incompressible flow, the density ρ becomes constant in incompressible Navier-Stokes Equation. Navier-Stokes Equation is then a group of non-linear Partial Differential Equation (PDE), owing to the convection term existing as the product of U_i and ϕ. The non-linear property makes the system against the principle of superposition. Both theoretical work and experimental work have proved that Navier-Stokes Equation is a chaotic system [112] [113], which is sensible to the initial value and boundary condition. A dimensionless number, Reynolds number, is used as the condition when the system totally turned into chaos

$$\mathrm{Re} = \frac{\rho U L}{\mu}, \tag{2.21}$$

where U and L are the characteristic velocity and length. Reynolds number stands for the rate of inertial force over viscous force.

Owing to large number of studies [114] [115], the flow will be turned into a highly irregular status with huge nearly random fluctuation, when the Reynolds number goes above certain amount, as shown in **Figure 18**. In such condition, even during a tiny time period, huge difference on the physical property of flow can be measured. Even more, by the same experimental facility with nearly the same input, two realizations can reach totally different results at same location and same time point. Since the flow turns into turbulent status, a slight mechanical perturbation can consist being amplified until a complete difference observed in macro-level.

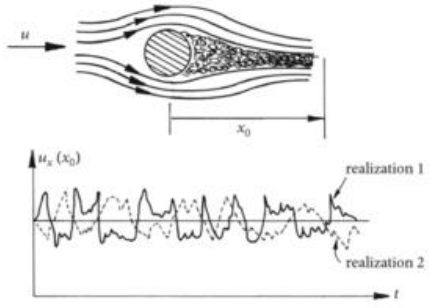

Figure 18 Turbulence fluctuation [116]

2.2.2 Statistical strategy on turbulence modeling

To further model the turbulent flow, statistical approaches have been used on turbulence modeling.

By statistic study on turbulence, an energy spectrum can be got as shown in **Figure 19**. According to the plot, turbulence can be decomposed into three parts with different ranges of wavenumber. Following Richardson's hypothesis [117], turbulence is composed of the basic unit, eddy, which carries the fluctuation in flow. In Kolmogorov's 1941 theory [118][119], further hypothesis is set up on eddies linked to the turbulent energy spectrum: the large eddies are got from inlet, then split into medium scale eddies. The medium eddies carry most of the inertial energy of flow, and will transfer the energy from the big ones to the small ones. Until when the scales of eddies become super tiny, the energy will come into the dissipation zoon, the turbulent kinetic energy will be consumed by heat loss. The tiny scale eddies in the dissipation range are assumed to be statistically isotropic, which have no influence on the macro flow and also not influenced by it. The motion of these tiny eddies only depends on the inner properties. Such eddies are also called Kolmogorov scale eddies.

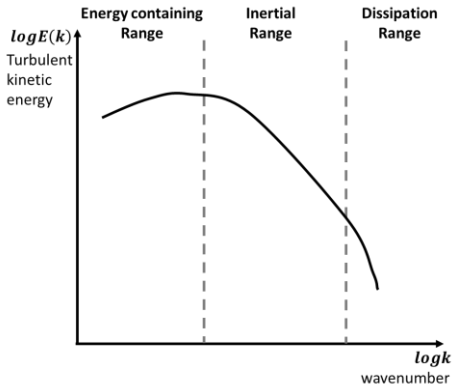

Figure 19 turbulence energy spectrum

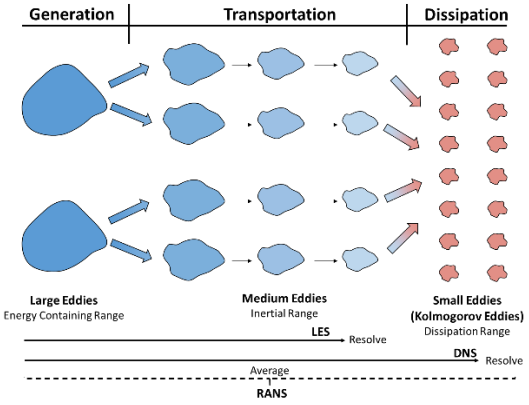

Figure 20 Kolmogorov theory and turbulence modeling

According to the scales resolved, the statistics-based modeling can be divided into DNS, LES and RANS, as shown in **Figure 20**.

2.2.2.1 DNS modeling

DNS (Direct Numerical Simulation) [120] tries to directly resolve all the turbulence scales in the flow. As the most straightforward approach on turbulence modeling, DNS controls the grid size and the time step both down to Kolmogorov scale,

$$\eta = \left(\frac{\nu^3}{\varepsilon}\right)^{1/4}, \tag{2.22}$$

According to Kolmogorov theory, the smallest scale in macro resolvable level of turbulence is the Kolmogorov scale, where all the other micro scales are beyond the scope of turbulence study, also certainly beyond the resolution requirement of the macro flow. With all the information in turbulence resolved down to Kolmogorov scale, DNS brings in high requirement for calculation amount and physical memory, which can only be possibly to apply on small-scale problems.

Based on the review of DNS approach, we can conclude:

DNS approach could stay as a tool of turbulence mechanics research in academic circle, but can rarely be used in engineering area. Like if DNS is applied to spray modeling, the mesh size must be down less than the droplet diameter, as way to resolve the boundary layer around the spray

droplet, as shown in **Figure 21**. Therefore, DNS is never able to be afforded by real large-scale industrial application like nuclear containment for now and for the near future.

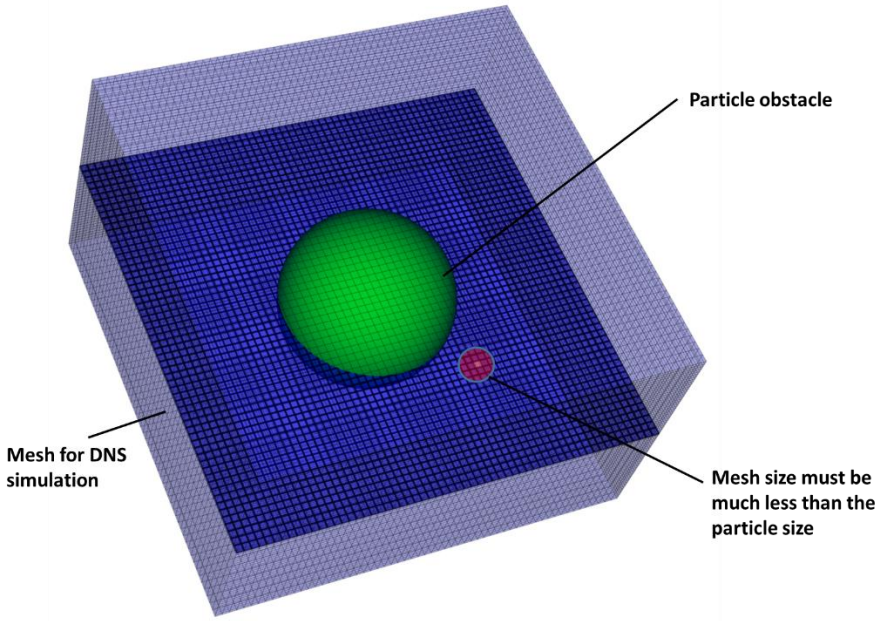

Figure 21 Direct Numerical Simulation

2.2.2.2 LES modeling

LES (Large Eddy Simulation) [121] tries to solve turbulence problem by real-time resolving the large eddies, while filtering out the small eddies.

According to Kolmogorov theory, the turbulent eddies can be categorized as energy containing eddies, inertial eddies and dissipation eddies. The former two categories always got a larger length and time scale, which loosen the requirement of grid size and time step. On the contrary, the dissipation eddies' scale on the contrary is down to the Kolmogorov level, which is the bottleneck of promoting time step and grid size. However, dissipation eddies share common statistically isotropic characteristics, which would be fit for macro-level modeling.

In LES method, a numerical filter is implemented as way to filter out the small Kolmogorov scale eddies from the flow [122], while only keeping the large eddies to resolve, as shown in **Figure 22**. By a proper setting of the filter scale, a certain precision can be maintained according to the requirement. Meanwhile, the dissipation-scale eddies' simulation will be taken place by proper modeling.

By applying a certain filter to velocity and pressure, we get

$$\overline{U(\boldsymbol{x},t)} = \int_{-\infty}^{\infty}\int_{-\infty}^{\infty} U(\boldsymbol{r},\tau)\, G(\boldsymbol{x}-\boldsymbol{r},t-\tau)d\tau d\boldsymbol{r} \tag{2.23}$$

$$\overline{p(\boldsymbol{x},t)} = \int_{-\infty}^{\infty}\int_{-\infty}^{\infty} p(\boldsymbol{r},\tau)\, G(\boldsymbol{x}-\boldsymbol{r},t-\tau)d\tau d\boldsymbol{r} \tag{2.24}$$

where $G(\boldsymbol{x}-\boldsymbol{r},t-\tau)$ is a filter function, which tries to cut off the wave with length scale less than a chosen one Δ and time scale less than a chosen one τ_C.

Therefore, the instant velocity and pressure at a certain location can be written as

$$U(\boldsymbol{x},t) = \overline{U(\boldsymbol{x},t)} + u' \tag{2.25}$$

$$p(\boldsymbol{x},t) = \overline{p(\boldsymbol{x},t)} + p' \tag{2.26}$$

Where u' and p' are the sub-scale information of velocity $U(\boldsymbol{x},t)$ and pressure $p(\boldsymbol{x},t)$.

If the filter is put on the incompressible Navier-Stokes Equation, the continuous equation will become

$$\frac{\partial \bar{U}}{\partial t} = 0 \tag{2.27}$$

The momentum equation will become

$$\frac{\partial \bar{U}}{\partial t} + \frac{\partial\left(\overline{U_i U_j}\right)}{\partial x_j} = -\frac{1}{\rho}\frac{\partial \bar{p}}{\partial x_i} + \nu\frac{\partial}{\partial x_j}\left(\frac{\partial \bar{U}_i}{\partial x_j} + \frac{\partial \bar{U}_j}{\partial x_i}\right) \tag{2.28}$$

By modeling the non-linear term as

$$\overline{U_i U_j} = \bar{U}_i \bar{U}_j + \tau_{ij}^{sub} \tag{2.29}$$

The momentum equation will turn into

$$\frac{\partial \bar{U}}{\partial t} + \frac{\partial\left(\bar{U}_i \bar{U}_j\right)}{\partial x_j} = -\frac{1}{\rho}\frac{\partial \bar{p}}{\partial x_i} + \nu\frac{\partial}{\partial x_j}\left(\frac{\partial \bar{U}_i}{\partial x_j} + \frac{\partial \bar{U}_j}{\partial x_i}\right) - \frac{\partial \tau_{ij}^{sub}}{\partial x_j} \tag{2.30}$$

where τ_{ij}^{sub} is the so-called sub-grid stress, which only contains the information of eddies with scales smaller than the grid size.

By properly modeling the sub-grid stress like Smagorinsky–Lilly model [123] and Germano dynamic model [124], etc. The momentum equation can be closed and then solved by numerical linear algorithm methods.

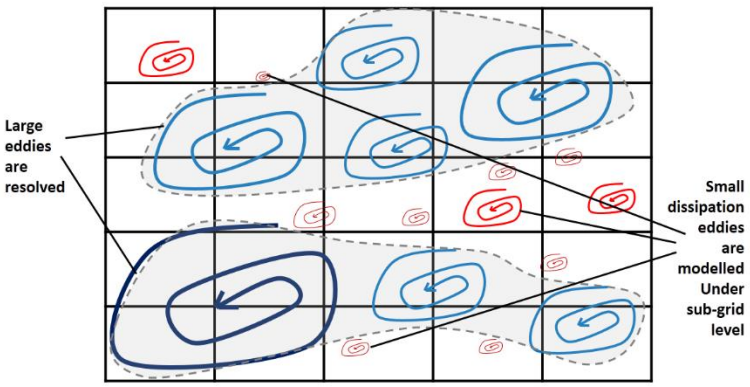

Figure 22 Large Eddy Simulation

According to the previous studies, we can conclude:

LES method makes detailed simulation possible in an industrial level application. However, the huge calculation amount still obeys the need of fast prediction in real industrial design, which makes the method only stay in academic exploration studies of engineering problems.

By real-time resolving large eddies in turbulence, LES can still be able to catch more details of the flow field, while got an acceptable amount of calculation compared with DNS, by properly modeling sub-grid stress. Therefore, some mechanism-study-oriented turbulence simulation in engineering applications like containment is possible, like shown in [125] [126]. However, to seek for enough precision, LES needs to resolve 95% of the turbulent kinetic energy, as way to ensure the isotropic assumption of the sub-grid eddies. The requirement of LES makes a simulation with million level grids as a basic, which makes it only an academic tool of studying macro scale

mechanism, but far away from the real industrial application design and prediction support.

2.2.2.3 RANS modeling

RANS (Reynolds-averaged Navier–Stokes) [127] tries to model turbulence by doing time-average over Navier-Stokes Equation, in order to further decrease the calculation requirements as shown in **Figure 23**. RANS modeling sets aside the capture of turbulence eddies resolution, but seek for the averaged performance of turbulence instead.

Assume the instant velocity can be described as

$$\mathrm{u}(\boldsymbol{x},t) = \langle U(\boldsymbol{x})\rangle + u'(\boldsymbol{x},t) \tag{2.31}$$

where $\langle U(\boldsymbol{x})\rangle$ is the averaged velocity and $u'(\boldsymbol{x},t)$ is the irregular fluctuation part.

The averaged velocity $\langle U(\boldsymbol{x})\rangle$ can be got through Reynolds average,

$$\langle U(\boldsymbol{x})\rangle = \lim_{T\to\infty}\int_{t_0}^{t_0+T} \mathrm{u}(\boldsymbol{x},t)dt \tag{2.32}$$

where T is a long-enough time period.

Therefore, by integrating over Navier-Stokes Equation, the Reynolds averaged Navier-Stokes Equation can be derived.

The Reynolds averaged continuous equation can be derived as

$$\langle\frac{\partial u_i}{\partial x_i}\rangle = \frac{\partial\langle U_i\rangle}{\partial x_i} = 0 \tag{2.33}$$

The Reynolds averaged momentum equation can be derived as

$$\langle\frac{\partial u_i}{\partial t} + u_j\frac{\partial u_i}{\partial x_j}\rangle = \langle f_i - \frac{1}{\rho}\frac{\partial p}{\partial x_i} + \nu\frac{\partial^2 u_i}{\partial x_j\partial x_j}\rangle \tag{2.34}$$

Which equals to

$$\frac{\partial\langle U_i\rangle}{\partial t} + \langle U_j\rangle\frac{\partial\langle U_i\rangle}{\partial x_j} + \langle u_j'\frac{\partial u_i'}{\partial x_j}\rangle = \langle f_i\rangle - \frac{1}{\rho}\frac{\partial\langle p\rangle}{\partial x_i} + \nu\frac{\partial^2\langle U_i\rangle}{\partial x_j\partial x_j} \tag{2.35}$$

Here, one additional term $\langle u_j'\frac{\partial u_i'}{\partial x_j}\rangle$ will be produced owing to the non-linear characteristics of Navier-Stokes Equation. If further construct controlling equation of this term, new additional terms with higher order moment will emerge again, which remain to be modelled. Therefore, the Reynolds-average Navier-Stokes Equation will suffer from unclosed terms. Such closure problem of turbulence is the most cumbersome issue in RANS family methods.

The additional term $\langle u_j'\frac{\partial u_i'}{\partial x_j}\rangle$ is also called Reynolds stress. The key issue of RANS family methods is to model the Reynolds stress. To solve the closure problem of Reynolds stress, RANS family always brings in additional physical values and make further assumption. By the different number of equations imported, RANS families can be extended into,

- 0 equation model: Mixing length model [128]
- 1 equation model: Prandtl's one-equation model [129], Spalart-Allmaras model [130]
- 2 equation model: k-epsilon models [130], k-omega models [131]

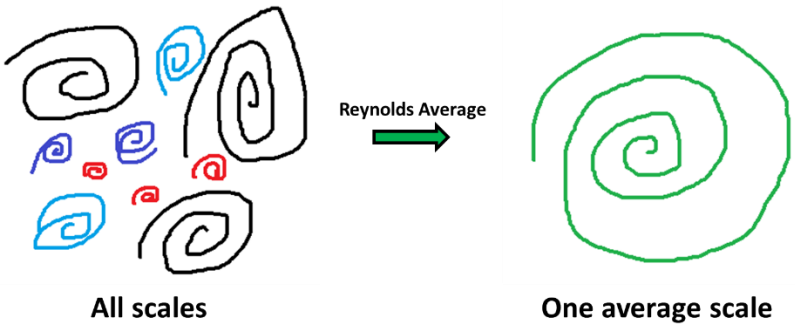

Figure 23 Reynolds Averaged Navier-Stokes Modeling

Based on the review of previous studies, we can conclude:

RANS family models provide a cheap way to solve turbulent problems, as large time step and grid size are permitted owing to the averaging approach. Rather than the irregular fluctuation, the averaged physical value would be of the main concern in real industrial application, which makes RANS model a good candidate for engineering study

RANS family models are cheap to model and fast to predict, but weak in extending to multi-phase and multi-component problems. The modeling-based closure approach in RANS family models throw new difficulties on multi-phase or multi-component problem, as new additional volume fraction or component will totally modify the terms in Reynolds-average Navier-Stokes Equation. The chemical reaction and phase change under turbulent effect will leave new unclosed terms remaining to model. Considering the diverse choices expression on the chosen experimental formula in source term of chemical reaction and phase change, RANS-based approach needs to provide closure models one by one to satisfy the given problem, which leaves a general model for multi-phase and multi-component problems no way to derive. Such situation is unacceptable in real industrial problems. The further solution for this issue will be discussed in Chapter 3.

2.2.3 Probability strategy on turbulence modeling: PDF modeling

PDF (Probability Density Function) method [132] has provided a new routine of solving turbulent problem from the probability viewpoint rather than statistics viewpoint. In PDF method, a stochastically equivalent system is constructed, as way to bypass the closure problem in traditional statistical based approaches. Therefore, PDF method is principally able to describe the performance of all scales, compared with approaches like RANS and LES.

PDF method converts the problem of solving physical values like velocity and pressure into an equivalent problem of solving a joint PDF of velocity and component,

$$\mathrm{f}(\boldsymbol{U}=\boldsymbol{V},\phi=\psi;\boldsymbol{x},t), \tag{2.36}$$

which stands for the probability of velocity $\boldsymbol{U}$ equals to a certain value $\boldsymbol{V}$, and a passive scalar ϕ equals to a certain value ψ at the location $\boldsymbol{x}$ and time t.

Similar to quantum mechanism theory, a PDF transport equation based on Navier-Stokes Equation can be derived following the method in [133],

$$\begin{aligned}\rho\left(\underline{\psi}\right)\frac{\partial f}{\partial t}+\rho\left(\underline{\psi}\right)V_j\frac{\partial f}{\partial x_j}-\frac{\partial\langle p\rangle}{\partial x_j}\frac{\partial f}{\partial V_j}+\frac{\partial}{\partial\psi_\alpha}\left[\rho\left(\underline{\psi}\right)S_\alpha\left(\underline{\psi}\right)f\right]\\=\frac{\partial}{\partial V_j}\left[\left\langle-\frac{\partial\tau_{ij}}{\partial x_i}+\frac{\partial p'}{\partial x_j}\middle|\underline{V},\underline{\psi}\right\rangle f\right]+\frac{\partial}{\partial\psi_\alpha}\left[\left\langle\frac{\partial J_i^\alpha}{\partial x_i}\middle|\underline{V},\underline{\psi}\right\rangle f\right],\end{aligned} \tag{2.37}$$

where ρ and S_α are the density and the source term. τ_{ij}, p' and J_i^α are the viscous stress, pressure fluctuation and component transfer flux. V_j and $\underline{\psi}$ are one chosen velocity and component realization in the velocity and component ensemble sample set.

As shown above, the joint velocity-component PDF transport equation is 6-variant Partial Differential Equation (PDE), which is hard to be solved by either theoretical or numerical approach. Moreover, the conditional expectations $\left\langle -\frac{\partial \tau_{ij}}{\partial x_i} + \frac{\partial p'}{\partial x_j} \middle| \underline{V}, \underline{\psi} \right\rangle$ and $\left\langle \frac{\partial J_i^\alpha}{\partial x_i} \middle| \underline{V}, \underline{\psi} \right\rangle$ are unclosed terms remaining to be modelled. As a result, a direct way of PDF transport equation solution is not practical.

To bypass the above problem, PDF method further derives a stochastic particle system following a well-established random process, which obeys the joint velocity-component PDF transport equation in concern of expectation. Therefore, by implementing a Monte-Carlo like simulation approach of large enough number particles, which follow the well-designed stochastic process, the joint PDF of velocity and component can be solved, as shown in **Figure 24**. Then engineering concerned values like averaged velocity, component or others can be further calculated by integrate over the sample space.

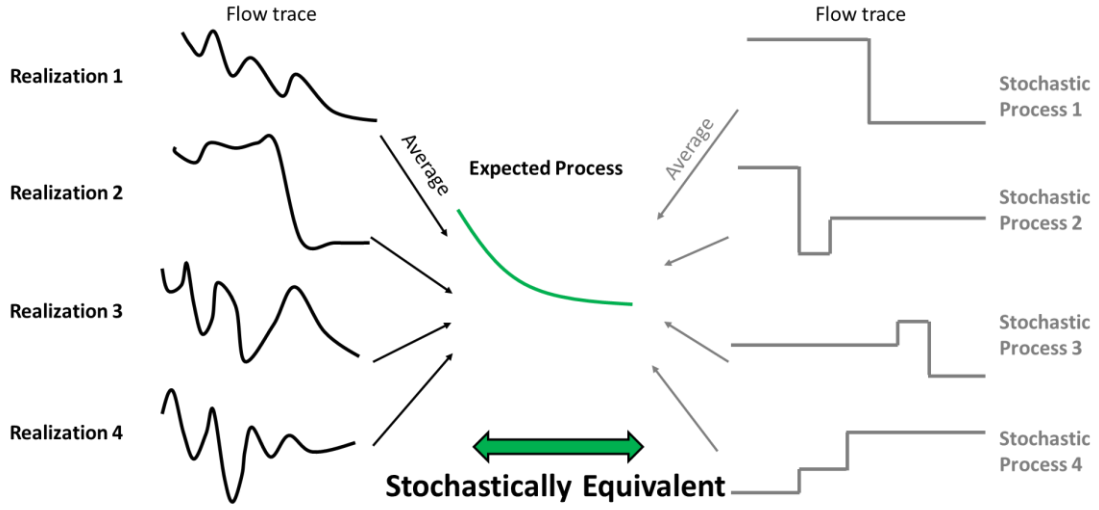

Figure 24 Probability Density Function approach

The stochastic process of the stochastic particles requires special treatments. In PDF method, two processes are used, Poisson Process and Diffusion Process. Poisson process is a random process which will stay unchanged or make a jump following Poisson distribution. Diffusion process is combined by a deterministic process and a Wiener process, which is defined as,

$$\Delta_{\delta t} W_i = W_{t+\delta t} - W_t, \tag{2.38}$$

and W_t is defined as,

$$W_t(t = t_n) = (\delta t)^{1/2} \sum_{i=1}^{n} \xi_i, \tag{2.39}$$

where ξ_i donates an independent standardized normal random variable with zero mean and unity variant.

To solve the joint velocity-component PDF transport equation, Pope provides a stochastic Lagrangian particle system following a 3-step process.

In Step 1, a stochastic process is constructed as way to simulate all the effects in turbulence except

the scalar diffusion and averaged pressure influence, which is

$$\Delta_{\delta t} U_i^* = G_{ij}\left[U_j^* - \widetilde{U}_j\right]\delta t + (C_0\varepsilon)^{1/2}\Delta_{\delta t} W_i, \tag{2.40}$$

$$\Delta_{\delta t}\phi_\alpha^* = S_\alpha\left(\underline{\phi}^*\right)\delta t, \tag{2.41}$$

$$\Delta_{\delta t} x_i^* = 0, \tag{2.42}$$

where G_{ij} is the coefficient to describe the anisotropic rate of turbulence and C_0 is the decay rate coefficient.

In step 2, the turbulent mixing of the scalar will be considered, which follows a Stochastic Mixing model

Each of N particle selected in Stochastic Mixing model got a probability,

$$C_\phi \delta t/\tau, \tag{2.43}$$

and a pair of the chosen particles being mixed got a probability,

$$C_\phi N \delta t/\tau, \tag{2.44}$$

where C_ϕ is a scalar mixing coefficient.

Then the scalars of the two particles will be exchanged following,

$$\underline{\phi}^{*(p)}(t+\delta t) = \underline{\phi}^{*(q)}(t+\delta t) = \frac{1}{2}\left[\underline{\phi}^{*(p)}(t) + \underline{\phi}^{*(p)}(t)\right] \tag{2.45}$$

In step 3, the convection and mean pressure gradient will be considered. The evolution equation can be derived as,

$$\frac{d\underline{U}^*}{dt} = -\frac{1}{\rho\left(\underline{\phi}^*(t)\right)}\nabla\langle p\rangle|_{\underline{x}^*(t)}, \tag{2.46}$$

$$\frac{d\underline{\phi}^*}{dt} = 0, \tag{2.47}$$

$$\frac{d\underline{x}^*}{dt} = \underline{U}^*(t), \tag{2.48}$$

Owing to the coupling of the variables and stability problem, the above process needs to further split into a 5 sub-step scheme to solve, which is even complicated. More details about the solution routine of PDF method can be found in [132].

Based on the review of previous studies, it can be concluded:

PDF method avoids the closure problem in statistics-based methods, by providing a stochastic particle system equivalent to the joint velocity-component PDF transport equation. Generally, PDF method doesn't require assumption and modeling of certain turbulent scales, which gives a better performance on fitting general problems compared with RANS and LES. In practical numerical simulation, PDF can be handled on a regular level size mesh. The stochastic particles follow simple stochastic processes, which cost less computer resource compared with detailed simulation in DNS. Especially, it should be noticed that PDF method is natural compatible with quantum computing [134], which makes it potential when next age of computer comes.

However, native PDF method shows its limit on engineering application in practice. As shown above, PDF method realization requires sophisticated physical mechanisms and mathematical tools on solution, which refer to the details beyond the scope of nuclear engineering on turbulence. The Lagrangian particle system will bring into the tracking problem as shown in Section 2.1.1. Furthermore, even the original solution algorithm on a simple problem will require for 3 steps and 5 sub-steps on dealing one stochastic particle. Considering the complex coupling among the

nuclear power plant simulation codes, the further extension of PDF method in the CFD module will produce additional difficulty on coding and debugging.
Therefore, PDF method has never been extended to engineering level problem, which only stay in academic area on studying turbulence mechanism.

2.2.4 Discussion of methodology choice in nuclear containment spray

Among the four methods, two categories can be introduced, the statistics-based and probability-based. The statistics-based methods include DNS, LES and RANS. DNS directly resolves all the scales in the flow, with detailed flow field information fetched. LES filters out the small dissipation eddies, while only keep large eddies to simulate. RANS averages over all the scales, leaving only one artificial averaged scale to resolve. On the opposite, the probability-based PDF method puts the Navier-Stokes Equations into probability space, and then solve the problem with a stochastic equivalent particle system. A detailed summary and comparison have been shown in Table 5.
Though not hard in modeling and coding, DNS and LES both relies a lot on the computing ability, which is far beyond the bearing of engineering design. PDF method shows a computing-friendly characteristic, but the sophistical derivation and realization restricts its extension on engineering application. At last, with low calculation amount and ease on practice, RANS family method remains as the best candidate for large-scale engineering applications like nuclear containment.
Though PDF approach shows its inconvenience on joint velocity-component coupling in turbulence, the method has shown its advantage on handling the unclosed terms of momentum equation produced by turbulent non-linear effect. It is therefore a routine to partly solve the turbulent transport problem of passive scalar, which includes non-linear convection and non-linear source term. The topic will be further discussed in Chapter 3.

Table 5 Summary of the turbulence models

Name	Strategy	Eddy Resolution	Calculation Amount	Coding Difficulty
RANS	Average	Single scale	Low	Easy
LES	Filter	Large eddies	High	Medium
DNS	Direct Resolution	All scales	Huge	Easy
PDF	Stochastically Equivalence	All scales	Medium	Hard

2.3 Inter-phase modeling

Phase-to-phase interaction is one special feature of the two-phase flow. Concerning it is unpractical to analytically solve the problem, the experimental-based modeling is always implemented instead, on mass, momentum and heat exchange. In nuclear containment simulation, the inter-phase modeling is the key component on predicting the cooling effect, as mass and energy transfer are the dominant processes during spray cooling.

2.3.1 Mass interaction

During the spray cooling process, the mass interaction can be divided into two parts: the material diffusion part and the phase change part. The phase change will be further discussed later in the following section. This section mainly focuses on the material diffusion part.

Under the assumption of a gas film between the liquid droplet and gas atmosphere, the steam vapor gas film is always under the saturation condition.

Certain amount of liquid phase will be turned into gas phase owing to the phase change. The mechanism-based simulation of phase change process requires the modeling scale down to the level of the droplet shape curvature and roughness, which far beyond the ability of scientific calculation and the need of engineering application. Therefore, in nuclear containment spray cooling process, experimental based models are widely used instead.

In the Eulerian framework, the mass interaction model can be summarized as [135],

$$\dot{m} = \rho \frac{6 \cdot \alpha \cdot \mathrm{Sh}}{d^2} \mu_m \left(Y_f - Y\right), \tag{2.49}$$

where μ_m is the mass diffusion coefficient, Y_f is the mass fraction of certain material at the gas film, Y is the mass fraction of certain material on gas side or liquid side.

The mass diffusion coefficient μ_m can be modelled as,

$$\mu_m = \frac{\alpha_{Thermo}}{\rho \cdot Le}, \tag{2.50}$$

where α_{Thermo} is the thermal diffusivity of certain material, ρ is the density and Le is the Lewis number,

$$Le = \frac{\kappa}{\rho C_p \mu}, \tag{2.51}$$

where κ is the thermal conductivity, C_p is the specific heat capacity, and μ is the viscous diffusion coefficient. Normally Lewis number is assumed to be unity.

Sh is the Sherwood number, which is the key parameter in mass interaction modeling. One commonly used model of Sherwood number is given by Frossling [136],

$$\mathrm{Sh} = 2 + 0.552 \mathrm{Re}^{\frac{1}{2}} \mathrm{Pr}^{\frac{1}{3}}, \tag{2.52}$$

Where Re is the Reynolds number and Pr is the Prandtl number.

2.3.2 Momentum interaction

Owing to the different mass and velocity carried by the two phases, there exist certain amount of momentum interaction between the liquid phase and gas phase. Owing to the difficulty of resolving droplet shape, the friction effect between the droplets and atmosphere is modelled by experimental correlation rather than real-time simulation.

The momentum interaction effects include drag force, lift force and virtual volume force. The lift force and virtual volume force are responsible for the effects in weak inertial flow, which is suitable for the bubble flow. During spray process, normally only drag effect is considered in the modeling.

By experimentally modeling of the friction force between the two phases, the drag force can be

modelled by

$$F^{drag} = -\frac{3}{4}\frac{D_{drag}\rho_g\alpha_l}{d}\left|U_g - U_l\right|\left(U_g - U_l\right), \tag{2.53}$$

where D_{drag} is the drag coefficient and d is the diameter.

The drag coefficient D_{drag} can be modelled by Schiller & Naumann model [137],

$$D_{drag} = \begin{cases} 0.44, & Re > 1000, \\ \frac{24}{Re}[1 + 0.15Re^{0.687}], & Re < 1000, \end{cases} \tag{2.54}$$

There also exist some other models like White model [138], Ishii & Zuber model [139], Dalla Valle model [140] and Moore model [141]. Following previous works on spray modeling, the commonly used Schiller & Naumann model is implemented in this work.

2.3.3 Energy interaction

The energy interaction is the most important effect during nuclear containment spray simulation, as it's used to cool down the atmosphere and depressurize the high pressure to safe level. The energy exchange between gas phase and liquid phase can be divided into two parts: convective heat transfer and phase change.

Traditionally, the energy interaction between gas phase and liquid phase can be modelled as

$$\dot{h}_l = \frac{6 \cdot \alpha_l \cdot \kappa \cdot \mathrm{Nu}}{d^2}\left(T_g - T_l\right) - \dot{m}h_l + \dot{m}L, \tag{2.55}$$

$$\dot{h}_g = \frac{6 \cdot \alpha_l \cdot \kappa \cdot \mathrm{Nu}}{d^2}\left(T_l - T_g\right) + \dot{m}h_g, \tag{2.56}$$

Where κ is the heat conductivity coefficient, Nu is the Nusselt number, $\dot{m}$ is the mass amount of evaporated liquid and L is the latent heat released from phase change.

The above model includes the assumption of the whole droplet sharing one common temperature and heat transfer directly happening between the droplet and the atmosphere, which lacks enough accuracy when large amount of heat exchange happened during evaporation. Therefore, the energy interaction model is further modified by

$$\dot{h}_l = \frac{6 \cdot \alpha_l \cdot \kappa \cdot \mathrm{Nu}}{d^2}\left(T_f - T_l\right), \tag{2.57}$$

$$\dot{h}_g = \frac{6 \cdot \alpha_l \cdot \kappa \cdot \mathrm{Nu}}{d^2}\left(T_g - T_f\right) + \dot{m}L, \tag{2.58}$$

where T_f stands for the temperature of the gas film between the gas phase and liquid phase.

In the new model, there assumed to be a gas film existing between the hot air and the water droplet, which is always under the saturated condition. During the evaporation process, the heat transfer will be balanced among the hot air, the water droplet and the gas film.

Therefore, the convective heat transfer will be modelled a gas-to-interface and interface-to-liquid two-stage process instead of a direct heat convection between gas and liquid.

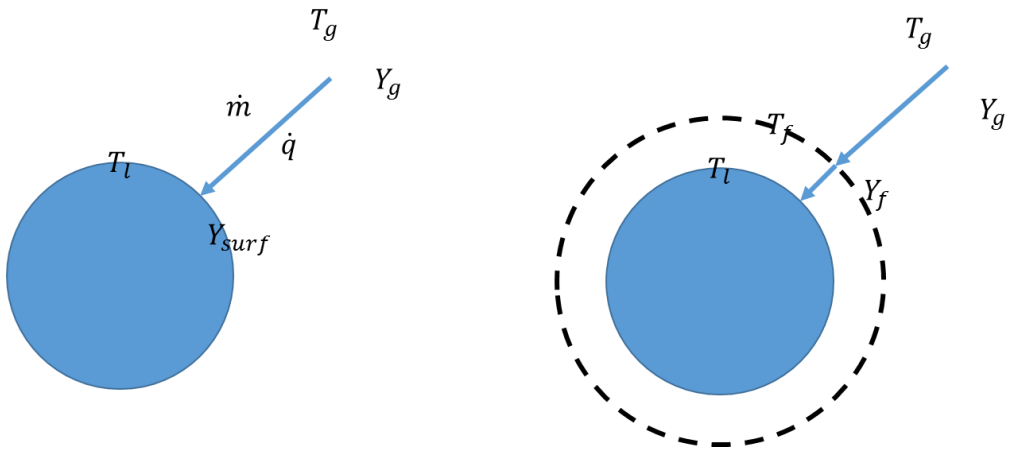

Figure 25 Comparison between direct inter-phase heat exchange model and gas-film-based heat exchange model

The Nusselt number is modelled by Ranz-Marshall model,

$$Nu = 2 + 0.6\mathrm{Re}^{\frac{1}{2}}\mathrm{Pr}^{\frac{1}{3}}, \tag{2.59}$$

The temperature and mass fraction of the gas film T_f and Y_f will be further modelled by phase change model in the following section.

2.3.4 droplet-droplet interaction

The droplet-droplet interaction in the liquid phase is decided by the spray type. The spray process can be divided into dense spray and dilute spray according to the volume fraction of the droplets. The dense spray mainly refers to the spray process, during which the liquid phase occupies the volume fraction more than 40%. The atomization process, droplet-droplet collision and coalescence are considered. The dilute spray refers to the spray process, during which liquid phase occupies less than 2% of the volume fraction. The droplets are widespread distributed and located far from each other. The droplet-droplet interaction can be neglected in dilute spray.

The dense spray is mainly used for the small-scale problems where the nozzle effect got a strong influence, like diesel engine. In nuclear containment spray process, the vessel volume is much larger than the nozzle. Therefore, in most of the spatial location in the containment, the liquid phase shares limited volume and spray droplets are widespread distributed. Owing to such characteristics, the studies in this work will implement the dilute spray model and neglect the droplet-droplet interactions.

2.4 Thermophysical modeling

Thermophysical models decide the physical properties during the energy exchange between the spray droplets and the surrounding atmosphere. In this section, the modeling of the phase change during evaporation, heat capacity and equation of state will be discussed

2.4.1 phase change modeling

2.4.1.1 Evaporation model

During the evaporation process, liquid phase water consists turning into the gas film, which makes water vapor component staying always as saturated in the gas film mixture. Following the saturation model, the mass fraction of water vapor component in the mixture can be modelled by

$$Y_f = \frac{W_{H2O}}{W \cdot p} p_{satur e}, \tag{2.60}$$

Where W stands for the mixture Mole mass weigh, p stands for the mixture pressure, W_{H2O} stands for the water vapor Mole mass weigh and $p_{satur e}$ stands for the saturated pressure at the gas film temperature.

The gas film temperature can be calculated by the balance of heat among gas phase, liquid phase and the gas film itself, which expresses as

$$T_f = \frac{K_l T_l + K_g T_g - \dot{m} L}{K_l + K_g}, \tag{2.61}$$

Where K_l stands for the heat transfer coefficient from liquid side and K_g stands for heat transfer coefficient from gas side. They could both be derived according to the models listed in Section 2.4.3.

The calculation of the gas film temperature T_f and the two phases' temperatures T_l and T_g will be calculation through a Newton iteration process between the coupling of the energy interaction model and phase change model.

2.4.1.2 Saturation model

Saturation refers to the status when the dynamic equilibrium between evaporation and condensation is reached. With the saturated pressure modelled by the saturation model, the mass fraction of the component can be further calculated according to Dalton's law.

The mass transfer amount of steam vapor from gas film to hot atmosphere is the key value in the whole spray cooling process, which is mainly decided by the mass fraction of steam vapor in the gas film mixture.

Two models are commonly used, the Clausius-Clapeyron Equation and Arden Buck Equation:

1. Clausius-Clapeyron Equation

Assume material got boiling point of T_B at 1 atm

$$p_{sat} = e^{\left[\frac{L_V(T)}{R/W}\left(\frac{1}{T_B} - \frac{1}{T}\right)\right]} \tag{2.62}$$

$$Y_f = \frac{W * p_{sat}}{W_{mix} * p_g} \tag{2.63}$$

2. Arden Buck Equation

The saturated pressure of water phase at certain temperature can be got following Arden Buck equation [143],

$$p_{sature} = Ae^{(T_f - 273.15)\frac{B(T_f - 273.15)}{C(D + (T_f - 273.15))}} \quad (2.64)$$

Where A, B, C and D are four parameters measured by Buck.

2.4.2 Thermodynamic model

The thermodynamic model describes how the specific heat capacity changes according to temperature. The models used in this work are constant model and JANAF model.

2.4.2.1 Constant

For the material whose physical property doesn't change too much, it is reasonable to assume the specific heat capacity keeps constant in a certain range of temperature. The way by specifying a constant value as the specific heat is used in this work for the liquid phase.

2.4.2.2 JANAF

Based on numerous experimental studies, it has been shown that the specific heat capacity may change rapidly for gas material over the temperature change, especially for large molecular material and high temperature condition. Therefore, a more precise model is derived, by linking specific heat to temperature in a polynomial function. To provide a more comprehensive model for calculating specific heat of certain material during chemical reaction, NASA [144] has done a lot of studies and set up JANAF (Joint Army-Navy-NASA-Air Force) table to provide the coefficients in the expression,

$$c_p(T) = R(a_1 + a_2 T + a_3 T^2 + a_4 T^3 + a_5 T^4), \quad (2.65)$$

where R is the gas constant, T is the temperature and a_1, a_2, a_3, a_4, a_5 are the coefficients provided for every materials in the JANAF table. Considering the temperature is not far from the saturation status, the gas phase physical property is changing critically, which is better fitted by JANAF model.

2.4.3 Equation of State

Equation of state refers to the relationship among the thermo physical variables like pressure, density and temperature. It is used in CFD study as the bridge to link temperature change to pressure. The equation of state models used in this work are perfect gas and perfect fluid.
During the physical process, the properties of physical materials can go through dramatic changes, which makes physical property modeling an important issue in spray cooling study.

2.4.3.1 Perfect gas

By assuming gas molecular as rigid particles with no volume and neglecting the interaction effects

between each other, the ideal gas model is set up. By taking such assumption, the density can be calculated through,

$$\rho = \frac{p}{RT}, \tag{2.66}$$

where p is the pressure, T is the temperature and R is the gas constant.
In this work, the perfect gas model is chosen as the equation of state model for gas phase.

2.4.3.2 Perfect fluid

The perfect fluid model may be considered as an extension of perfect gas model to fluid material. In perfect fluid model, the fluid material density is assumed to change from a certain value, while keeps on increasing following the promotion of pressure over temperature, which can be written as,

$$\rho = \frac{p}{RT} + \rho_0, \tag{2.67}$$

where ρ_0 is the reference density.
Normally, the reference density is relatively much larger than the density change triggered by pressure and temperature change, which matches the common sense that fluid material is nearly incompressible.
In this work, the perfect fluid model is chosen as the equation of state model for liquid phase.

2.5 Numerical solution of two-phase model

With all the physical processes well modelled in the previous sections, the way on numerically solving the governing equations remain as the last issue.
As shown in Section 2.1, both the Lagrangian-based approach and the Eulerian-based approach choose to model the continuous phase as Eulerian field. In Eulerian approach, the spray droplets are again modelled as Eulerian field through a volume fraction equation. In this section, the numerical solution algorithms of the single-phase problem will be first reviewed, then the solution for two phase flow will be further introduced.

2.5.1 Numerical solution of the single-phase problem

Owing to the way on dealing with mass conservative equation, the solution algorithms of single-phase problem can be divided into two families: Density-based and Pressure-based.

2.5.1.1 Pressure-based algorithm

The pressure and velocity are coupled though the incompressibility constraint, which results in a saddle-point problem when applying a coupled algorithm on solving the partial differential equation group. Therefore, the Pressure-based segregated algorithm is always used instead.

1. Theoretical derivation of projection method

The Pressure-based algorithms can be all treated as the mutation of the classic projection method, which is given by [145] in 1967. In 1970s, the computer efficiency and memory capacity are hard to handle large-scale matrix iteration, which makes direct coupling solution of PDEs near impossible. The projection method tries to solve the velocity and pressure separately by decoupling the incompressible Navier-Stokes equations, which provides an affordable way on flow simulation problem.

In a physical viewpoint, the way on decoupling the incompressible equations comes from the decomposition of velocity vector. A certain vector can be split into a solenoidal part and an irrotational part by Helmholtz–Hodge Decomposition, as

$$\boldsymbol{v} = \boldsymbol{v_{sol}} + \boldsymbol{v_{irrot}} \tag{2.68}$$

Assume a certain potential scalar function related to the irrotational part as

$$\boldsymbol{v_{irrot}} = \nabla\phi \tag{2.69}$$

The decomposition can be further expressed as

$$\boldsymbol{v} = \boldsymbol{v_{sol}} + \nabla\phi \tag{2.70}$$

Owing to the characteristics of the divergence-free part v_{sol}, by applying divergence operator on the decomposition equation, it becomes,

$$\nabla^2\phi = \nabla \cdot \boldsymbol{v} \tag{2.71}$$

which is a Poisson equation of the scalar ϕ.

Therefore, if the certain vector $\boldsymbol{v}$ is already known or initially guessed, the scalar can be solved from equation 2.76. Then the solenoidal part $\boldsymbol{v_{sol}}$ of the vector $\boldsymbol{v}$ can be got by,

$$\boldsymbol{v_{sol}} = \boldsymbol{v} - \nabla\phi \tag{2.72}$$

Such theory illuminates the possible solution routine of velocity, as velocity follows the divergence-free property owing to the continuous equation and the pressure gradient can be treated the potential scalar on constructing irrotational part, as shown in

$$\nabla \cdot \mathrm{U} = 0 \tag{2.73}$$

$$\frac{\partial U}{\partial t} + U \cdot \nabla U = -\nabla p + \frac{1}{Re}\nabla^2 U \tag{2.74}$$

By firstly setting a guessed velocity U^* and follow the way in deriving equation 2.71 on 2.74, the pressure Poisson equation can be got, the pressure can be solved. Then by using equation 2.72, U^* will be updated to keep mass conservation.

2. Numerical linear algebra derivation of projection method

Following a detailed discussion in [146], the projection method can be understood as a LU decomposition of the coupled coefficient matrix. By applying certain numerical scheme on the transient, convection, gradient and Laplacian terms, the discrete matrix system can be derived as

$$\begin{bmatrix} A & G \\ D & 0 \end{bmatrix} \begin{pmatrix} U^{n+1} \\ p \end{pmatrix} = \begin{pmatrix} r^n \\ 0 \end{pmatrix} + \begin{pmatrix} bc_1 \\ bc_2 \end{pmatrix} \tag{2.75}$$

where A stands for the discrete coefficient from the transient and Laplacian operators. G stands for the discrete coefficient from gradient operator and D stands for the discrete coefficient from divergence operator. r^n stands for the contribution of explicit parts by latest time step. bc_1 and bc_2 stands for the boundary conditions for momentum equation and continuous equation.

If Crank-Nicolson scheme [147] is implemented on time discretion and explicit second-order Adams-Bashforth scheme [148] is implemented on the convection discretion. A can be further expressed as

$$\mathrm{A} = \frac{1}{\Delta t} M - \frac{1}{2} L \tag{2.76}$$

where M stands for time discrete coefficient and L stands for the viscous term discrete coefficient.

In addition, the gradient and divergence operators are one pair of symmetric operators, which makes $\mathrm{D} = -G^T$.

By applying LU decomposition on the discrete coefficient matrix, it can be expressed as,

$$\begin{bmatrix} A & G \\ D & 0 \end{bmatrix} = \begin{bmatrix} A & 0 \\ -G^T & G^T A^{-1} G \end{bmatrix} \begin{bmatrix} I & A^{-1} G \\ 0 & I \end{bmatrix} \tag{2.77}$$

By further extending the coefficient matrix A into Nth order Taylor series, it can be expressed as,

$$A^{-1} \cong B^N = \Delta t M^{-1} + \frac{\Delta t^2}{2} (M^{-1} L) M^{-1} + \frac{\Delta t^N}{2^{N-1}} (M^{-1} L)^{N-1} M^{-1} \tag{2.78}$$

If neglect the truncation error in B^N, the discrete system can be rewritten as,

$$\begin{bmatrix} A & 0 \\ -G^T & G^T B^N G \end{bmatrix} \begin{bmatrix} I & B^N G \\ 0 & I \end{bmatrix} \begin{pmatrix} U^{n+1} \\ p \end{pmatrix} = \begin{pmatrix} r^n \\ 0 \end{pmatrix} + \begin{pmatrix} bc_1 \\ bc_2 \end{pmatrix} \tag{2.79}$$

The LU decomposition provides the possibility to solve the problem by 3 segregated fractional steps, which successfully decouples the velocity-pressure coupling problem.

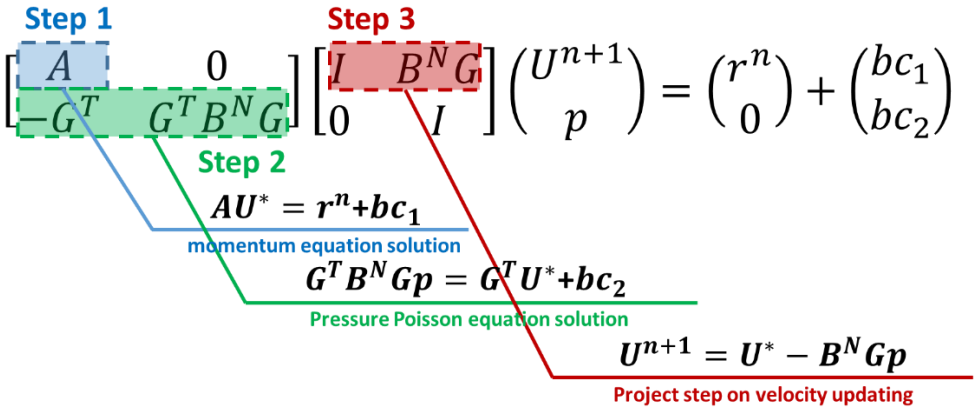

Figure 26 The solution routine of projection algorithm

3. Simple family methods and its application on collocated grid

One of the most famous extension of Pressure-based algorithm is the SIMPLE (Semi-Implicit Method for Pressure Linked Equations) method [149] and its transient mutation, PISO (Pressure-Implicit with Splitting of Operators) algorithm [150]. However, the original SIMPLE family methods heavily rely on the staggered grid [151], as way to overcome the odd-even decoupling during discretion. The staggered mesh calls for differential storage locations for pressure and velocity component, which makes data structure complicated and interpolation frequent to use.

By using Rhie-Chow interpolation [152] and combine SIMPLE and PISO, a collocated-grid based Pressure-based algorithm is given by Jasak in [153], which is widely applied in OpenFOAM on all pressure-based solvers.

First by implementing the full implicit scheme of time, the momentum equation can be derived into a semi discrete form as,

$$a_p U_p + \sum_n a_n U_n = -\nabla p, \tag{2.80}$$

Where U_p and a_p stand for the velocity of the mesh central point and the diagonal discrete coefficient related to it, U_n and a_n stand for the velocity of the mesh neighbor points and the off-diagonal discrete coefficients related to them. p stands for the pressure.
The equation can be re-written as

$$U_p = \frac{H(U)}{a_p} - \frac{\nabla p}{a_p}, \tag{2.81}$$

where $H(U) = -\sum_n a_n U_n + \frac{U_p^0}{\Delta t}$.

Different from traditional projection method, Jasak takes advantage of the discrete form of the continuous equation rather than the exact form on constructing the pressure equation.
By discretizing continuous equation, it can be derived as,

$$\sum_i U_f \cdot S_i = 0, \tag{2.82}$$

where U_f stands for the velocity at the mesh cell surface, and S_i stands for the surface area vector.
By interpolating from the neighbor centers, the surface velocity can be derived as,

$$U_f = \left(\frac{H(U)}{a_p}\right)_f - \frac{(\nabla p)_f}{(a_p)_f}, \tag{2.83}$$

Combine equation 2.82 and 2.83, the pressure equation can be derived as,

$$\sum_i \left(\frac{1}{a_p}\nabla p\right)_f \cdot S_i = \sum_i \left(\frac{H(U)}{a_p}\right)_f \cdot S_i, \tag{2.84}$$

The equation of 2.81 and 2.84 will be kept iterated until the difference of velocity and pressure have been decreased to a certain criterion.
A so-called relax factor ω can be used onto the iteration process, which add

$$U^{k+1} = \omega U^{k+1} + (1-\omega)U^k, \tag{2.85}$$

$$p^{k+1} = \omega p^{k+1} + (1-\omega)p^k, \tag{2.86}$$

at the last step of each iterative loop. Relax factor can mathematically enhance the pivot dominate position, as way to improve the convergence speed of the calculation.

2.5.1.2 Density-based algorithm

Density-based algorithm [154][155] directly targets on solving the density, while the pressure change will be further derived by the density. The method was first set up in aerodynamics area, which tried to solve compressible flow problem with density as a variable of both time and space,

$$\frac{\partial \rho}{\partial t} + \frac{\partial \rho U_i}{\partial x_i} = 0 \tag{2.87}$$

Owing to the compressibility, the density is related to pressure according to equation of state. Therefore, the solution process can be easily discretized by both explicit scheme and implicit scheme.
Density-based algorithm is strong on solving compressible flow problem. By using high-resolution schemes [156] [157], special phenomenon like shock wave can be successfully captured. However, when comes to the incompressible flow, density and pressure are not related,

which makes the Density-based algorithm not able to directly implement. Though there's methods like artificial compressibility approach [158], the application of Density-based algorithm into incompressible problem is still not common.

2.5.1.3 Fully-coupled algorithm

Recently, with the fast development of CPU ability and memory content, the fully-coupled algorithm has become possible. Some recent works [159] [160] have shown the exploration of the approach on incompressible flow.

Traditionally, under the restriction of memory content, it is hard to store the huge coefficient matrix of the continuous-momentum PDE system, which makes the decoupled approach referred in the previous section popular in solving incompressible problem.

The form of the linear system can be written as,

$$[J]\begin{pmatrix} U^{n+1} \\ p \end{pmatrix} = \begin{pmatrix} r^n \\ 0 \end{pmatrix} + \begin{pmatrix} bc_1 \\ bc_2 \end{pmatrix} \tag{2.88}$$

where J is the Jacobi coefficient matrix, similar to the form shown in Equation 2.75.

Instead of a Picard iteration like procedure between momentum equation and the pressure equation, the method tries to directly solving the system by implementing the non-linear methods like Newton iteration.

The fully-coupled algorithm provides synchronous of velocity and pressure, which gives a more robust performance on convergence. In addition, large time step is possible owing to the fully implicit characteristics. However, though able to handle the problem in modern computer, the calculation efficiency is still far from fast prediction requirement in engineering applications. Furthermore, the saddle point problem needs extra treatment like particular pre-condition methods. As a conclusion, the fully-coupled algorithm still stays at an early stage, which got a certain distance away from practical application in industry.

2.5.2 Numerical solution of the two-phase problem

By using Eulerian approach on modeling the discrete phase, the spray process becomes a Euler-Euler system problem. In such system, the governing equations of the two phases will be coupled through an addition volume fraction equation. Therefore, the solution of two-phase system can be extended from the approach of single-phase treatment.

The solution algorithm of the system will follow an updated version of projection method:

Step 1 Solution of volume fraction

The governing equation of the liquid phase volume fraction can be written as,

$$\frac{\partial(\alpha_l \rho_l)}{\partial t} + \nabla \cdot (\alpha_l \rho_l U_l) = 0, \tag{2.89}$$

where α_l, ρ_l and U_l stand for volume fraction, density and velocity of the liquid phase.

The above equation is equivalent to

$$\frac{\partial \alpha_l}{\partial t} + \nabla \cdot (\alpha_l U_l) + \frac{\alpha_l}{\rho_l}\frac{d_l \rho_l}{dt} = 0, \tag{2.90}$$

where the operator $\frac{d_l}{dt}$ is defined as,

$$\frac{d_l}{dt} = \frac{\partial}{\partial t} + U_l \cdot \nabla \tag{2.91}$$

By further reforming the equation, it can be written as,

$$\frac{\partial \alpha_l}{\partial t} + \nabla \cdot (U\alpha_l) + \nabla \cdot \left(U_r \alpha_l (1-\alpha_l)\right) + \frac{\alpha_l}{\rho_l}\frac{d_l \rho_l}{dt} = 0, \tag{2.92}$$

where U stands for the mixture velocity and U_r stands for the relative velocity between the two phases, which are defined as,

$$\mathrm{U} = \alpha_g U_g + \alpha_l U_l, \tag{2.93}$$

$$U_r = U_l - U_g \tag{2.94}$$

The equation of gas phase volume fraction can be modelled following the same approach, which is derived as,

$$\frac{\partial \alpha_g}{\partial t} + \nabla \cdot \left(U\alpha_g\right) + \nabla \cdot \left(-U_r \alpha_g \left(1-\alpha_g\right)\right) + \frac{\alpha_g}{\rho_g}\frac{d_g \rho_g}{dt} = 0 \tag{2.95}$$

By summing the above two equations, we get,

$$\nabla \cdot \mathrm{U} = -\frac{\alpha_g}{\rho_g}\frac{d_g \rho_g}{dt} - \frac{\alpha_l}{\rho_l}\frac{d_l \rho_l}{dt} \tag{2.96}$$

By put Equation 2.96 back into Equation 2.95, the final expression for liquid volume fraction equation is constructed, which is,

$$\frac{\partial \alpha_l}{\partial t} + (U \cdot \nabla)\alpha_l + \nabla \cdot (U_r(1-\alpha_l)\alpha_l) = (1-\alpha_l)\left(\frac{1}{\rho_g}\frac{d_g \rho_g}{dt} - \frac{1}{\rho_l}\frac{d_l \rho_l}{dt}\right)\alpha_l \tag{2.97}$$

By integrating over the whole controlling volume and use finite volume method upon the equation, the discrete form of the volume fraction equation can be derived as,

$$\begin{aligned} \frac{1}{V}\frac{[\alpha_l]^{n+1} - [\alpha_l]^n}{\Delta t} &+ \sum U_f S_f \, [\alpha]_{convect\ scheme} \\ &+ \sum (1-\alpha_l)_f U_{rf} S_f \, [\alpha]_{convect\ scheme} \\ &= \frac{1}{V}(1-\alpha_l)\left(\frac{1}{\rho_g}\frac{d_g \rho_g}{dt} - \frac{1}{\rho_l}\frac{d_l \rho_l}{dt}\right)[\alpha_l] + \frac{\sum U_f S_f}{V}[\alpha_l] \end{aligned} \tag{2.98}$$

where $[\cdot]$ stands for the variable treated as unknown and going to be solved. $[\cdot]_{convect\ scheme}$ stands for the discrete form of the variable following certain convection scheme. $(\cdot)_f$ stands for the interpolation of the physical value from volume center to the face center.

Step 2 Solution of the component in gas mixture

$$\frac{\partial(\rho_g \alpha_g Y_i)}{\partial t} + \frac{\partial(\rho_g \alpha_g U_g Y_i)}{\partial x_j} = \frac{\mu_t}{Sc}\nabla^2 Y_i + \dot{m} \tag{2.99}$$

Following the way of evaporation process modeling in Section 2.5.1, $\dot{m}$ will be further expanded as,

$$\dot{m} = \rho_1 * \mathrm{K}_m * \mu_m * \left(Y_f - Y_i\right) \tag{2.100}$$

By finite volume method on discretion, the component equation can be derived as,

$$\frac{\rho_g^k \alpha_g^k [Y]_i^{k+1} - \rho_g^n \alpha_g^n [Y]_i^n}{\Delta t} + \frac{1}{V}\sum \rho_f \alpha_f U_f S_f \, [Y]_{convection\ scheme}^{k+1}$$
$$= \frac{1}{V}\sum \frac{\mu_t}{Sc_f} \nabla [Y]^{k+1}{}_f + \rho_1 * \mathrm{K}_m * \mu_m * \left(Y_f - [Y]^{k+1}\right) \quad (2.101)$$
$$+ \left(\frac{\partial \rho_g}{\partial t} + \frac{\partial (\rho_g U_g)}{\partial x_j}\right)[Y]^{k+1}$$

Then following the saturation model, the droplet gas film component will be updated by,

$$Y_f = \frac{W * p_{sat}}{W_{mix} * p_g} \quad (2.102)$$

Step 3 Momentum solution

The governing equation of gas phase momentum can be written as,

$$\frac{\partial (\rho_g \alpha_g U_g)}{\partial t} + \frac{\partial (\rho_g \alpha_g U_g U_g)}{\partial x_j} = \nabla \cdot \left((\mu + \mu_t)(\nabla U + (\nabla U)^T)\right) + K_g U_g \quad (2.103)$$

where K_g is the coefficient modelled though interphase momentum interaction model as shown in Section 2.4.2, which can be expressed as,

$$K_g = 0.75 C_D \frac{\alpha_g \mu_g}{d^2} \quad (2.104)$$

By discretizing the above equation, the discrete form of momentum equation can be written as,

$$\frac{\rho_g^k \alpha_g^k [U_g]_i^{k+1} - \rho_g^n \alpha_g^n [U_g]_i^n}{\Delta t} + \frac{1}{V}\sum \rho_f \alpha_f U_{gf} S_f \, [U_g]_{convection\ scheme}^{k+1}$$
$$= \frac{1}{V}\sum (\mu + \mu_t)[U_g]_{lapacian\ scheme}^{k+1} + \mathrm{K}_g [U_g]^{k+1} \quad (2.105)$$

where U_{gf} is the gas phase velocity of the control volume surface. $[\cdot]_{lapacian\ scheme}$ stands for the discrete form of the variable following certain Lapalacian scheme.

By the same way, the discrete form of liquid phase momentum equation could also be derived, which will not be shown here.

Step 4 Energy solution

Concerning the latent heat will be released during the evaporation process. Enthalpy will be used instead of inner energy on solving the temperature change during spray cooling.

The governing equation of gas phase enthalpy can be written as,

$$\frac{\partial (\rho_g \alpha_g h_g)}{\partial t} + \frac{\partial (\rho_g \alpha_g U_g h_g)}{\partial x_j} = \frac{\alpha_h}{Pr_t} \nabla^2 (\alpha_g h_g) + \dot{h} \quad (2.106)$$

where $\dot{h}$ is the heat source from latent heat released during phase change and inter-phase heat exchange.

By discretizing the above equation, the discrete form of energy equation can be written as,

$$\frac{\rho_g^k \alpha_g^k [h_g]_i^{k+1} - \rho_g^n \alpha_g^n [h_g]_i^n}{\Delta t} + \frac{1}{V}\sum \rho_f \alpha_f U_{gf} S_f \, [h_g]_{convection\ scheme}^{k+1}$$
$$= \frac{1}{V}\sum \frac{\alpha_h}{Pr_t} \alpha_g [h_g]_{lapacian\ scheme}^{k+1} + \dot{h} \quad (2.107)$$

Here, the heat source $\dot{h}$ will be calculated by an explicit way,

$$\dot{h} = K_h (T_f - T_g) + \dot{m}\left(h(T_f) - h(T_g)\right) + \dot{m}\left(\frac{U_l^2}{2} - \frac{U_g^2}{2}\right) \quad (2.108)$$

where K_h is the heat transfer coefficient modelled as shown in Section 2.5.2. $h(T_f)$ and $h(T_g)$

stand separately for the enthalpy of the water vapor at the temperature of the gas film and the atmosphere mixture.

The discrete form of liquid phase energy equation and its heat source could also be derived in the same way, which will not be shown here.

After both gas phase and liquid phase enthalpy are got, the temperature of gas phase T_g and liquid phase T_l will also be updated as well. Then a further updating will be proceeded for the gas film temperature T_f through,

$$K_{hg}(T_g - T_f) + K_{hl}(T_l - T_f) = \dot{m}L, \tag{2.109}$$

where K_{hg} and K_{hl} are the modelled heat transfer coefficient of has phase and liquid phase. L is the latent heat of phase change, which is calculated by,

$$\mathrm{L} = \rho_g * \mathrm{K}_m * \mu_m * (Y_f - Y_g) * (h_{ag} - h_{al}) \tag{2.110}$$

where h_{ag} and h_{al} are the absolute enthalpy of gas phase and liquid phase.

Obviously, the controlling equation of T_f is non-linear. Here, a one-step Newton iteration is implemented on linearizing the problem, which is derived as,

$$T_f = \frac{K_{hg}(T_f - T_g) + K_{hl}(T_f - T_g) + \dot{m}L}{K_{hg} + K_{hl} + \frac{\partial L}{\partial T_f}} \tag{2.111}$$

Here the derivative of latent heat $\frac{\partial L}{\partial T_f}$ will be calculated according to the constant pressure heat capacity model as shown in Section 2.5.2.

The iteration loop will be kept proceeded from Step 1 to Step 3 until the difference of physical values between latest iteration k and this iteration $k+1$ has decreased to a certain criterion, similar to the traditional pressure correction method.

2.6 Summary

In this chapter, the two-phase flow modeling of spray has been widely discussed. Concerning the balance among calculation amount, coding difficulty and model precision, Eulerian approach has been chosen to model the discrete droplets in spray cooling process. Following, the mass, momentum and energy interaction models between gas phase and liquid phase are also discussed. The thermo-dynamical models for water droplet and atmosphere are listed. At last, the numerical solution algorithm of Eulerian two-phase model is discussed from both physical and mathematical angle.

3. Stochastic Field Method on modeling spray cooling process

In the previous chapter, the physical modeling of the spray process is discussed in detail. However, the interaction between turbulent fluctuation and spray droplets still remain to be modelled. In this chapter, the additional turbulence influence upon spray droplet transport and evaporation cooling will be studied. A Eulerian based branch of the PDF family methods, Stochastic Field Method, will be implemented to overcome the closure problem in turbulent scalar transport. With the contribution of the work in this chapter, the study of spray cooling modeling will be more comprehensive, which set up a solid fundamental of modeling for fine simulation in containment cooling.

3.1 Turbulent effect on scalar transport modeling

Scalar transport is an important topic of CFD analysis in multiple areas. In reactive flow, the chemical component dissolved at certain location is the key variable of the whole reaction process. In combustion, the mass fraction of the fuel in the mixture decides the ignition process. In multiphase flow, the volume fraction links closely to the performance of the discrete phase. The volume fraction of the bubbles will decide the flow pattern in the gas-liquid two-phase flow. The volume fraction of the solid particles will decide the total dynamics behavior of the gas-solid two-phase flow. The volume fraction of the spray droplets will decide the whole spray cooling process.

When combined with the turbulent effect, the scalar transport phenomenon will become even more complex. The passive scalar transport equation can be written as

$$\frac{\partial c}{\partial t} + \nabla \cdot (Uc) = \nabla \cdot (\gamma \nabla c) \tag{3.1}$$

where c is the scalar component carried by the flow and γ is the diffusion coefficient.

Under turbulent condition, the scalar component and the velocity can be written as

$$c = \langle c \rangle + c', \tag{3.2}$$

$$U = \langle U \rangle + u', \tag{3.3}$$

where $\langle c \rangle$ and $\langle U \rangle$ stand for the averaged component and velocity, c' and u' stand for the fluctuation part of them.

The product of the velocity and scalar in the convection term of equation 3.1 could bring in the turbulent closure problem similar to the momentum equation discussed in Section 2.2.

3.2 Discussion on turbulent fluctuation of scalar transport

Under turbulent condition, the scalar component carried by the flow will also get fluctuated characteristics, which are always mathematically written as equation 3.2.

However, the way of the expression requires further discussion. Traditionally the scalar

component fluctuation was believed to be the result of turbulent convection [161][162], which throws doubt on the above expression 3.2. Concerning the scalar fluctuation carried by the flow a result of the velocity fluctuation, the expression of transient scalar would be written as

$$c = \langle c \rangle + c'(u'), \tag{3.4}$$

where the fluctuation term of the scalar term is a function of velocity fluctuation u'. Instead of the equation 3.2, the fluctuation part of the scalar c' is not an independent random variable, but a function of the velocity fluctuation u'.

Under the new expression 3.4, the Reynolds averaged equation of the scalar component transport equation will be derived as

$$\frac{\partial \langle c \rangle}{\partial t} + \nabla \cdot (\langle U \rangle \langle c \rangle) - \nabla \cdot (\gamma \nabla \langle c \rangle) + \nabla \cdot (\langle c'(u')u' \rangle) = 0 \tag{3.5}$$

The unclosed term $\nabla \cdot (\langle c'(u')u' \rangle)$ now becomes a non-linear term of u', which will be even harder to deal with, as traditional hypothesis like Boussinesq eddy viscosity assumption can't be implemented any more.

Though a possible misunderstanding it could be, the new study has shown the traditional way of expressing scalar fluctuation like equation 3.2 has luckily hit on the right point. A recent study of Drivas and Eyink [163] has given a new explanation of scalar component fluctuation in turbulent flow. Owing to the new theory, turbulence in the flow is more like a trigger rather than the engine in scalar component fluctuation. The tiny stochastic perturbations resulted from molecular diffusivity will be amplified into a persistent fluctuation even after the initial perturbation vanished over certain time period. More works on this topic can be referred to [164][165][166]. Therefore, the fluctuation part of the scalar component is independent from the velocity fluctuation u', and can still be written as

$$c = \langle c \rangle + c', \tag{3.6}$$

Therefore, similar to the situation in momentum fluctuation modeling, one additional term like the Reynolds stress, $\nabla \cdot (\langle c'u' \rangle)$ remains to be modelled, as shown in the following equation,

$$\frac{\partial \langle c \rangle}{\partial t} + \nabla \cdot (\langle U \rangle \langle c \rangle) - \nabla \cdot (\gamma \nabla \langle c \rangle) + \nabla \cdot (\langle c'u' \rangle) = 0 \tag{3.7}$$

The additional term can be modelled though traditional statistics-based approach like RANS and LES, by taking the eddy viscosity assumption, the unclosed term $\nabla \cdot (\langle c'u' \rangle)$ can be modelled by

$$\nabla \cdot (\langle c'u' \rangle) = \nabla \cdot (\gamma_t \nabla \langle c \rangle), \tag{3.8}$$

where γ_t stands for the turbulent kinetic viscosity, which can be calculated according to the turbulent models as shown in Section 2.2.

However, concerning the importance of the volume fraction and temperature change during the mass and heat transfer in spray cooling process, the error brought from the statistics modeling may have stronger influence on the containment cooling estimation compared with the momentum unclosed term modeling.

For one-dimensional scalar like volume fraction and temperature, rather than the three-dimensional vector like velocity, the expression and modeling of the non-linear unclosed terms become much simpler, which makes the realization of PDF family methods easier and cheaper. Therefore, PDF family methods become strong potential candidates in scalar turbulent transport simulation.

3.3 PDF modeling in scalar transport modeling

In some engineering problems like spray cooling, the scalar transport under turbulence, rather than momentum transport, would be the priority. Turbulent scalar transport shares the same non-linear convection term problem like normal turbulent momentum transport. Meanwhile, the source terms during scalar transport always got a more complex non-linear expression than the convective terms, which therefore unable to handle directly by statistics-based turbulence models like RANS and LES.

Owing to the algorithm and realization complexity, PDF modeling has not been widely used in turbulence momentum modeling, but has shown its potential in turbulent scalar transport studies. As shown in Section 2.2, PDF method totally avoid the closure problem brought from statistics-based methods, with the calculation amount under an acceptable level. However, the joint velocity-component PDF modeling calls for a complex mathematical derivation, and also requires the assumption of turbulent time scale. Luckily, the PDF transport equation of the passive scalar in flow will be much simpler than the joint velocity-component PDF equation, which can be decoupled from velocity modeling and take traditional RANS or LES instead.

Following the way in Pope's work [132], the turbulent scalar transport modeling is going to be derived by integrating the velocity-component joint PDF transport equation 2.37 over velocity sample space, a component PDF transport equation can be derived as

$$\rho\left(\underline{\psi}\right)\frac{\partial f}{\partial t}+\frac{\partial}{\partial x_j}\left(\rho\left(\underline{\psi}\right)\left\langle U_j\middle|\underline{\psi}\right\rangle f\right)+\frac{\partial}{\partial \psi_\alpha}\left[\rho\left(\underline{\psi}\right)S_\alpha\left(\underline{\psi}\right)f\right] = \frac{\partial}{\partial \psi_\alpha}\left[\left\langle\frac{\partial J_i^\alpha}{\partial x_i}\middle|\underline{\psi}\right\rangle f\right] \tag{3.9}$$

Here, the convection term can be rewritten as

$$\left\langle U_j\middle|\underline{\psi}\right\rangle = \langle U_j\rangle + \left\langle u_j''\middle|\underline{\psi}\right\rangle \tag{3.10}$$

which makes the equation becomes,

$$\rho\left(\underline{\psi}\right)\frac{\partial f}{\partial t}+\rho\left(\underline{\psi}\right)\frac{\partial}{\partial x_j}\left[\left(\langle U_j\rangle+\left\langle u_j''\middle|\underline{\psi}\right\rangle\right)f\right]+\frac{\partial}{\partial \psi_\alpha}\left[\rho\left(\underline{\psi}\right)S_\alpha\left(\underline{\psi}\right)f\right] = \frac{\partial}{\partial \psi_\alpha}\left[\left\langle\frac{\partial J_i^\alpha}{\partial x_i}\middle|\underline{\psi}\right\rangle f\right] \tag{3.11}$$

Considering momentum fluctuation term not key component in scalar transport equation, the unclosed velocity fluctuation term is always modelled by traditional statistics-based turbulence modeling. Such a simplification makes the application of PDF family methods on scalar transport much simpler and easier to realize.

By following the well-established Boussinesq assumption, the unclosed velocity fluctuation term can be rewritten as

$$\rho\left(\underline{\psi}\right)\left\langle u_j''\middle|\underline{\psi}\right\rangle \mathrm{f} = -\Gamma_T\frac{\partial f}{\partial x_j} \tag{3.12}$$

The way of solving scalar PDF transport equation 3.11 can be done via Original PDF modeling, MOM family modeling and Stochastic Field Method modeling.

3.3.1 Original PDF modeling

Pope has already provided an original PDF modeling on scalar transport coupled with k-epsilon model in [132]. Considering the averaged velocity has already been got through certain turbulence model calculation, a new Lagrangian stochastic particle system can be derived in concern of scalar transport.

Compared with the joint velocity-component PDF modeling, now the velocity has been achieved by other turbulence modeling. The stochastic Lagrangian particles will only carry certain scalar realization in the sample space. Therefore, a new three-step fractional approaches can be derived as:

Step 1 considers the source term effect, the stochastic process can be derived as

$$\Delta_{\delta t}\phi_{\alpha}^{*} = S_{\alpha}\left(\underline{\phi}^{*}\right)\delta t \tag{3.13}$$

$$\Delta_{\delta t}x_{i}^{*} = 0 \tag{3.14}$$

Step 2 considers the turbulent dissipation in scalar transport. The corresponding stochastic process is proceeded the Stochastic Mixing model, following the way on dealing with the term $\frac{\partial}{\partial\psi_{\alpha}}\left[\left\langle\frac{\partial J_{i}^{\alpha}}{\partial x_{i}}\middle|\underline{\psi}\right\rangle f\right]$ in Section 2.2.4.

Step 3 tries to deal with the convection-diffusion process on location movement. The stochastic process is derived as

$$\Delta_{\delta t}x_{i}^{*} = D(x_{i}^{*},t)\delta\mathrm{t} + [B(x_{i}^{*},t)]^{1/2}\Delta_{\delta t}W_{t} \tag{3.15}$$

Where

$$\mathrm{D} = \langle U\rangle + \frac{1}{\langle\rho\rangle}\nabla\Gamma_{T} \tag{3.16}$$

$$\mathrm{B} = \frac{2\Gamma_{T}}{\langle\rho\rangle} \tag{3.17}$$

The PDF modeling on scalar transport itself is much simpler than the velocity-scalar coupled modeling. However, the method still relies on Lagrangian particle system, which needs further treatment on tracking and interception.

3.3.2 MOM family modeling

MOM family modeling refers to a family of methods including MOM, QMOM and DQMOM, which tries to overcome the closure problem by assigning a certain shape to the probability distribution.

Assume a simple problem is controlled by a PDF transport equation like

$$\frac{\partial f(\psi;x,t)}{\partial t} = -\frac{\partial}{\partial\psi}\big(g(\psi)f(\psi;x,t)\big) \tag{3.18}$$

MOM (Method of Moment) [168] tries to model the unknown function $g(\psi)$ as

$$g(\psi) = \sum_{i=0}^{k} w_{k}\psi^{k} \tag{3.19}$$

QMOM (Quadrature Method of Moments) [169] tries to model the term $g(\psi)f(\psi;x,t)$ as a

whole by

$$\int g(\psi)f(\psi;x,t)d\psi = \sum_{i=1}^{n} g(\psi_i)\, w_i(x,t) \tag{3.20}$$

DQMOM (Direct Quadrature Method of Moments) [170] tries to directly expand the PDF using delta function as

$$f(\psi;x,t) = \sum_{i=1}^{n} w_i(x,t)\delta\big(\psi - \psi_i(x,t)\big) \tag{3.21}$$

By coupling the equation of N higher order moments, all the N coefficients $w_i(x,t)$ can be solved from a large linear system, then the unclosed term can be able to express with them.
The MOM family methods implement a Eulerian-based approach, which avoids the complicated Lagrangian particle system. However, new higher moment equations are brought, which further increase the calculation amount and coding difficulty.

3.3.3 Stochastic Field modeling

The original PDF method depends on Lagrangian system, which needs further effort on particle tracking system construction. At same time, the complex derivation also puts limits on application in real engineering problem. To extend the application of PDF method, Valiño derives a Eulerian-based PDF method, Stochastic Field Method [171], in order to provide a simple and reliable solution for the scalar PDF transport equation.
Different from the usage of stochastic particles in Pope's original method, Valiño [171] has implemented a new concept of stochastic Eulerian field,

$$\tau^n(\boldsymbol{x},t) = F_c^{-1}(\psi^n(\boldsymbol{x},t);\boldsymbol{x},t) \tag{3.22}$$

Where F_c stands for the probability distribution function of a certain scalar $\psi^n(\boldsymbol{x},t)$ in the sample space.
By properly modeling the turbulent diffusion term in equation 3.11, it could be rewritten as

$$\frac{\partial f}{\partial t} + U_i\frac{\partial f}{\partial x_i} - \frac{\partial}{\partial x_i}\left[(\Gamma_T + \Gamma_l)\frac{\partial f}{\partial x_i}\right] = \frac{\partial}{\partial \psi}\left[\frac{\omega_C}{2}(\psi - C)f\right] - \frac{\partial}{\partial \psi}[S(\psi)f] \tag{3.23}$$

To solve the equation 3.15, Valiño borrows the mathematical tool on solving statistical mechanics problem, stochastic differential equation, on deriving the solution.

3.3.3.1 Brief introduction of stochastic differential equation: case study by Fokker–Planck equation

In a brief way to understand, stochastic differential equation can be defined as partial differential equation containing stochastic process as the variable. Typical physical problems like Brownian motion and financial problems like price fluctuation can all be modelled as a mathematical system controlled by stochastic differential equations.
Fokker–Planck equation is one of the most important theoretical foundation in statistical mechanics, which describes the probability density function of particle's movement during

Brownian motion. The shape of equation is similar to scalar PDF transport equation 3.15, which therefore deserves further introduction.

Following the theory introduced in [133], Fokker–Planck equation can be written as

$$\frac{\partial}{\partial t}f(x,t) = -\frac{\partial}{\partial x}[\eta(x,t)f(x,t)] + \frac{\partial^2}{\partial x^2}[D(x,t)f(x,t)], \tag{3.24}$$

Where $f(x,t)$ stands for the probability density function of the particle existing at certain location x at certain time t.

Owing to the characteristics of Brownian motion, a stochastic process can be derived following the Fokker–Planck equation, as

$$dX_t = \eta(X_t,t)dt + \sqrt{2D(X_t,t)}dW_t, \tag{3.25}$$

where X_t is a certain realization of possible particle movement trace, $\eta(X_t,t)$ is the drift coefficient, $D(X_t,t)$ is the diffusion coefficient. W_t is the Wiener process (white noise).

Where the convection term $-\frac{\partial}{\partial x}[\eta(x,t)f(x,t)]$ gives a contribution as the drift $\eta(x,t)dt$ in the particle movement, while the diffusion term $\frac{\partial^2}{\partial x^2}[D(x,t)f(x,t)]$ gives a contribution as the diffusion $\sqrt{2D(x,t)}dW_t$ in the particle movement.

Since white noise process dW_t proceeded during each realization, the final location X_t will be always slightly different from each other sample, which is just like the irregular fluctuation during real chaos process.

If large enough number of realizations have been provided, the probability density function $f(x,t)$ can be approximated by

$$f(x = X,t) = \frac{N_X}{N}, \tag{3.26}$$

Where N is the total number of the realization sample set, N_X is the number of realizations during which $X_i = X$. The construction of the realization sample set can be built up with methods like Monte Carlo method.

With the help of the above mathematical tool, the n-order statistical moment M_n can be got by

$$M_n = \int_{-\infty}^{\infty} x^n p(x,t)dx = \frac{1}{N}\sum_{i=1}^{N} X_i^n, \tag{3.27}$$

Which totally bypass the moment closure problem in turbulence modeling

3.3.3.2 Application of stochastic differential equation in turbulent scalar transport problem: Stochastic Field Method

As shown above, the probability density function of the passive scalar component can be written as,

$$\frac{\partial f}{\partial t} + U_i\frac{\partial f}{\partial x_i} + \frac{\partial}{\partial x_i}\left(\gamma_t\frac{\partial f}{\partial x_i}\right) + \frac{\partial}{\partial x_i}\left(\gamma\frac{\partial f}{\partial x_i}\right) - \frac{\partial}{\partial \phi}\left[\frac{\omega_C}{2}(\phi - \langle c\rangle)f\right] = 0, \tag{3.28}$$

Valiño [171] makes use of the way on solving PDF transport equation introduced in the previous section, and derive the solution of equation 3.28 in the following way.

Compared with Fokker–Planck equation, $U_i \frac{\partial f}{\partial x_i}$ and $\frac{\partial}{\partial \phi}\left[\frac{\omega_C}{2}(\phi - \langle c \rangle) f\right]$ can be treated as the convection term, which give a contribution as,

$$d\tau^k = -U_i \frac{\partial \tau^k}{\partial x_i} dt - \frac{\omega_C}{2}(\tau^k - \langle c \rangle) dt, \tag{3.29}$$

Similarly, the terms $\frac{\partial}{\partial x_i}\left(\gamma_t \frac{\partial f}{\partial x_i}\right) + \frac{\partial}{\partial x_i}\left(\gamma \frac{\partial f}{\partial x_i}\right)$ can be treated as the diffusion term, which give a contribution as,

$$d\tau^k = \frac{\partial}{\partial x_i}\left((\gamma + \gamma_t)\frac{\partial \tau^k}{\partial x_i}\right) dt + \sqrt{2(\gamma + \gamma_t)} \frac{\partial \tau^k}{\partial x_i} dW_i^k, \tag{3.30}$$

Together, the stochastic process derived from the scalar component PDF transport equation got the expression as,

$$\begin{aligned} d\tau^k = -U_i \frac{\partial \tau^k}{\partial x_i} dt + \frac{\partial}{\partial x_i}\left((\gamma + \gamma_t)\frac{\partial \tau^k}{\partial x_i}\right) dt + \sqrt{2(\gamma + \gamma_t)} \frac{\partial \tau^k}{\partial x_i} dW_i^k \\ - \frac{\omega_C}{2}(\tau^k - \langle c \rangle) dt, \end{aligned} \tag{3.30}$$

By large enough number of random Eulerian fields τ^k following the above stochastic process, the PDF can be calculated by statistics of the result sample fields. In the sense of probability, such process successfully goes through all the possible realizations of the scalar field value under turbulence. Therefore, all the statistical moments or the non-linear reaction source terms of the scalar field can be easily and accurately calculated through the PDF.

The averaged scalar component, or 1st order moment, is normally of most concern in engineering problems. It can be directly calculated by

$$\langle c \rangle = \frac{1}{N} \sum_{k=1}^{N} \tau^k, \tag{3.31}$$

Stochastic field method is straightforward on modeling and easy to implement, which makes it a potential approach on passive scalar transport under turbulence.

3.3.4 Discussion of methodology choice in nuclear containment spray

Three branches of the PDF family methods on turbulent scalar transport have been introduced in the previous sections, as summarized in Table 6. Among the three, the original PDF method still relies on the Lagrangian particle system to solve scalar transport, which provides a high precision, but the high calculation amount and the difficulty on coding. The MOM family methods try to use higher order moments on constructing the polynomial expansion, in order to approximate the true solution. MOM family method scarifies part of the precision, as way to decrease the complexity of the algorithm. However, the process of constructing higher order moments still require certain degree of calculation and specified coding. The Stochastic Field Method tries to re-derive the component PDF transport equation into a Eulerian field form. By solving the new Eulerian equation using the SDE tool, the method exchanges part of the calculation amount and precision with the coding difficulty.

Concerning that the spray cooling problem of nuclear containment stays on an engineering level, the precision of Stochastic Field Method is still acceptable. However, the advantage of overcoming non-linear property through PDF methodology can be remained. In addition, the convenience in coding and the compatibility with other Eulerian based modeling make the method easily to be extended in the existing codes. Therefore, stochastic field method stays as the best choice for nuclear spray cooling modeling.

Table 6 Summary of PDF family methods on turbulent scalar transport

Name	Strategy	Calculation Amount	Precision	Coding Difficulty
Original PDF	Lagrangian stochastic particle system	High	High	Hard
MOM	High order moment closure	Medium	Medium	Medium
Stochastic Field	Stochastic Eulerian fields	Medium	Medium	Easy

3.4 Turbulent effect on spray modeling

As volume fraction and temperature are typical passive scalars in spray cooling process, turbulence therefore also impresses strong influence on spray process.

When the continuous phase of the two-phase flow turns into turbulence, the transportation of volume fraction and energy will also be influenced. Under turbulent flow, the spray droplets will get additional transportation carried by the fluctuation of gas phase. Owing to the non-linear chaotic characteristics of turbulent flow, the real transient value of volume fraction and temperature can never be achieved only except in the real-time experiment. Therefore, the effort to seek for the “real” physical value is useless and meaningless. Certain way on modeling the time-averaged or spatial-averaged value meets the practical requirement in real engineering application.

The way of modeling averaged volume fraction transport equation traditionally follows the way on modeling the averaged mass fraction transport equation. However, it is obvious that chemical component and spray droplets have strong difference in both physical property and behavior. Therefore, the modeling of volume fraction transport governing equation will be further discussed in this section. The difference between the two equations will be stressed, which leading to different construction of the stochastic processes when using PDF family methods.

In the spray modeling case under nuclear containment study, the averaged Eulerian field describing spray droplets is key value to solve in CFD analysis. To overcome the difficulty of turbulence closure problem, the implementation of stochastic field method can be used. In this section, the details of applying stochastic field method on solving volume fraction transport equation will also be discussed in detail.

3.4.1 Discussion on Eulerian equation of spray droplet volume fraction

As discussed in Section 2.1, the spray droplets are modelled together as a field in the Eulerian viewpoint, instead of a group of independent particles in the Lagrangian viewpoint. Therefore, a

new governing equation of the new physical field needs to be added, in order to distinguish gas phase and liquid phase.

For Eulerian treatment of spray droplets, it could follow the mass fraction transport equation in chemical engineering area. Concerning chemical component well dissolved in the chemical flow, it is always assumed to occupy the whole controlling volume and able to diffuse to the neighbor cells [172]. Therefore, the equation is modelled as

$$\frac{\partial}{\partial t}(\rho Y) + \nabla \cdot (\rho U Y) = -\nabla \cdot (\gamma \nabla Y), \tag{3.32}$$

where Y is the mass fraction shared by liquid droplets in the gas-liquid mixture, and γ is the molecular diffusion coefficient of the liquid phase.

when comes to the two-phase flow like spray problem, volume fraction is used instead, as way to describe the liquid droplet location in the gas-liquid mixture. The equation is modelled as

$$\frac{\partial}{\partial t}(\rho \alpha) + \nabla \cdot (\rho U \alpha) = 0, \tag{3.33}$$

where α stands for the volume fraction occupied by the spray droplets in the two-phase mixture at certain location.

This volume fraction equation set up by the nuclear engineering community is part of the famous two-fluid model [110]. Compared with the traditional way on modeling mass fraction transport, the molecular diffusion term $-\nabla \cdot (\gamma \nabla Y)$ is wiped out, under the consideration that "volume", as a description of spatial occupation, has no molecular diffusive characteristics like real physical values, as shown in **Figure 27**. As the volume occupied less and less by the liquid phase, the assumption of discontinuity become more and more effective. At the same time, it is also more reasonable to assume no molecular diffusion happening during the transport process.

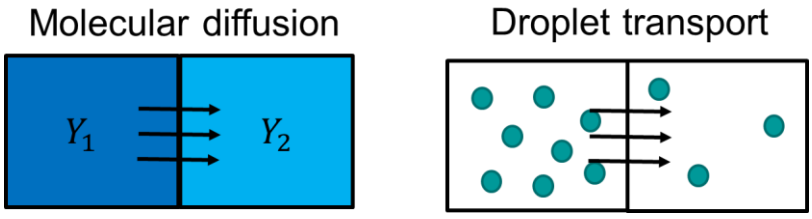

Figure 27 Molecular diffusion and droplet transport

Spray processes can be divided into two different categories: dense spray and dilute spray. On condition that spray liquid stay as bulks and occupied a relatively big volume of space, the spray is treated as dense spray, which is largely seen in engine fuel spray. On condition that the spray liquid has already been fully atomized and wide spread distributed in the large space (droplet volume fraction less than 2%), the spray is treated as dilute spray, like the spray cooling case in nuclear containment in this work.

In dilute spray problem, though water phase owning a much stronger viscous effect than the atmosphere, the droplets stay far from each other, which results in a very weak droplet-droplet interaction, way much different from the viscous effect. Therefore, the volume fraction equation is used to describe the field of the spray droplets in this study.

3.4.2 Stochastic Field Method on volume fraction equation

Conerning the difference of the governing equations between volume fraction transport and scalar

component transport. Valiño's original form of stochastic process for each Eulerian sample field will not properly work. In this section, following the spirit of Stochastic Field Method, the stochastic process will be re-derived for volume fraction transport.

It is no doubt to see volume fraction α is also one kind of passive scalar. Therefore, the PDF transport equation of volume fraction can also be derived following the same way in [171]. However different from equation 3.11, the molecular diffusion part in the scalar transport equation 3.7 is not existing any more. Therefore, a new volume fraction PDF transport equation is derived as,

$$\frac{\partial f_\alpha}{\partial t} + U_i \frac{\partial f_\alpha}{\partial x_i} + \frac{\partial}{\partial x_i}(\langle u'_i | c = \phi \rangle f_\alpha) = 0, \tag{3.34}$$

where f_α is the probability density function that $\alpha = \mathrm{A}$ in a certain turbulent realization, where A is a certain realization of volume fraction α in the sample space.

By proper turbulent modeling on the momentum term, the equation 3.34 can be rewritten as

$$\frac{\partial f_\alpha}{\partial t} + U_i \frac{\partial f_\alpha}{\partial x_i} + \frac{\partial}{\partial x_i}\left(\gamma_t \frac{\partial f_\alpha}{\partial x_i}\right) = 0, \tag{3.35}$$

where γ_t is the turbulent viscous coefficient following the eddy viscosity assumption.

With the same approach on Fokker–Planck equation solution, the stochastic process related to volume fraction PDF transport equation can be derived as,

$$d\alpha^k = -U_i \frac{\partial \alpha^k}{\partial x_i} dt + \frac{\partial}{\partial x_i}\left(\gamma_t \frac{\partial \alpha^k}{\partial x_i}\right) dt + \sqrt{2\gamma_t} \frac{\partial \alpha^k}{\partial x_i} dW_i^k \tag{3.36}$$

where α^k is the volume fraction in a certain realization following the above process.

Like shown in equation 3.31, by providing large enough number of samples, the average volume fraction can be got by

$$\langle \alpha \rangle = \frac{1}{N} \sum_{k=1}^{N} \alpha^k, \tag{3.37}$$

3.5 Turbulent effect on spray cooling modeling

Since the mass transfer process is also a non-linear process during spray cooling, it will as well be influenced by the fluctuated characteristics of gas phase turbulence, similar to the volume fraction solution in previous section.

During the evaporation process, certain amount of mass at the surface of liquid spray droplets will be transferred to the atmosphere though both convection and diffusion process. Concerning the highly complicated process during evaporation, an experiment-based approach by the dimensionless Sherwood number is used on modeling in engineering applications. By assuming droplet as a sphere, analytical work and experimental work are done together by Frossling [136] on modeling the transfer process when the impact of droplet motion and surface boundary layer existing.

As shown in Section 2.4.1, the Sherwood number can be modelled by

$$\mathrm{Sh} = 2 + 0.552 \mathrm{Re}^{\frac{1}{2}} \mathrm{Pr}^{\frac{1}{3}}, \tag{3.38}$$

Different from the flow Reynolds number, here Re refers to the particle Reynolds number, which describes the relative motion between the droplet and the surrounding atmosphere over the viscous

effect. It is modelled as,

$$\mathrm{Re} = \frac{\rho_g U_r d}{\mu_g}, \tag{3.39}$$

Where ρ_g is the density of gas phase, μ_g is the viscous coefficient of gas phase, d is the diameter of spray droplets, and U_r is the relative velocity between the spray droplets and surrounding atmosphere.

Under turbulent condition of the gas phase, it is no doubt that the relative velocity U_r will also get fluctuation part following the turbulent effect of gas phase flow.

$$U_r = \langle U_r \rangle + u_r \tag{3.40}$$

where $\langle U_r \rangle$ is the averaged relative velocity, and u_r is the fluctuated part.

Since Sherwood number is a non-linear function of U_r as shown in equation 3.38, the Reynolds averaging of Sherwood number also suffers from non-closure problem, as it is obvious that

$$\langle \mathrm{Sh} \rangle = 2 + 0.552 \mathrm{Pr}^{\frac{1}{3}} \langle \mathrm{Re}^{\frac{1}{2}} \rangle \tag{3.41}$$

However, the Reynolds averaging part follows

$$\langle \mathrm{Re}^{\frac{1}{2}} \rangle \propto \langle (\langle U_r \rangle + u_r)^{\frac{1}{2}} \rangle \neq \langle U_r \rangle^{\frac{1}{2}} \tag{3.42}$$

Owing to non-linear property, the fluctuated part u_r can't be eliminated during Reynolds averaging process, which means an additional effect on mass transfer needs to be further modelled.

A pure analytic-based derivation of the additional turbulent effect will be hard, concerning the complexity of evaporation process and the uncertainty of the experimental model. Bini and Jones [173] implemented a dimension analysis method, together with experimental approach, to build up models concerning the turbulent effect on spray mass transfer in LES study on acetone spray evaporation process. Following the previous work, a stochastic Sherwood number considering the addition turbulent effect in RANS-based simulation can be modelled in this work as

$$Sh_{st} = C_V Sc_g^{1/3} \left(\rho_g \frac{k^{1/2} d}{\mu_g} \right)^{1/2} |dW_t|^{1/2} \tau_p^{3/4}, \tag{3.43}$$

Different from Bini's work [173] on modeling Sh_{st} with sub-grid scale turbulent fluctuation, the gas phase turbulent kinetic energy k is directly used on modeling the additional mass transfer effect brought by turbulent flow of gas phase.

In equation 3.43, Sc is the Schmidt number, k is the gas phase turbulent kinetic energy, C_V is the coefficient for tuning, and τ_p is the particle time, which is

$$\tau_p^{-1} = \frac{3}{4} \frac{\rho_g}{\rho_l} C_D \frac{U_r}{d}, \tag{3.44}$$

where ρ_g and ρ_l are the densities of gas phase and liquid phase. C_D is the drag coefficient as discussed in Section 2.4.2. U_r is the relative velocity defined as equation 3.40. d is the diameter of the spray droplet.

During the simulation of each time step, the energy equation will be solved N times as samples for different turbulent realization. Each realization will differ from each other owing to the white noise dW_t in equation 3.43. At the final stage of each realization, h_g^k will be calculated under the influence from the stochastic Sherwood number, Sh_{st}^k in each sample. The averaged enthalpy of gas phase will be calculated by

$$\langle h_g \rangle = \frac{1}{N}\sum_{k=1}^{N} h_g^k \tag{3.45}$$

3.6 Validation of Stochastic Field Method: chemical reactor

To validate the basic performance of Stochastic Field Method, a simple 1D plug-flow chemical reactor case is used to check the modeling of reactive flow. A basic overview of the chemical reactor can be referred to **Figure 28**.

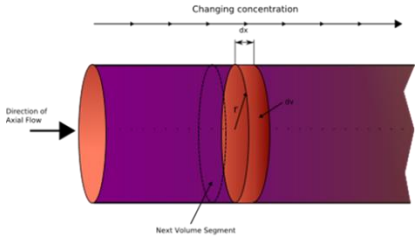

Figure 28 Plug flow reactor[171]

By simplification, the reactive flow is assumed to be only along one direction, with the chemical reaction during the process is modeled as a source term $S(\psi)$, which is

$$S(\psi) = a_1(1-\psi), \tag{3.46}$$

where ψ is the chemical component in the flow, and a_1 is a coefficient.

At initial time, there's no chemical materials in the flow, which means

$$\psi = 0, \tag{3.47}$$

Therefore, the probability density function at each field is,

$$f(\psi = 0; x, 0) = 1, \tag{3.48}$$

where x means the location along the flow direction.

It is assumed a constant chemical flow with a certain component fraction is kept injecting, which means a Dirichlet type boundary is defined at the inlet as

$$\psi = \phi \tag{3.49}$$

where ϕ is the chemical component carried by inlet flow.

Following it, the boundary condition of PDF at the inlet is defined as

$$f(\psi = \phi; x = 0, t) = 1, \tag{3.50}$$

The boundary condition at the outlet is defined as a normal outflow condition, therefore a Neumann type boundary is defined as

$$\frac{\partial \psi}{\partial x} = 0 \tag{3.51}$$

Following it, the boundary condition of PDF at the outlet is defined as

$$\frac{\partial}{\partial x} f(\psi; x = L, t) = 0, \tag{3.52}$$

where L is the length of calculation domain.

During the simulation, the coefficient in the source term 3.46 is chosen as constant in this case by,

$$a_1 = 3, \tag{3.53}$$

The coefficients in the stochastic field transport equation are chosen as,

$$\omega_C = 20, \tag{3.54}$$

$$\gamma + \gamma_t = 0.1. \tag{3.55}$$

The problem is solved numerically by stochastic field method, 50 cells are generated by discretizing the calculation domain and 100 stochastic fields are generated at every cell to cover the possible chemical component sample space. 2nd Central Scheme is used on the discretion of the governing equation and 0.001 is chosen as the time step. The realization of stochastic field method approach is coded by MATLAB.

With the well-established coefficient assumption in the simple 1D case, a theoretical solution according to it can be derived, which is used as a comparison on validation of the performance of the simulation. The theoretical solution is derived as,

$$c(x) = 1 - e^{-2.416x} \tag{3.56}$$

The result of the simulation by stochastic field method on the plug-flow reactor can be got like shown in **Figure 29**.

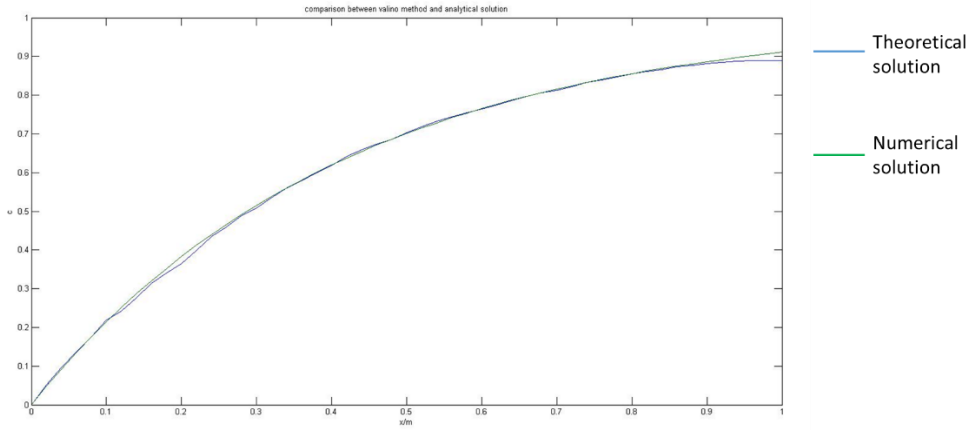

Figure 29 Simulation result of the plug flow chemical reactor

As shown in **Figure 29**, the code has basically realized Stochastic Field Method. In the whole domain of the plug-flow reactor, the chemical component got from simulation has matched well with the theoretical solution. Some certain differences can be found in the inner space and near the outlet. The difference in the inner space is owing to the limited number of stochastic fields. Based on the theoretical study in [171], only when the stochastic field number approximates to infinite, the statistics moment of the sample field will be equal to the real physical filed. If number not large enough, the stochastic performance may still bring in some non-physical fluctuation during the simulation. Such error can be decreased by increasing the number of stochastic fields, and finally eliminated when the number reaches infinite. The difference near the outlet boundary part is owing to the difficulty of boundary treatment in PDF family methods. PDF family methods try to implement an equivalent system of artificial sample fields following stochastic process to approximate the real physical realization sample space. However, at the boundary part, the physical value is certain, without any influence from the chaos feature. This characteristic will be even stronger in the theoretical solution, as possible device error and measure error are possible experiment but never exist in theoretical world. Therefore, the boundary condition may require special consideration in the circumstance of stochastic field transport, which deserves further study in future.

3.7 Summary

In this chapter, the modeling on turbulent scalar transport has been widely studied. To provide fine simulation of nuclear containment spray process under turbulent atmosphere, Stochastic Field Method is implemented as way to overcome the turbulent closure problem in traditional turbulence modeling.

Among the methods, the PDF method has shown its advantage over other turbulence models. By the import of the stochastic equivalent system, the method has successfully overcome the closure problem brought by non-linear property. Among the 3 branches of PDF family methods, Stochastic Field Method turns out as the most potential approach, which is easy on coding and acceptable on calculation amount.

At the last part of the chapter, a simple 1D plug-flow chemical reactor case has been provided as a benchmark to validate the basic performance of Stochastic Field Method, which shows the method is sound on dealing with scalar transport under turbulence.

With the work in this chapter, solid fundamental is set up for detailed simulation on nuclear containment cooling. In addition, the available working condition is further extended to turbulent situation. With the contribution of this part, fine simulation of nuclear containment spray modeling is complete, which is able to be implemented for the prototype design prediction and data generation for coarse case prediction.

4. Modeling on spray cooling in nuclear containment

As discussed in Chapter 2, the spray cooling process in nuclear containment is coupled with multiple physical effects, which therefore deserves a further study. In this chapter, all the models on simulating the spray in stable atmosphere will be validated based on the nuclear containment benchmark, THAI. The result has shown that the models are reliable in detailed simulation of nuclear containment spray process. With the effort done in these two parts. The source of data generation for coarse simulation has been provided.

4.1 Introduction

The spray system plays as the key role in nuclear containment to ensure the completeness and functionality when nuclear accident happened. During design-based accident, the primary loop is assumed to be broken, large amount of coolant will be leaked into the containment and vaporized into steam. When comes to severe accident, the situation will become more complicated and dangerous. The reactor core could be melted and fission products will be released into the containment. Owing to the reaction between the nuclear fuel rod claddings and water, Zirconium will be oxidized and hydrogen will be produced. Following the previous studies [174] [175], the containment faces 3 thorny problems:

(1) High temperature and High pressure of the atmosphere
(2) Iodine and aerosols dispersed in the atmosphere
(3) Large amount of hydrogen distributed in the containment with certain degree of stratification.

On the commission of nuclear containment safety, the spray system is implemented in the containment, which will be triggered by the temperature and pressure level of the system. Liquid water will be injected from the nozzle located at the upper part and atomized into small droplets. Owing to the large heat capacity and evaporation effect of the water droplet, the atmosphere will be cooled down and depressurized slowly. Moreover, the spray water will be used to wash the polluted atmosphere and remove suspended reactive and non-reactive aerosol particles. Lastly, the spray droplets will disturb the distribution of hydrogen in the atmosphere mixture owing to the momentum interaction with the surrounding gas. As a result, the hydrogen stratification will be partly weakened, which decreases the chance of deflagration and make it easy for hydrogen elimination.

In this chapter, the behavior of spray in stable atmosphere will be studied. Concerning the large volume and complex structure of the real nuclear containment, the performance of the spray model may partly be interrupted by other effects. Therefore, a commonly used benchmark in the containment area, THAI, will be taken instead, as way to validate the performance of the Eulerian two-phase modeling, as well as the basic characteristics of the spray process in nuclear containment.

4.2 Experiment facility

As briefly introduced in Section 1.4.1, THAI (Thermal Hydraulics, Aerosol and Iodine) facility is

one of the most common-used international benchmarks of nuclear containment study. The THAI facility was constructed in 2000 [43], aimed at experimental studies on light water reactor several accidents. The THAI experimental programs include THAI-I (1998-2003), THAI-II (2003-2007), THAI-III (2006-2009), THAI-IV (2009-2013), THAI-V (2013-) and OECD benchmarks, OECD/NEA THAI (2007-2009), OECD/NEA THAI2 (2011-2014).

THAI test facility covers various topics in nuclear containment safety study, including gas distribution and stratification, condensation effect, turbulence effect, iodine mass transfer, multi-compartment iodine distribution and behavior, iodine-painted-surfaces interaction, hydrogen deflagration, aerosol wash-down behavior, pressure suppression pool hydro-dynamics, and many other issues related to containment.

THAI facility is also involved as a component of OECD-NEA/ISP-47 on Containment thermal hydraulics, OECD-NEA/ISP-49 on Hydrogen combustion, the framework of SARNET-1 on Iodine mass transfer and oxide behavior, the framework of SARNET-2 on Passive autocatalytic recombiners and German CFD network on gas distribution.

An overall view of THAI facility can be found in Figure 30. As shown in Figure 31, the geometric structure of THAI facility follows the basic characteristics of real nuclear containment in a technical scale. THAI consists a large vessel with a total surface area of 163 m^2 including the inner structures, while 100 m^2 if only single compartment is considered. The vessel got a total volume of around 60 m^3, including a 1.7 m^3 sump compartment, a 17.7 m^3 dome compartment, and a 6.05 m^3 inner cylinder compartment. The outer diameter of the vessel is 3.2 m and the height is 9.2 m. The material of the wall is made by Stainless steel DIN, which got a thickness of 22 mm.

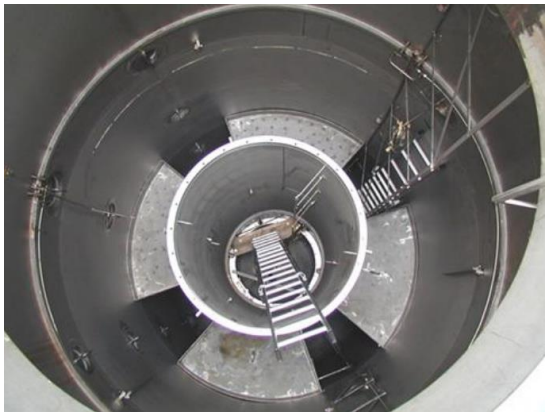

Figure 30 Overall view of THAI[35]

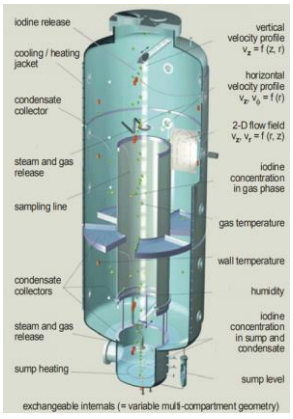

Figure 31 Structure design of THAI[35]

The outer wall of the vessel is covered by an oil-filled cooling jacket, which helps keep the wall temperature constant. A 20 kW electrical heating coil is equipped around the wall to provide heat source. In addition, a 12 cm mineral wool is further used on the outer side as way to realize the thermal insulation function and keep the heat loss into a minimum degree. The limit of the facility is 14 bars at 453K, which covers the scope of pressure and temperature change during accident condition.

The full cone type nozzle is used in THAI facility, which provides a cone shape distribution of the spray nozzle in the near-nozzle part. The nozzle is installed at 1.8 m from the center of the roof, with an outer diameter of 8 mm. Based on the measurement, the spray angle is 30º and the

Sauter-diameter of the spray droplets is around 830 μm.
Initially, the vessel is occupied by humid air with absolute pressure of 1.5 bar and homogenous distributed temperature of 90 ℃. The air consists 25% volume fraction of water vapor and it assumed to be constant distributed overall over the whole vessel. The wall has been heated up to 90 ℃ before the activation of spray and is kept such temperature over the whole experimental process. After the wall has been heated, the spray water will be injected from the nozzle, which got a temperature of 20 ℃ and mass flow rate of 1 kg/s. During the experiment, the spray water will be collected in the sump part of THAI facility and the removal action will not be done only until the experiment stops. Several thermocouples are installed in the vessel to measure the gas temperature change. More details on the experiment facility can be found in [35].

4.3 Numerical settings

To validate the physical models of the spray, a detailed simulation is proceeded based on THAI benchmark. The discrete liquid phase is modelled by a Eulerian approach. All the interaction effects between two phases are considered, including mass transfer, momentum transfer and energy transfer. Gas film is assumed existing between the water droplet and atmosphere, which is filled by saturated water vapor. The saturation model follows Arden-Buck Equation. More details on modeling can be referred to Chapter 2.

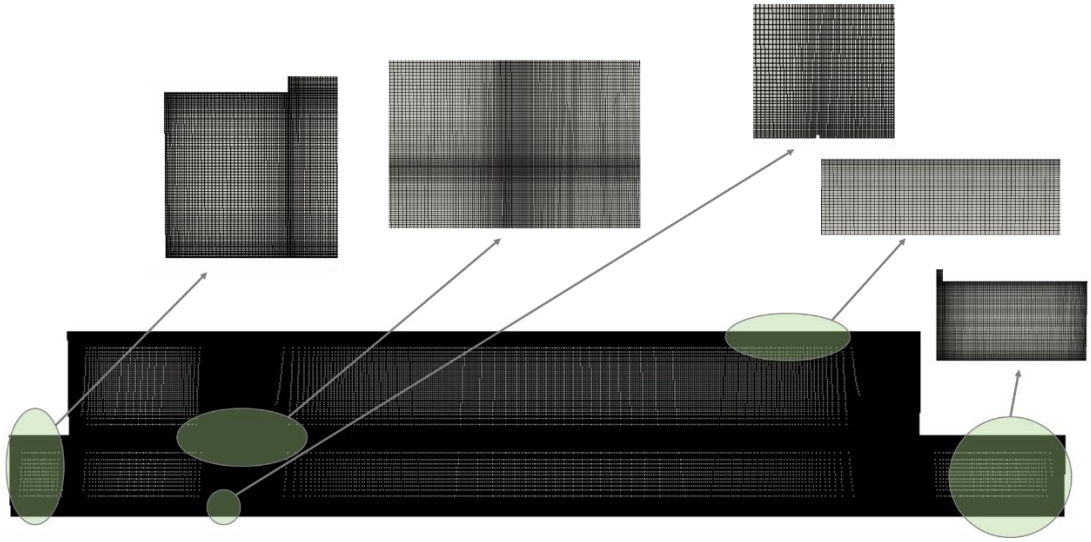

Figure 32 Mesh used in THAI spray simulation

The mesh structure used in the simulation is like shown in **Figure 32**, which totally consists of 109819 cells. To avoid the possible numerical problem and analysis difficulty, the mesh implements pure blocked Cartesian mesh. To well fit the small size of spray nozzle, the local refinement is proceeded on the mesh down to the nozzle diameter. All the near wall part in the head part, body part and base are also refined to fit the near-wall boundary layer. The smallest size of the mesh is 4 mm.
Owing to high reliability and free access, the open-source package OpenFOAM is used on simulating the problem. The time step is chosen as 0.0001 s to satisfy the CFL criterion. Following the measure time of THAI benchmark experiment, the total simulation time has been set as 160s. The details on setting can be found in **Table 7**.

Table 7 Setting of OpenFOAM simulation on THAI benchmark

Time step	0.0001 s
Total time	160 s
Mesh size	4 mm
Total mesh cells	109819

4.4 Results and discussion

The simulation is proceeded for 160 s as way to make a comparison with the experimental data. The time-dependent temperature changing at the certain measured locations in THAI facility have been extracted from the result data, which are shown in **Figure 33**.

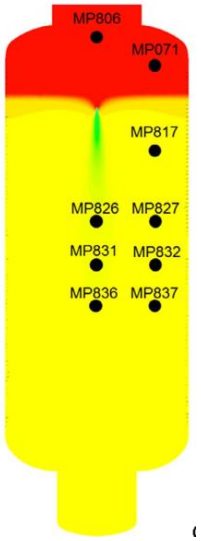

Figure 33 Thermo couple locations in THAI [37]

The temperature change in MP806, MP817, MP826, MP827, MP831, MP832, MP836, MP837 have been provided in Figure 34-41. As shown in the figures, the simulation results have successfully captured the basic trend of the temperature change during experiment. As time goes on, the temperature at all measure points keeps decreasing. Compared with the experiment data, the over temperature predicted from the numerical simulation is lower. This is because only one group of droplet diameter size is not considered, which neglects the variation of droplet size and magnifies the cooling effect. Such phenomenon can be improved by assuming poly-dispersed droplet size model. However, it can be observed that the temperature prediction near the nozzle part is much more precise at MP806 than other parts. This is because the liquid water is much closer to the continuous status around the nozzle, which makes the field concept more reasonable in Eulerian approach and therefore get a better matching than other dilute parts. In addition, the prediction of temperature at MP817, MP827, MP832, MP837 is better than the near-axis parts. This is because the Eulerian simulation has not applied the atomization model, which gives a

prediction of more water droplets compared with real process. As a result, there would be an overestimation of cooling in the center part.

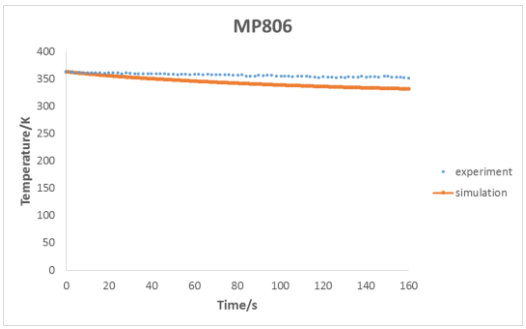

Figure 34 transient temperature change at MP806

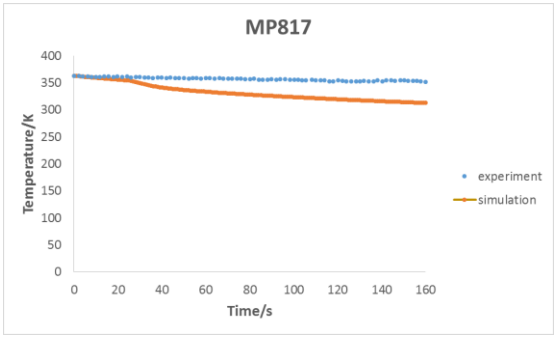

Figure 35 transient temperature change at MP817

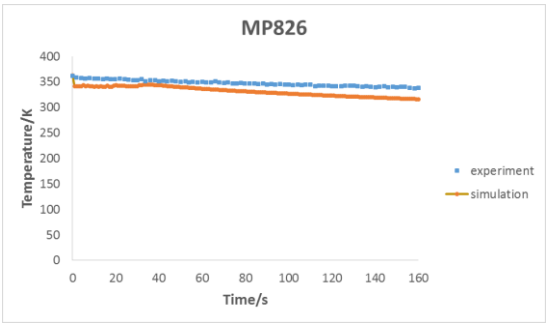

Figure 36 transient temperature change at MP826

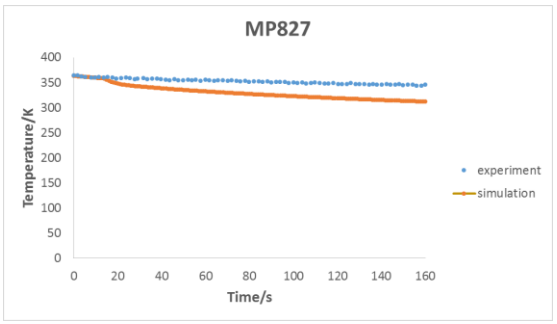

Figure 37 transient temperature change at MP827

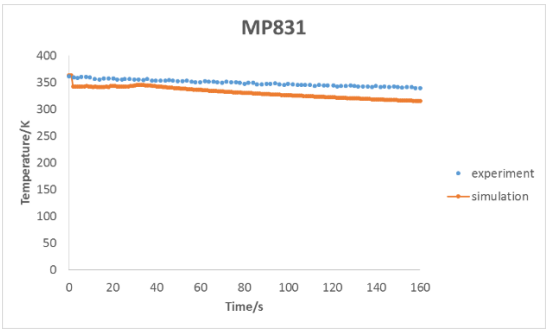

Figure 38 transient temperature change at MP831

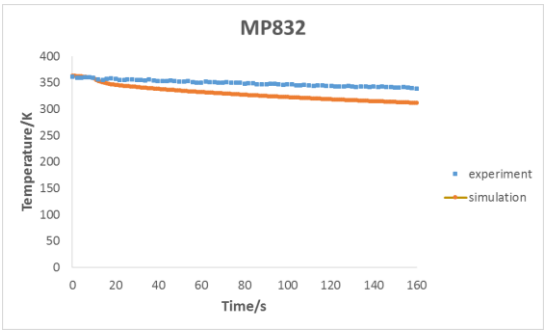

Figure 39 transient temperature change at MP832

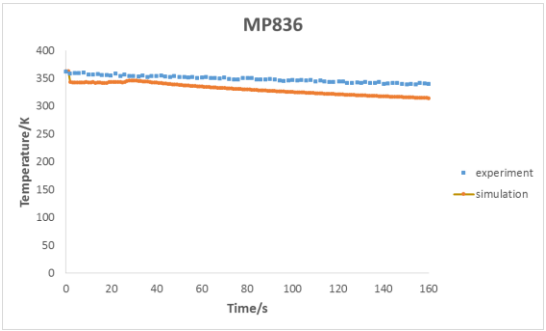

Figure 40 transient temperature change at MP836

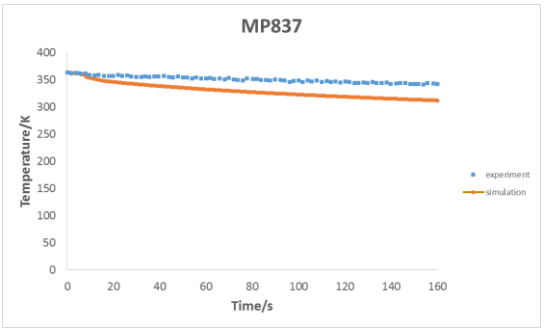

Figure 41 transient temperature change at MP837

The overall pressure change has been provided in **Figure 42**. As shown in the figure, the total pressure in the vessel keeps decreasing, and finally reach a near-to-atmosphere status. The simulation has provided a well matching with the experiment, which means CFD analysis has given a reliable result on cooling depressurization.

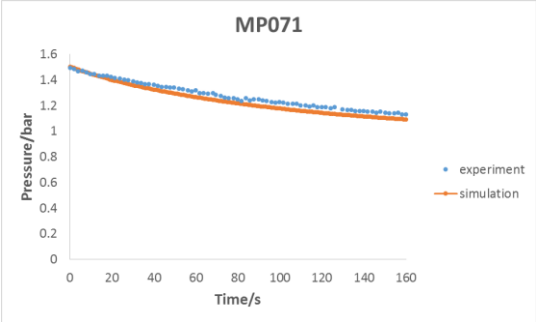

Figure 42 transient pressure change at MP071

The contours of liquid phase velocity and gas velocity have been provided in **Figure 43** and **Figure 44**. As shown in the figures, high velocity zone can be found near the central axis part. The liquid phase keeps spanning in width from the spray nozzle. The relative high velocity spray droplets produce strong momentum interaction with the surrounding atmosphere, which also generates a high velocity zone in the central part of the containment. The gas flow will be blocked by the solid wall at the lower part, which generates two re-circling zones at the outer wall and the bottom, as shown in **Figure 45**. The re-circulation is stronger near the outer wall owing to the large space. A low velocity zone can be found at the bottom for the liquid phase. This is because the liquid water felled on the vessel bottom will not be discharged during the experiment, which result in a stable accumulation water pool during the time period.

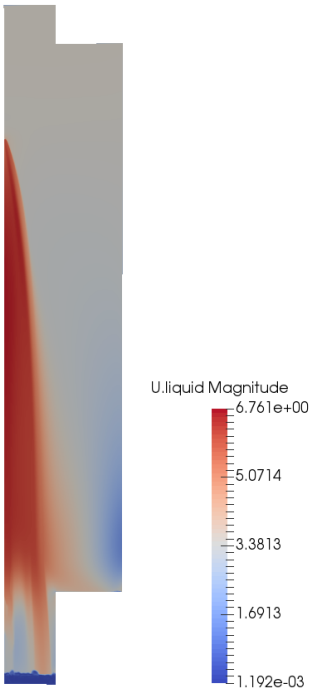

Figure 43 Liquid phase velocity distribution

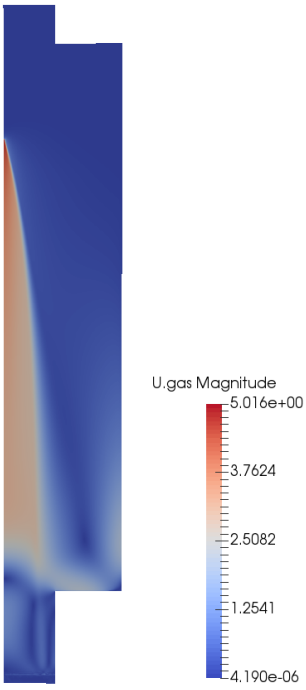

Figure 44 Gas phase velocity distribution

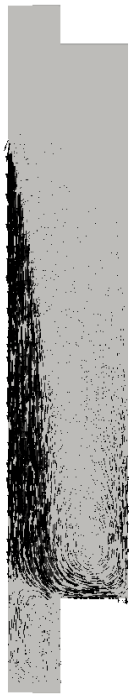

Figure 45 Vector plot of gas velocity

The contour of atmosphere temperature and liquid volume fraction have been shown in **Figure 46** and **Figure 47**. As shown in **Figure 46 Gas phase temperature**, there is significate gas temperature distribution in the containment, where the upper part of the containment has not been cooled enough. This is because the water nozzle is installed at the roof of the containment, and the upper part of the containment can only be cooled down mainly by the lower part, instead of direct energy exchange with the water droplets. As shown in **Figure 47 Liquid phase volume fraction**, the spray area mainly occupies the middle part which follows the spray angle at the nozzle. There is a clear profile of the liquid phase, while a lower volume fraction can be observed in the inner part compared with the outer part. This is because the diffusion effect of the liquid phase can't be modelled well compared with the Lagrangian particle tracking. The Eulerian approach models spray droplets as a continuous field set, which takes tiny space of a certain mesh cell. The modeling of particle dispersion can only be done though statistical based experimental study, which may neglect the individual behavior of droplets and may underestimate the dispersion when the spray is super dilute.

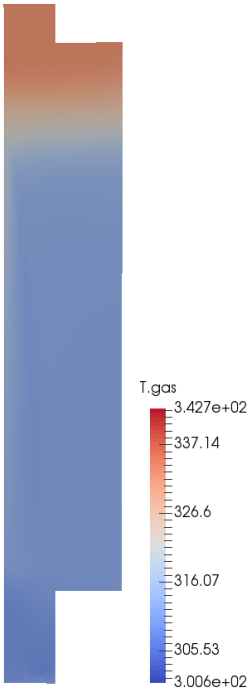

Figure 46 Gas phase temperature distribution

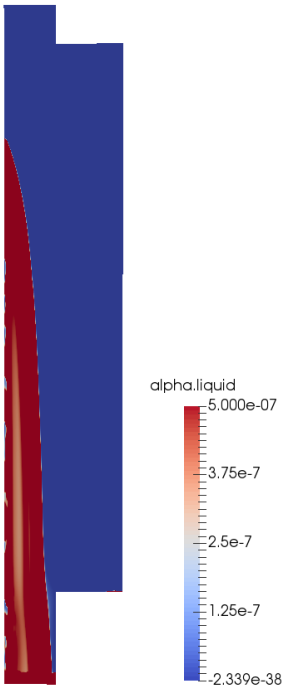

Figure 47 Liquid phase volume fraction distribution

The contours of transient temperature in the vessel at 30s, 60s, 90s, 120s and 160s are provided in **Figure 48**. As shown in the figure, there exists always a low temperature zone at the bottom, which comes from the consisting cooling from the accumulated spray water during the process. The atmosphere will be cooled down slowly along the time period. The area following the tracing line along the nozzle injecting angle will first get cooled, which is influenced by the weak atomization considered in Eulerian approach. During the process, the atmosphere will be first cooled down in the lower part then slowly transfer to the upper part. This is because the liquid phase is much closer to continuous phase in the near nozzle part, and diffuse step by step into a dilute status. Owing to high concentration of liquid phase in the near nozzle part, the interface contacting the atmosphere is much smaller than the dispersed status at the lower part. Therefore, the heat transfer is more efficiency from the lower part than the upper part. The stratification of gas temperature will slowly form and be enhanced along the experiment process.

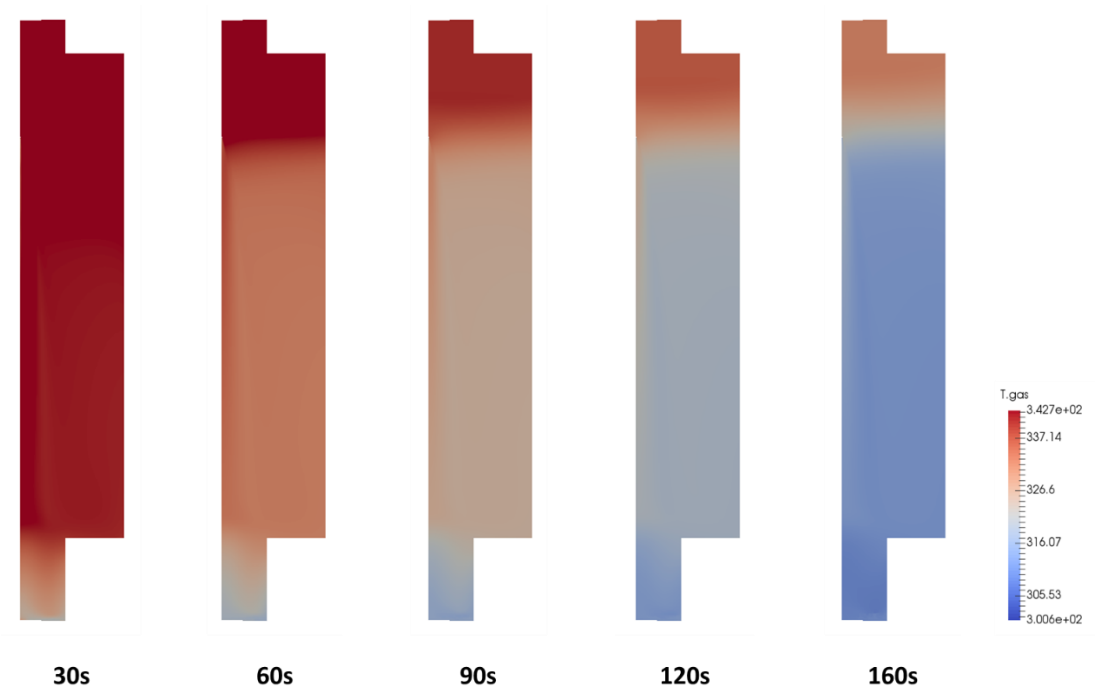

Figure 48 Temperature change during the whole period

4.5 Conclusion and summary

The validation of the Eulerian-based spray cooling model system introduced in Chapter 2 has been proceeded in this chapter. The international severe accident benchmark THAI has been taken as the benchmark in the numerical study. According to the comparison between the simulation and experiment, it has been shown that the physical models can be able to provide a reliable prediction on spray evaporation cooling problem in nuclear containment.

With the contribution of the work in this chapter, the detailed simulation of nuclear containment spray cooling in a stable atmosphere has been guaranteed. However, in a general situation of spray cooling, the turbulence may also exist in the containment, concerning the high-speed flow jet injected from the broken pipe.

The turbulence effect can be brought into the depressurization process, as the turbulent mixing can provide a much stronger effect on cooling. It is also reasonable to bring turbulence into consideration, as the jet flow leaking from the primary coolant pipe could easily turn the atmosphere into turbulent status by its free shear effect when severe accident happened. Such topic will be further discussed in next chapter, as way to provide a comprehensive modeling of containment spray process.

5. Stochastic Field Method modeling on turbulent spray evaporation in a containment-like case

With all the physical modeling of mass transfer, momentum transfer and energy transfer widely studied and validated in the previous chapters, the detailed CFD simulation containment spray in stable atmosphere is ensured. However, turbulence is also a common phenomenon during accident status of nuclear containment, as discussed in previous work [176]. Therefore, a simulation work of spray cooling process in a containment-like case will be further studied, in order to validate the Stochastic Field Method modeling on turbulent scalar transport discussed in Chapter 3. With the work of this chapter, the effort on detailed CFD simulation on containment spray cooling is complete, which set up a practical guideline for real containment study and also provide data source for the coarse grid CFD simulation going to be discussed in the following chapters.

5.1 Introduction

The emergency cooling of hot atmosphere heated by primary loop leaking is one of the most important tasks in nuclear safety study [177]. During accident condition, the spray system installed on the top of the containment will be active, which tries to depressurize the pressure to a safe level and also cool down the atmosphere, as way to decrease the thermal and mechanical stress harming on the containment structure. At the same time, some subordinate functions like radiative aerosol washing and removal will also be realized, as way to enhance environmental protection mission of nuclear reactor during severe accident condition.

The behavior of nuclear containment spray has been widely studied during the last two decades [49]. However, the focus is mainly put on the spray cooling of the stable atmosphere. The flow is slow and weak during such a situation, which mainly triggered by the shear from the spray injection and the natural convection. However, when server accident condition happened, large amount of the coolant would be released into containment with high velocity. If the break in the LOCA accident large enough, there would be supersonic coolant jet injected into the containment and flashed into steam vapor. Therefore, there could be strong turbulence in the containment atmosphere, owing to the free shear effect from the break flow.

Several nuclear containment benchmarks have been set up during the past two decades, like TOSQAN, MISTRA, THAI and PANDA introduced in Section 1.4.1. However, nearly all the experiments done based these facilities only target on the spray cooling process under stable or laminar atmosphere, while leaving the study of spray evaporation under turbulence still blank. In this chapter, the study based on a dryer facility experiment [178] will be given instead, which got similar geometric characteristics and working conditions compared with nuclear reactor containment.

5.2 Methodology on turbulent spray evaporation simulation

The spray process in nuclear containment is a two-phase multi-component flow problem, which includes gas phase and liquid phase, while the gas phase is further mixed by the air component and the water vapor component. During the cooling process, evaporation effect needs to be considered, which includes energy transfer and phase change process. All the above phenomenon can be influenced, when the atmosphere flow is under turbulent condition. Therefore, the spray cooling process under turbulence is an even more complicated physical process.

For the continuous phase, the property of continuity like a single-phase flow is well kept. Therefore, the traditional Eulerian approach is used. For the discrete phase, both Lagrangian approach and Eulerian approach can be the possible choices. Lagrangian approach shows as more elegant way on modeling discrete droplets compared with Eulerian approach, as each single droplet can be traced during the process and individual characteristics like diameter, temperature and velocity can be well kept. However, the Lagrangian approach put heavy stress on the computing ability and memory capacity, as the location, momentum and energy should be saved for the moment in computer memory and updated for the next moment by calculation. Normally, an injection with 10 million – 100 million droplets is not rare in large-scale problem like nuclear containment, which makes the calculation even tougher. On the contrary, the Eulerian approach implements cell volume fraction instead to locate spray droplets, which is cheap and fast on prediction, while the averaged property of Eulerian approach fits the requirements of engineering applications. Therefore, Eulerian approach wins over Lagrangian approach, and is chosen as the modeling approach of discrete phase in this work.

When the gas phase in the containment turns into turbulence, the fluctuations from the air flow will influence the volume fraction transport and mass transfer process, as both phenomena include non-linear parts. Details about this topic can be referred to Chapter 3. The traditional statistics-based turbulence models, like RANS and LES approaches, are widely used on passive scalar transport simulation. However, the non-linear term can’t be well treated through traditional Reynolds averaging process, which makes RANS family methods heavily rely on experimental models. Though LES can in a degree relieve the closure problem by real-time resolving the volume fraction or temperature carried by the large eddies, the spatial scale resolution and the time scale resolution make LES hard to handle upon large-scale industrial applications.

Based on a realization of PDF method on Eulerian fields, Stochastic Field Method is easy to construct and cheap to calculate. In addition, Stochastic Field Method avoids the closure problem by bringing into a stochastic equivalent system, which gives better performance on keeping non-linear characteristics of the convection and source terms. Owing to the good compatibility with Eulerian solver, the method is easily extended to the traditional CFD code platforms. Therefore, the turbulent fluctuation of gas flow effect on volume fraction transport and phase change during energy transfer is modelled by Stochastic Field Method.

5.3 Dryer experiment introduction

Concerning the limitation of spray cooling experiment done under turbulent flow in nuclear community, the benchmark is chosen from food industry, with the geometric characteristics and

the physical effects similar to nuclear containment.

As shown in previous studies [179] [180], the spray dryer is a widely-used facility in chemical industry, like food, detergent and pharmaceutical product processing. It is designed to turn wet materials into dry form. During the process, liquid feed like milk or maltodextrin will be injected into the large volume space of the dryer. Owing to the hot atmosphere and turbulence mixing, the liquid fraction in the feed will be vaporized, leaving the pure material as powders. Compared with other technologies, less volatile or thermal labile compounds will be sacrificed by spray drying, which makes the method widespread adopted in food industry.

The spray benchmark in the work follows the experiment done by Kieviet [180]. The facility is a small-scale test case, with total volume around 10.3 m^3. The dryer consists a cylinder part as the main area of the liquid feed drying, as well as a cone part at the lower part to collect the product powders. The structure of the vessel is designed to prevent the dry powders from accumulating on the wall or bottom. The dryer got a diameter of around 2.2 m and a total height of 3.7 m, where the height of the cylinder part is 2 m and the height of the cone part takes 1.7 m. The details of the geometric design can be found in **Figure 49** and the work [180].

The nozzle is put on the center of the roof. In this case, the pure water spray experiment is taken as the benchmark, which got a mass flow rate of 42 kg/hr. Based on the measurement during the experiment, the spray forms an angle of 73º in the near-nozzle part. On the roof of the dryer, there's also an annulus inlet around the nozzle, which provides co-current hot air flow into the vessel. The air flow inlet got a width of around 4 cm and a volume flow rate of 0.421 m^3/s. Based on the measurement of the air distributor, the hot air got a temperature of around 468 K, turbulent kinetic energy of around 0.027 m^2s^{-2} and turbulent energy dissipation rate of around 0.37 m^2s^{-3}. The turbulent air flow is used to enhance the heat-exchange between the products and atmosphere, so as to offer a better drying effect.

Initially, the chamber of the dryer has already been preheated to 468K, with humidity of 0.009 kg per kg dry air. At the lower part near the outlet of the cone part, a discharging pipe is installed with a diameter of around 17 cm. The pipe is connected to an air pump, which generates a relative pressure of -150 Pa, as way to discharge the hot, which stops over-drying of the products.

5.4 Numerical settings

In this work, the OpenFOAM package is extended with the module of Stochastic Field Method in its two-phase turbulence model library, in order to treat the turbulent effect on spray cooling in the dryer case.

To overcome the non-linear turbulent effect on volume fraction transport and energy transfer, 10 Stochastic fields on volume fraction and temperature are constructed during each time step, as way to implement the Stochastic Field Method. Another group is done during the meantime with pure Eulerian approach, which has no modeling on turbulent scalar transport. The comparison between two groups of simulation will be proceeded to study the influence of the Stochastic Field Method on turbulent spray cooling.

Since the vessel is geometrically axis-symmetric, a 2D mesh is used to simulate the problem, with total mesh cell number of 16600 and mesh size of 0.02m. The time step is chosen as 0.001 s.

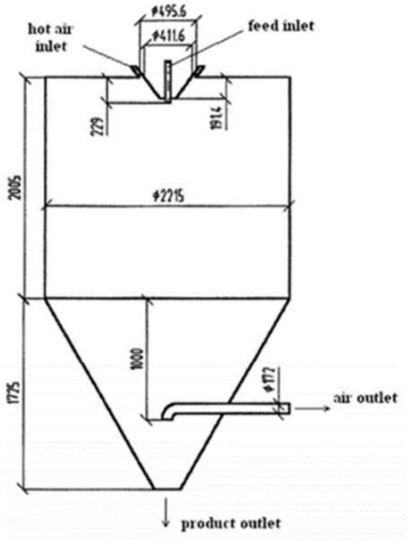

Figure 49 Geometric design of the dryer [180]

Figure 50 Dryer mesh used in simulation

The modeling settings and numerical settings are chosen as shown in **Table 8 and Table 9**.

Table 8 Modeling setting in OpenFOAM simulation

Physical Process	**Modeling**
Continuous Phase	Eulerian
Discrete Phase	Eulerian
Turbulent effect on volume fraction	Stochastic Field Method
Turbulent effect on mass transfer	Stochastic Field Method

Table 9 Numerical setting in OpenFOAM simulation

Time step	0.001s
Total time	160s
Mesh size	0.02m
Total mesh cells	16600

5.5 Results and discussion

During the experiment, the thermocouples are put at 5 different locations along the vertical direction, while also 5 ones along the radical direction, which totally makes 25 measure points in the dryer. The details of measurement configuration can be found in [180]. The simulation is proceeded for 160 s. The comparison of temperature between the simulation and experiment is provided in **Figure 51-56**.

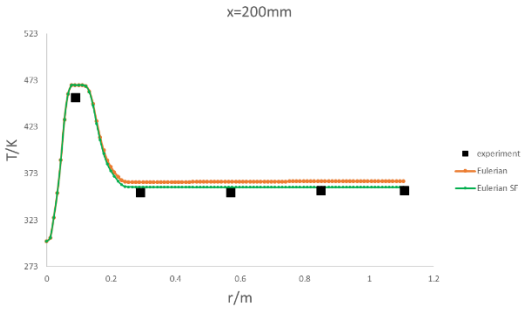

Figure 51 Result at the height of 200mm

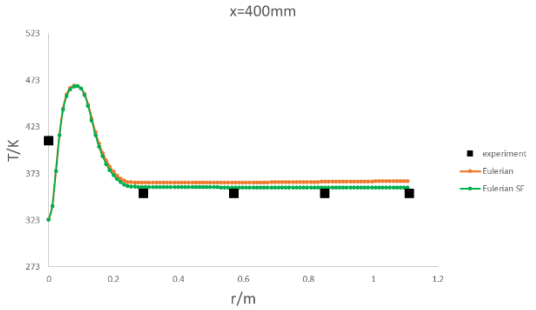

Figure 52 Result at the height of 400mm

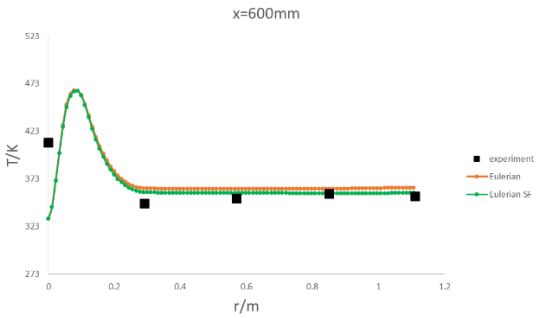

Figure 53 Result at the height of 600mm

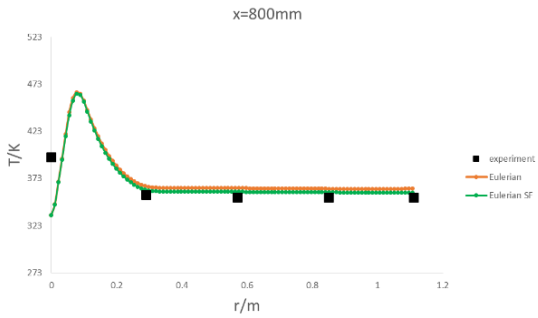

Figure 54 Result at the height of 800mm

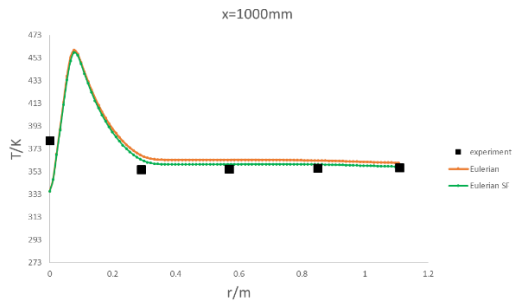

Figure 55 Result at the height of 1000mm

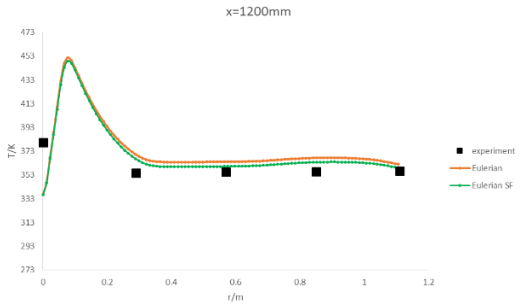

Figure 56 Result at the height of 1200mm

Based on the results shown in the above figures, it can be observed that Eulerian approach has successfully provided a good prediction of the real process, with acceptable error compared with the experiment. The performance near the axial centerline part has larger difference than other measure points. The overestimation of the cooling effect comes from the weakness of particle diffusion in Eulerian modeling, which makes the assumption treating liquid droplets as continuous liquid injected from the nozzle with strong inertial property. In real process, the atomization process will happen near the nozzle part, which results in a wider spreading of the liquid droplets. However, real-time simulation of atomization process demands grid size much smaller than nozzle diameter, which beyond the ability of computing in real engineering circumstance. Therefore, rather than real simulation of particle dispersion for a single droplet, Eulerian approach implements a field-based modeling considering all the physical effect influencing the diffusion of liquid phase, which underestimates the process. As a result, large bulk of liquid still accumulated around the nozzle down part, which generates a low temperature zone near the center line. However, around the measure points in the large space where the liquid phase only occupies negligible volume fraction, Eulerian approaches have offered a reliable prediction compared to the

experiment.

Owing to the results in Figure 51-56, it can also be seen that Eulerian simulation coupled with stochastic field method gives a better performance compared with the normal Eulerian simulation. This is because the additional turbulence effect upon droplet evaporation has been considered by the stochastic field method modeling, while the further turbulent transport of droplets in the means of volume fraction has been taken into account at the same time. Therefore, the cooling process is closer to the real physical process, which provides a better matching between the numerical simulation and the experiment.

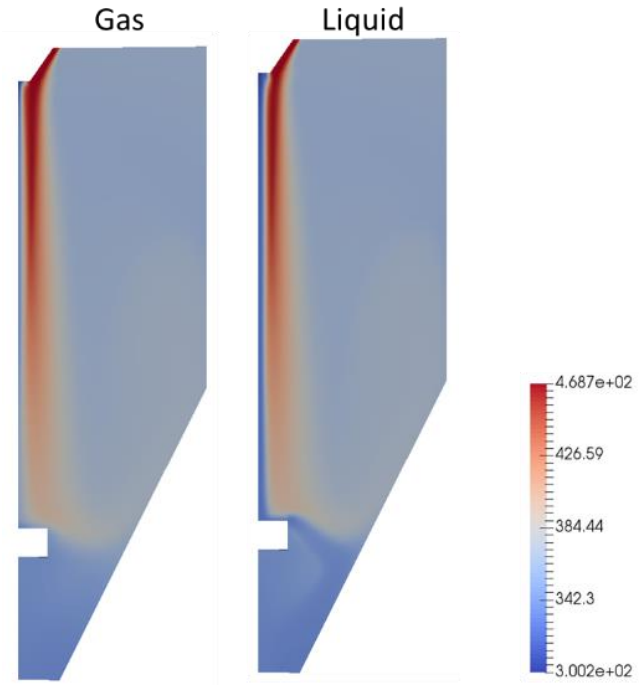

Figure 57 Temperature contour of gas and liquid phases

The final distribution of temperature of gas and liquid phase have been shown in the **Figure 57**. According to the simulation result, gas and liquid nearly reach a temperature homogenous status at 160s. The liquid temperature is much cooler in the axis part compared with the gas phase. This is because the liquid droplet got a much higher volume fraction in the central part, where the evaporation effect is much weaker compared with other locations. Therefore, the temperature is also much lower. Near the outlet discharging pipe area, there's also a lower temperature area. This phenomenon shares a similar reason like above. The liquid phase hit on the pipe and drop down, the air flow will carry those droplets to the wall of the dryer, which forms a lower temperature region in liquid temperature contour.

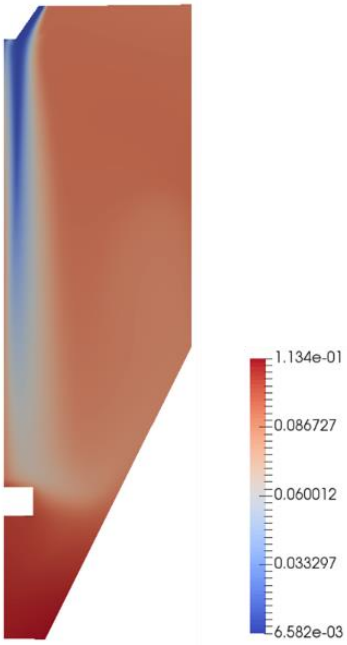

Figure 58 Steam vapor mass fraction distribution

There's a low steam vapor mass fraction area near the axis, as shown in **Figure 58**. This area is mainly the near-nozzle area. The hot air has been injected into the vessel from the nozzle on the roof with a high velocity, which makes the area mainly occupied by the gas phase. Therefore, such a low steam vapor mass fraction part existing here. Such area also shows the potential to enhance the heat exchange on nozzle location and vessel geometric design.

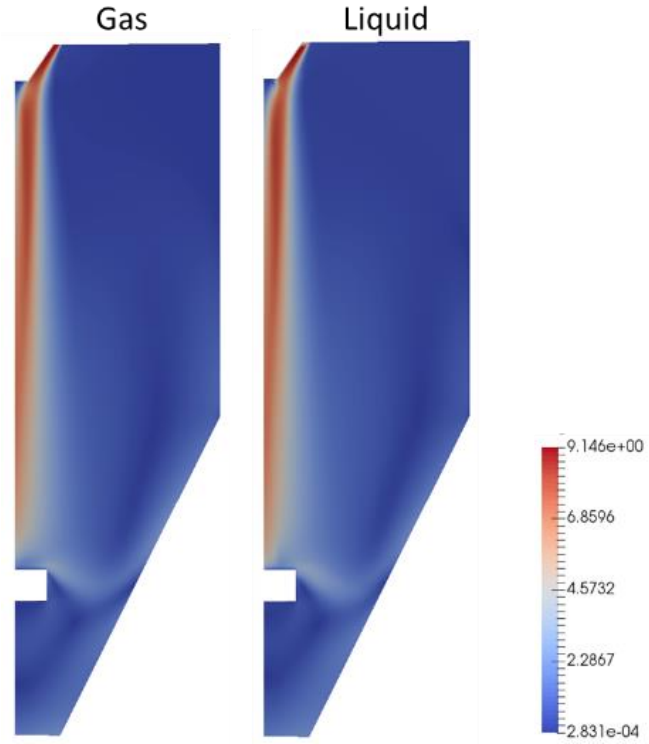

Figure 59 Velocity contour of gas and liquid phases

As shown in **Figure 59**, the gas phase and the liquid phase have nearly reached the momentum equilibrium status at the time 160s. In the spray cooling process of containment-like size problem. The spray can be treated as dilute spray, during which the liquid phase only occupied a quite small volume fraction. Owing to the little momentum liquid phase carries, the two phases will be balanced following the gas phase, as shown in the figure. There's some tiny difference between the gas phase and the liquid phase in the upper part near the spray nozzle. This is because the place got large volume of liquid cumulated around the water inlet.

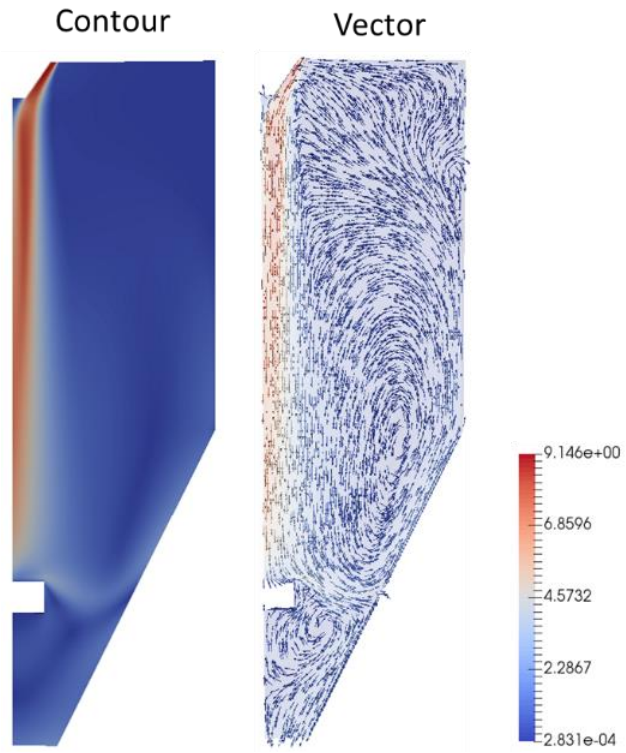

Figure 60 Vector plot of gas phase velocity distribution

The right part of **Figure 60** has shown the gas phase velocity contour and its vector field. As shown in the vector field of the velocity. The high velocity zone is located at the central part, owing to the hot air injection. There's strong re-circling in the middle part of the vessel. This comes from the free shear effect from the central high velocity zone, the wall shear from the vessel and the blockage of the discharging pipe. There's also weak re-circling area in the bottom part, which resulted from the free shear of the air flow blocked by the discharging pipe.

5.6 Conclusion

This chapter has further studied the turbulence effect on the spray evaporation cooling process in nuclear containment. By theoretical study given in Chapter 3, the non-linear characteristics of volume fraction transport and droplet evaporation model will be both influenced by the turbulent fluctuation. Owing to the restricts of traditional statistics-based turbulence modeling approaches, Stochastic Field Method will be implemented coupled with the Eulerian spray model discussed and modelled in previous chapter on studying the effect.

Considering the experiments done in benchmarks of nuclear engineering community mainly focus

on evaporation in steady atmosphere, a dryer evaporation case is taken instead, which is similar to the geometric and physical characteristics of the nuclear containment case. The open source package OpenFOAM is used and further extended on realizing Stochastic Field Method onto the spray model. Based on the comparison between the traditional method and the Stochastic Field Method, it can be observed that additional cooling effect existing during spray process when turbulence existing. By implementing the new method, the turbulent effect can be taken into account and get a better prediction performance.

With the studies in the recent two chapters, the detailed physical modeling of nuclear containment spray process has been set up. With this work, the mechanism-based CFD study on new type containment or new working condition can be guided by the modeling approach here. Furthermore, the well-established modeling provides solid fundamental on Coarse Grid CFD of nuclear containment studied in the following chapters.

6. Coarse Grid CFD

With the exhaustive study on modeling of spray cooling process in nuclear containment, the practical guideline for detailed CFD analysis on containment spray issues has been proposed. As shown in the previous chapters, the sophisticated modeling approaches on spray cooling and turbulence are able to provide a reliable result on the containment simulation, but low speed in practice owing to the treatment of each sub-module.

In real engineering design, the fast prediction is necessary for the industrial planning. Concerning duplicated times of modification in geometry and working condition may be required during the design stage, the fine numerical simulation of the containment will largely delay the schedule of the whole engineering plan. Therefore, the acceleration solution on numerical simulation could promote the efficiency and the economy of the engineering project.

Coarse Grid CFD is a new-born method on speeding up the traditional CFD analysis. The method implements a data-driven approach, which is popular since the evolving of data science. Concerning large amount of data have been produced and saved in the past two decades, Coarse Grid CFD will generate proper coarse models by well taking advantage of the existing data, in order to provide fast simulation on nuclear project design. In this chapter, the Coarse Grid CFD will be introduced in detail. The improvement by physical-based flux correction will be derived and compared with the geometric-based flux correction approach. Later on, the validation of the method will be proceeded on a wired bundle sub-channel flow case.

6.1 Introduction

Coarse Grid CFD is a new method targeting on engineering CFD simulation of the super large-scale industrial problems. The mechanism-based simulation of physical process upon engineering designs will face challenges from both the mesh size and the time step, concerning its large scale and long lasting. The mesh size always has to be set to a super tiny scale, in order to fit the complicated structure of the nuclear equipment. Like in the nuclear containment problem, a real containment in commercial nuclear power plant will have a volume of 100 m^3 as a normal case. However, the small-scale structures like manway, stair, double roof are also existing with geometric scales much smaller than the containment size. The resolution of those tiny designs requires small mesh size setting, as well as the unstructured grid cells, which add further calculation amount to the simulation and influence the iteration convergence. In addition, the time step has also been required to be a small value. Following the CFL (Courant–Friedrichs–Lewy) condition, the CFD calculation will get diverged after CFL number over 1. The CFL number is defined as

$$CFL = U\frac{\Delta t}{\Delta x'}, \tag{6.1}$$

where U is the local velocity, Δt is the time step and Δx is the mesh size.

Therefore, the time step has to keep small, concerning the tiny mesh size used in engineering applications, which further increase the total calculation amount and promote the total simulation time cost.

In the spray cooling problem discussed in previous chapters, several days are needed until one group of results is caught, if traditional sequential running is implemented. Though able to handle by parallel running on modern scientific computing cluster, the solution is still far away from the requirements of fast iteration in industrial design and modification and cheap in operation. Therefore, the import of Coarse Grid CFD on solving large-scale problem provides a potential solution for practical engineering applications

6.2 Related Works

Coarse Grid CFD is a new-born method aimed at solving repeated problem in engineering by taking use of fine simulation data. The early work has been on Class, Andreas G. et al [181] at APS 2010 meeting, which introduced the basic idea and strategy on applying Coarse Grid CFD. Later on, the work has been done on anisotropic porosity formulation of the method [182]. Some studies [183] [184] [185] [186] [187]have been further done on application of Coarse Grid CFD on wire wrapped fuel assembly. Some recent work [188] [189] have also been done discussing the possible way of flux correction and sub-channel blockage treatment.
Most of the previous work mainly focus on the geometric-based flux correction approach on realizing Coarse Grid CFD. The application is also limited to the open channel flow case. In this work, the extension of Coarse Grid CFD by physical-based flux correction and treatment of blocked channel flow will be further studied.

6.3 Coarse Grid CFD

6.3.1 Classic CFD simulation with turbulence modeling

Though Navier-Stokes Equations has already been set up by Claude-Louis Navier and George Stokes two centuries ago, there still has been no analytical solution derived even until now. Actually, even the existence and smoothness of the Navier-Stokes Equations are not proved yet, which still stay as one of the seven most important open problems in mathematics. Owing to the difficulty on analytically solving Navier-Stokes Equations, the experimental approach has been adopted instead as the main choice on fluid mechanism studying. However, certain drawbacks have been revealed over the past century. Firstly, experimental facility plays as an expensive solution. Experiment of industrial application always got large volume, together with special measurement devices, which could occupy a large part of the engineering budget. Secondly, experimental approach is dull on modification. During the design of the experiment facility, the usage of Similarity Laws restricts its freedom of further extension. Lastly, experimental studies can be time-consuming. Though a real process on proceeding the experiment is high efficiency in time, the construction of the experimental facility can take several months as a minimum. Therefore, the experimental approach is facing challenge, since the industrial application becomes more and more complex in both geometry and physics.
Numerical approach, as a method to solve partial differential equations in a discrete way, turns out as a third solution of fluid mechanics problem. The application of finite difference method in fluid

mechanism was first discussed in Richarson's book [117]. Later on, new methods [155] are derived on numerically solving fluid mechanics problem, like FVM (Finite Volume Method) and FEM (Finite Element Method). It is believed to be the first work on CFD-based solving 3D Navier-Stokes Equations that the T3 group has done at Los Alamos National Lab. Ever since then, lots of studies and commercial codes on CFD analysis have evolved to solve all kinds of problems related to flow, like aerodynamics, combustion, magneto-dynamics, etc.

The difficulty and complexity of fluid mechanics problem mainly come from turbulence. As discussed in Section 2.2, turbulence is a non-linear chaotic process, which not only has influence on the momentum prediction, but also got strong effect on the passive scalar solution. The treatment of turbulent flow still relies on turbulence modeling, like RANS, LES, DNS, PDF, etc. Following popular engineering turbulence model, RANS, the governing equation of fluid mechanics with turbulence model can be derived as

$$\nabla \cdot U = 0, \tag{6.2}$$

$$\frac{\partial U}{\partial t} + U \cdot \nabla U = -\frac{1}{\rho}\nabla p + (\upsilon_l + \upsilon_t)\nabla^2 U, \tag{6.3}$$

where U is the velocity, p is the pressure, ρ is the density, υ_l is the laminar viscous coefficient. Following the Boussinesq eddy viscosity assumption, υ_t is the turbulent viscous coefficient, which is modelled by the turbulence model.

RANS family models include a bundle of models like k-ε model, k–ω model, RSM, etc. Normally one or two additional equations will be attached to the solution process. Moreover, further treatments are necessary in special areas like the near-wall area. Sometimes, even with the simplest turbulence model like RANS, CFD prediction still requires super computer if industrial application large enough.

In a brief summary, the classic CFD got the following drawbacks,

1. **Large Calculation Amount**. A rigorous CFD needs to resolve all the flow structures like boundary layer, which therefore ask for enough mesh cells capturing the local phenomenon. Even simple models used, additional equations of the turbulent statistical values are still needed on turbulence modeling, which brings in more computing requirements.
2. **Complex Treatment**. Extra attention needs to be paid in classic CFD analysis, like the wall function. The 1st floor of mesh cells needs to be step-by-step modified until the wall function can be implemented, which demands certain times of iterations.
3. **Meshing Difficulty**. In real engineering products or solutions, the irregular geometric profile is a common situation during designing process. By classic CFD, sophisticated skills are needed on meshing, which generate a great deal of tiny unstructured mesh cells. The meshing task is a tough job on both time and energy. The quality of mesh could be the trigger on divergence in solution iteration.

6.3.2 Derivation of Coarse Grid CFD

Coarse Grid CFD aims to promotes the simulation efficiency, while still maintain the basic characteristics of Classic CFD approach. As discussed in previous section, the fine simulation done by Classic CFD is both expensive and time-consuming. In nuclear engineer, even more difficulties can be found, due to the large separation of scale range. The smallest scale in nuclear reactor can be down to sub-millimeter level within fuel assemblies, while as large as tens of

meters when comes to the dimensions of the reactor core or even the reactor vessel and containment.

In industrial applications, the repeated phenomenon is quite common in both geometric and physical viewpoint. It is not rare to see the similar parts or components in the engineering devices. Like in the nuclear containment spray, the nozzles are always symmetrically distributed on the roof, which got similar cooling effect compared with each other. It is also common situations to proceed groups of simulations with only slight change on initial or boundary conditions. Like in pipe flow and channel flow, a group of CFD analysis will be done with partly modification on the velocity boundary condition, but leaving geometric information unchanged. Large amount of data is generated during the process, but not well dug for further value.

Coarse Grid CFD is designed to overcome the deficits of Classic CFD, by well exploring the fine simulation data. By using proper flux correction, the fine simulation data can be mapped onto the coarse mesh cell, as way to provide a data-driven model for industrial applications. Therefore, an industrial-level resolution can be achieved, which is lower than Classic CFD, but substantially higher than system code level.

By integrating over the incompressible Navier-Stokes Equations at an industrial-level scale, the governing equation of Coarse Grid CFD can be derived as

$$\nabla \cdot \boldsymbol{\alpha} U = 0, \tag{6.4}$$

$$\frac{\partial U}{\partial t} + (U \cdot \boldsymbol{\beta} \nabla) U = \boldsymbol{F_T} - \frac{1}{\rho} \nabla p, \tag{6.5}$$

where $\boldsymbol{\alpha}$ is the volume porosity of the flow, $\boldsymbol{\beta}$ is the surface permeability of the flow, and $\boldsymbol{F_T}$ is the Coarse Grid volumetric force.

The key idea of Coarse Grid CFD is trying to reuse the fine simulation data from Classic CFD, as way to parameterize and modeling α, β and F_T in the flow of a certain industrial facility, which can be further employed to predict other working conditions under the similar applications.

6.3.3 Volume porosity and volumetric force

One of the advantages of Coarse Grid CFD is the permission of implementing a simplified mesh from the real complex geometry. The inconsistence between the real geometry and the coarse mesh will be covered by volume porosity.

By concerning the solid structures in the flow field, the volume porosity α is used, which is defined as,

$$\alpha = \frac{V_s}{V}, \tag{6.6}$$

where V_s is the volume occupied by the solid part, and V is the volume of the mesh cell, as shown in **Figure 61**.

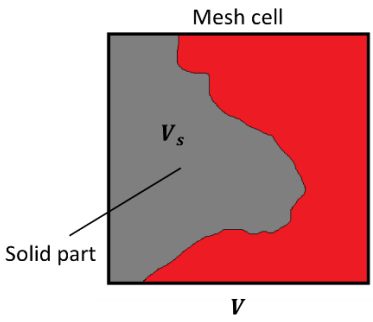

Figure 61 volume porosity

To avoid the complicated modeling of turbulence, a volumetric force model is used instead. The volumetric force stands for the viscous and turbulent influence on the mesh cell, which are mapped into the volume as,

$$F_T = \frac{1}{V}\iiint_V \left((\upsilon_l + \upsilon_t)\nabla^2 U\right)dv, \tag{6.7}$$

where v is the cell volume of the fine simulation mesh, and V is the cell volume of the coarse simulation mesh.

6.3.4 Flux Correction: Geometric-based and Physical-based

Under the influence of geometric inconsistence and the resolution difference between the fine simulation by classic CFD and the coarse simulation by Coarse Grid CFD, the convection term in momentum equation of Coarse Grid CFD requires further modification, which is kind of flux correction from a physical viewpoint. The way of implementing flux correction can be divided into two kinds: Geometric-based and Physical-based.

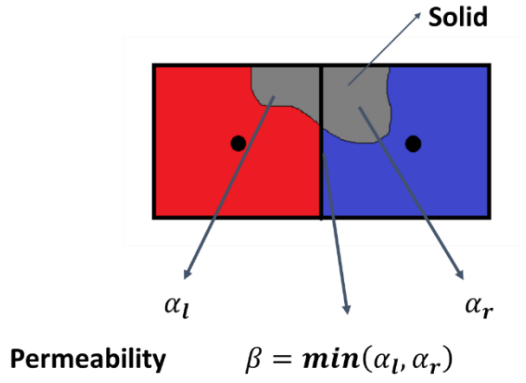

Figure 62 Surface permeability

The Geometric-based flux correction tries to fix the error in a straightforward way by only considering the area on the surface blocked by the solid structure. Therefore, the correction mainly stands for the permeability of flow though the control volume's profile. Considering the difficulty on calculating the real blocked area on the surface, the permeability is got by a cheap way as,

$$\beta = min(\alpha_l, \alpha_r), \tag{6.8}$$

where α_l and α_r are the volume porosities of the neighbor mesh cells, as shown in **Figure 62**.

The Physical-based flux correction further considers the influence of the coarse mesh scale on the flux calculation. As shown above, the Geometric-based flux correction only considers the effect of

the geometric blockage on the surface, while neglecting the error on discretion and interpolation between the two coarse mesh cells. However, under super coarse size of the mesh, the error can be amplified in a certain degree. Like in a coarse mesh with 10 times the size of fine mesh, the error of interpolation will increase from $o(\Delta x^2)$ to $o\left(((10\Delta x)^2)\right)$, which is possible to be more than 100 times when large velocity or pressure gradient existing around the surface, as shown in **Figure 63**.

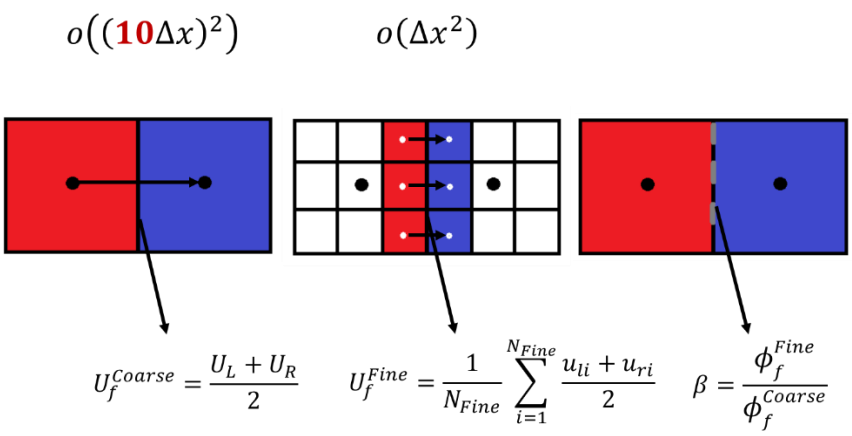

Figure 63 Physical-based correction

The Physical-based flux correction builds up the surface permeability from a way of physical flux difference, which can be calculated by,

$$\beta = \frac{\phi_f^{Fine}}{\phi_f^{Coarse}} \tag{6.9}$$

where ϕ_f^{Fine} is the fine mesh flux defined by,

$$\phi_f^{Fine} = \iint_S U_f ds, \tag{6.10}$$

which is calculated by integrating of the velocity U_f in the fine mesh cell interpolated onto its surface s over the coarse mesh cell surface S.

And ϕ_f^{Coarse} is the coarse mesh flux defined by,

$$\phi_f^{Coarse} = U_f\big|_S S, \tag{6.11}$$

which is calculated by the product of the interpolated velocity $U_f\big|_S$ from the fine simulation to the coarse mesh and the coarse mesh cell surface S.

Considering the task of geometric mapping of surface as more difficult one compared with volume mapping, a simplified way of calculating the fine flux is proceeded by implementing a Gaussian-kernel. It can be derived as,

$$d = \vec{n} \cdot \left(\vec{C}_{FineCell} - \vec{C}_{CoarseSurface}\right), \tag{6.12}$$

$$l = \frac{\sum_{i=1}^{N_{Fine}} \sqrt[3]{v}}{N_{Fine}}, \tag{6.13}$$

$$\phi_f^{Fine} = \frac{\sum_{i=1}^{N_{Fine}} e^{\sqrt{d_i/l_i}} u_i}{e^{\sqrt{d_i/l_i}}} S, \tag{6.14}$$

where $\vec{C}_{FineCell}$ and $\vec{C}_{CoarseSurface}$ are the cell center of the fine mesh cell and the surface center of the coarse mesh cell, $\vec{n}$ is the norm vector of the coarse mesh cell surface, d is the distance between the fine cell center and coarse surface. v is the fine mesh cell volume, N_{Fine} is the fine mesh cells involved into a certain space, which should be an appropriate space with length substantially smaller than the coarse cell dimensions while larger than fine cell dimensions, and l is the characteristic length of the fine cells. u_i is the velocity of the fine cell i, and ϕ_f^{Fine} is calculated through the Gaussian-kernel.

6.3.5 Treatment of the complete solid cells

In the sub-channel flow problem, it is common to meet blockage situation. However, from a numerical aspect, the existing of pure solid cells could bring into the singular problem. Therefore, the treatment on the blockage would need further studies.

Around the pure solid cell, surface permeability will be limited to zero, which makes the pivot coefficient turns into zero and form a singular matrix. Though a small value can be set instead to avoid the problem, the large rate of blockage will give back a high velocity feedback, which produces fake velocity values spreading over the solid cells. From the mathematical viewpoint, a small pivot value will possibly generate large condition number, which brings into further convergence problem.

Target on the problem, two tricks are provided to dump the fake velocity,

1. Implement an artificial high viscosity to physically diffuse the fake velocity, which is derived as

$$\frac{\partial U}{\partial t} + (U \cdot \boldsymbol{\beta}\nabla)U = \upsilon_{art}\nabla^2 U + \boldsymbol{F_T} - \frac{1}{\rho}\nabla p, \tag{6.15}$$

where υ_{art} is the artificial viscosity used to dump the fake velocity.

2. Directly target on the matrix coefficient, by adding large value to the diagonal element of the matrix, which enhances the diagonal dominant property,

$$\left(a_P + a_{dump}\right)U_P^{n+1} + \sum a_N U_N^{n+1} = F_T + Gp^n, \tag{6.16}$$

where a_P and a_N are the diagonal and off-diagonal coefficients. U_P^{n+1} and U_N^{n+1} are the velocities of the center cell and the neighbor cell. G is the discrete gradient operator. a_{dump} is the dumping coefficient used on improving the matrix conditional number.

6.3.6 Numerical Solution of Coarse Grid CFD: Coarse Grid Projection Method

With governing equations modified in Coarse Grid CFD, as shown in equation 6.4 and 6.5, the numerical solution of the system requires further treatment.

As discussed in Section 2.6, a saddle-point problem will be caught when constructing the coefficient matrix from the discrete form of the equations, owing to the velocity-pressure coupling characteristics of incompressible Navier-Stokes Equations. Therefore, a straight-forward way of numerical solving the velocity and pressure at the same time is not possible. Though in the recent

years, some new studies have provided new matrix iteration approaches for the saddle-point problem, the large memory requirement is not welcomed, which makes the decoupled projection methods still the mainstream in incompressible flow solution.

The projection method is derived to solve the incompressible problem, as discussed in Section 2.6.1.1. In a mathematical viewpoint, it's actually a general expression of LU decomposition. The method can be treated as the prototype of the later popular SIMPLE family methods.

As the governing equation of Coarse Grid CFD is different from the classic Navier-Stokes Equation, therefore, a new modification of the projection method needs to be derived, which we name as Coarse Grid Projection Method.

The solution routine of Coarse Grid Projection Method can be summarized as following,

1. Discrete the momentum equation with certain numerical scheme,

$$a_P U_P^{k+1} + \sum a_N U_N^{k+1} = F_T + G p^k, \tag{6.17}$$

where a_P is the diagonal coefficient of discrete matrix for momentum equation, while a_N is the off-diagonal part. G is the discrete coefficients of pressure gradient following certain numerical scheme.

2. If U^{n+1} got from the last step is named U^*, by reforming equation 6.5, a new expression of U^* can be derived as

$$U^* = \frac{H(U^*)}{a_P} + \frac{\frac{1}{\rho}\nabla p}{a_P}, \tag{6.18}$$

$$H(U^*) = \sum a_N U_N^* + F_T, \tag{6.19}$$

Different from original projection method, the governing equation of Coarse Grid CFD doesn't keep the divergence-free condition of velocity, owing to the existence of volume porosity. Therefore, Coarse Grid Project Method tries to derive a new pressure Poisson equation, by putting equation 6.4 into equation 6.19 and integral over velocity, which got an expression as,

$$\sum \left(\frac{1}{a_P \rho}\nabla p\right)_f \alpha S_f = \sum \left(\frac{H(U^*)}{a_P}\right)_f \alpha S_f, \tag{6.20}$$

3. If p got from the last step is named p^*, based on equation 6.19, the final velocity solution after correction from continuity is derived as

$$U^{**} = \frac{H(U^*)}{a_P} + \frac{G p^*}{a_P}, \tag{6.21}$$

Only until the norm of difference between the new solution U^{k+1} and the latest iteration step solution U^k is held below a certain criterion, the iteration will be kept proceeding. A detailed procedure can be found in **Figure 64**.

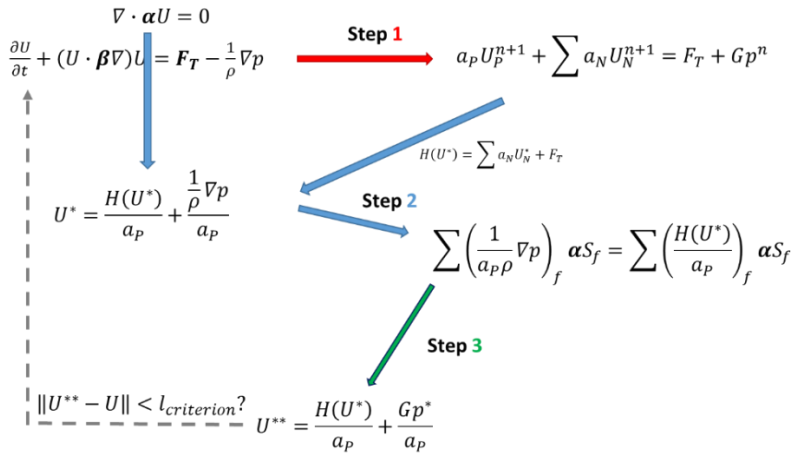

Figure 64 Workflow of coarse grid projection method

6.4 Case Study

To validate the performance of Coarse Grid CFD on real industrial applications. The simulation of the flow in blocked liquid-metal-cooled fuel assemblies will be proceeded. The result will be compared with the experiment data in the MAXSIMA project.

6.4.1 Experiment description

The thermo-hydraulics is a key topic in the nuclear reactor core study. Under the framework of EU FP7, the MAXSIMA (Methodology, Analysis and eXperiments for the Safety In MYRRHA Assessment) project was set up. The objective of MAXSIMA is to provide a solid fundamental of safety study in MYRRHA assessment, which is a flexible fast spectrum research reactor with a capacity of 50-100 MWth. MYRRHA (Multi purpose hYbrid Research Reactor for High tech Applications) is one type of the accelerator driven system (ADS), which works under sub-critical and critical conditions. A multiplying core made by MOX fuel is used in MYRRHA, which implements liquid lead-bismuth (Pb-Bi) as the coolant. The flow characteristics in the core is one of the targets in MAXSIMA project.

7 work packages are included in MAXSIMA. Owing to the objectives of Work Package 3, the experimental study was done on the interaction between the fuel pin and the coolant at the Karlsruhe Liquid Metal Laboratory (KALLA). Under operation condition, MYRRHA is able to generate inacceptable high temperature of the fuel cladding around the blocked fuel assembly. The experiment is set up to study the extent of the potential blockages' influence, which resulted from the corrosion products of the liquid metal coolant.

The experiment of the blocked liquid-metal-cooled fuel assemblies is performed by a 19-rod bundle with wire-wrap spacers to fix it. Two solid blockages are put along the bundle at the height of 492 mm and 711 mm as shown in **Figure 65**, which stand for the crude deposition from the interaction between the fuel assembly and the liquid metal coolant. A more detailed description of MAXSIMA project and summary of experimental and numerical study can be found in [193].

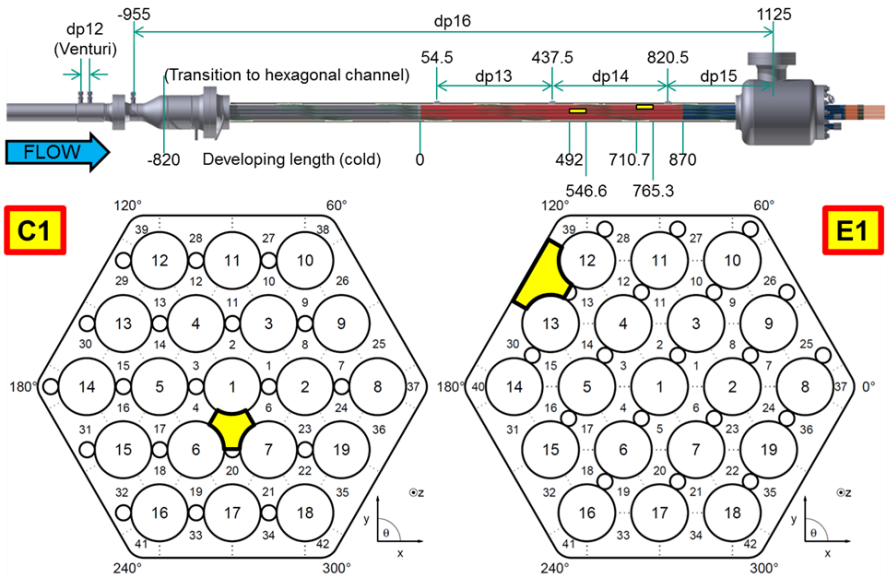

Figure 65 Experiment facility in MAXSIMA project[193]

CAD model following the experiment is built as shown in **Figure 66** and **Figure 67**. The whole bundle contains 19 pins, together with wire-wrap spacers surrounding each of them. The fuel rod got a length of 870 mm and a diameter of 8.2 mm. Compared with the pin, the wire-wrap got an axial pitch of 328 mm and a wire diameter of 2.2 mm. Under the experiment condition, the liquid metal, Lead-Bismuth-Eutectic (LBE) is chosen as the working material and a velocity of 1.7m/s is chosen as the inlet boundary condition.

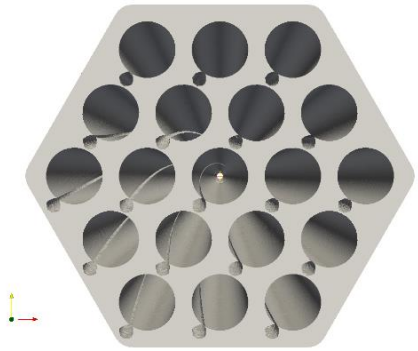

Figure 66 Front view of the CAD

Figure 67 Overall view of the CAD

6.4.2 Numerical settings of the fine simulation

To validate the behavior of Coarse Grid CFD. A fine simulation is first done to provide data for the coarse modeling, as well as a reference to validate the performance of the coarse grid simulation. Following the MAXSIMA experiment, a fine mesh is constructed according to the sub-channel structure with blockage, as shown in **Figure 68** and **Figure 69**.

In order to provide detailed flow field information, all the geometric characteristics must be covered by the fine mesh, which including the wedged region between the wire and the rod, well also between the wire and contact points. The fine cells are clustered in the vicinity of surfaces of the rod and the wire surfaces, so as to well resolve boundary layers developing process in the

sub-channel. At least two layers of thin cells will be put upon the surfaces of the rods, the wires and the bundle wall, as shown in **Figure 70**. At last, a highly unstructured mesh is generated with about 3 million cells.

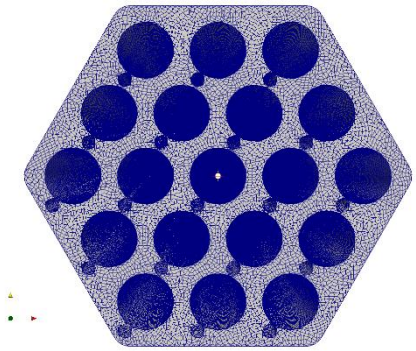

Figure 68 Front view of the fine mesh

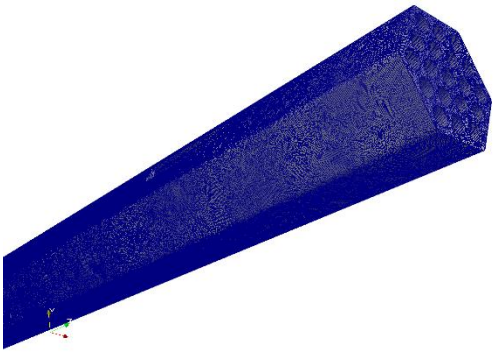

Figure 69 Overall view of the fine mesh

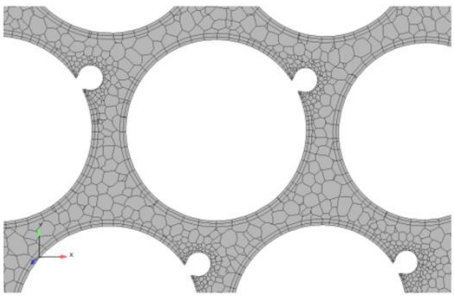

Figure 70 Near wall meshing on treating the boundary layer

For fine simulation, the boundary conditions and numerical schemes are set as Table 10, Table 11 and Table 12.

Table 10 Boundary settings of the fine simulation

Location	**Boundary Type**
Velocity inlet	Dirichlet Type (fixed value of 1.7m/s)
Velocity outlet	Neumann Type (gradient of 0)
Pressure inlet	Neumann Type (gradient of 0)
Pressure outlet	Dirichlet Type (fixed value of 0)

Table 11 Turbulence model and numerical schemes used in fine simulation

Equation terms	**Model and numerical scheme**
Turbulence modeling	k-epsilon model
Wall function	two-layer all y+ wall treatment
Momentum convection term	Second-Order Upwind
Turbulent kinetic energy convection term	Second-Order Upwind
Turbulent dissipation rate convection term	Second-Order Upwind
Diffusion term	Linear discretion with correction
Gradient term	Hybrid Gauss-Least Squares Method

Table 12 Linear solver setting in the fine simulation

Solver	**Choice and value**
Velocity solver	Algebraic Multi-grid (AMG)
Pressure solver	Algebraic Multi-grid (AMG)
Momentum equation relaxation factor	0.7
Pressure equation relaxation factor	0.3
Convergence tolerance	0.1

By SIMPLE iteration until the steady condition reached, the contour and streamline of the overall flow field are shown in **Figure 71** and **Figure 72**. According to the result, some basic characteristics of the bundle flow can be caught.

The velocity distribution over the whole bundle is regular and smooth. Compared with the inner sub-channels, the outer ones and the near-outline area got higher velocity. The areas near the wire-wrap spacer part have generated a low-velocity area. Around and after the two blockages, low velocity zone can also be observed.

Figure 71 Velocity contour of the flow in fine simulation

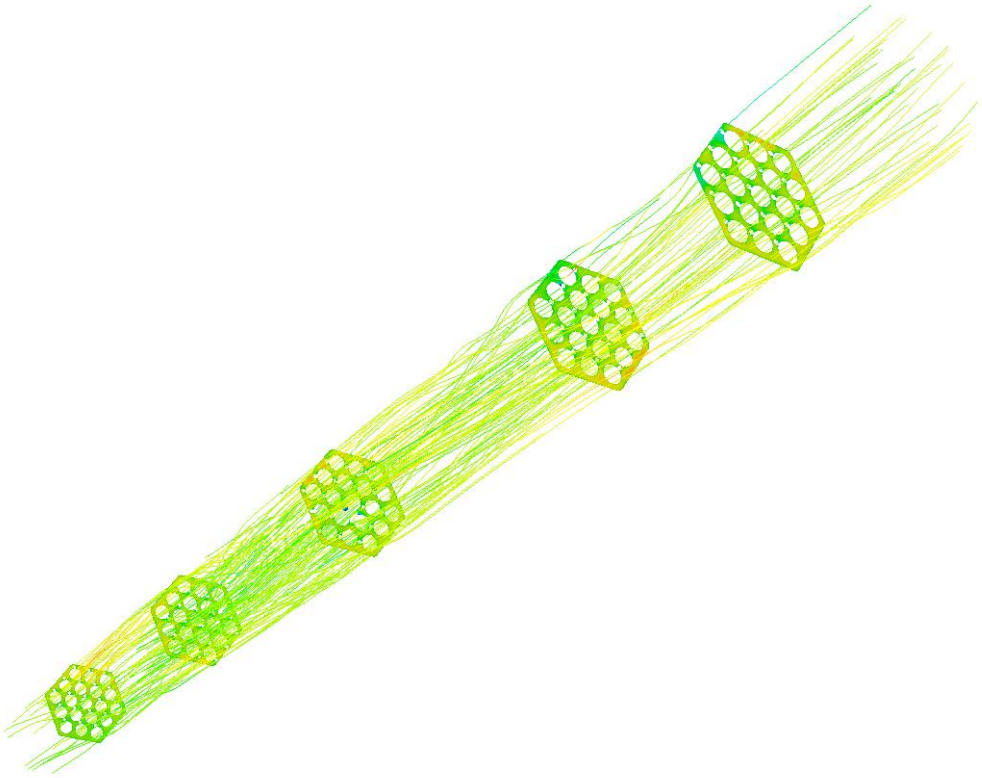

Figure 72 Streamline of the flow in fine simulation

6.4.3 Numerical settings of the coarse simulation

The coarse grid simulation will be proceeded, following the Coarse Grid CFD approach as described in Section 6.3. Compared with the fine mesh, the coarse case only applies a mesh with around 15000 cells, as shown in **Figure 73** and **Figure 74**.

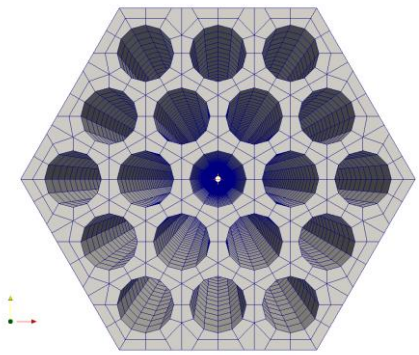

Figure 73 Front view of the coarse mesh

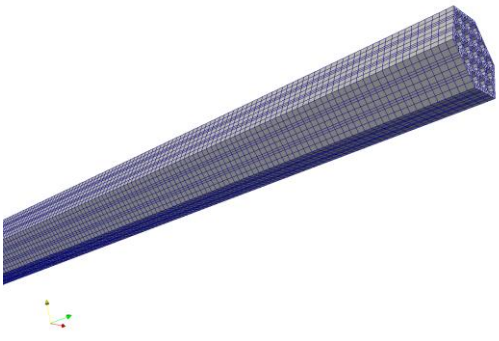

Figure 74 Overall view of the coarse mesh

The detailed meshing near the solid is not required any more, as the resolution of boundary layer effect will be considered in volumetric force when extracting data from the fine simulation. In addition, the irregular structures like blockage and wire will also be neglected during the meshing process, while using a volume porosity by mapping CAD onto the coarse mesh instead. As shown in **Figure 75** and **Figure 76**, the volume porosity field around the blockage got a zero value, while

less than unity value when the wire-wrap spacers occupying part of the sub-channel.

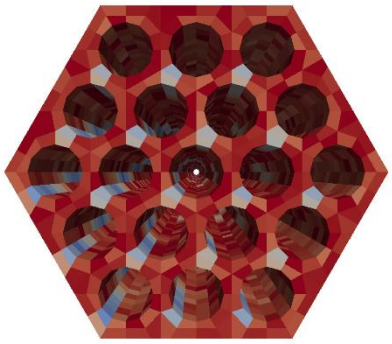

Figure 75 Front view of the volume porosity

Figure 76 Overall view of the volume porosity

Same setting of the parameter in fine simulation is used on coarse simulation. By the coarse grid simulation, an overall view of the velocity field contour and streamline tracing are shown in **Figure 77** and **Figure 78**. According to the simulation result, the coarse grid CFD has basically captured the fundamental structures of the flow field. The overall simulation got a similar performance of velocity distribution compared with the fine case. There's also velocity decreasing following the two blockages. Moreover, the slightly higher velocity area around the outline wall part has also been got. As shown in the streamline plot, though blockages are not geometrically inserted into the coarse mesh, it can still be observed that the fluid is flowing around the blockage rather than directly penetrate through it, which means Coarse Grid CFD has successfully overcome the geometric inconsistence problem brought by mesh simplification.

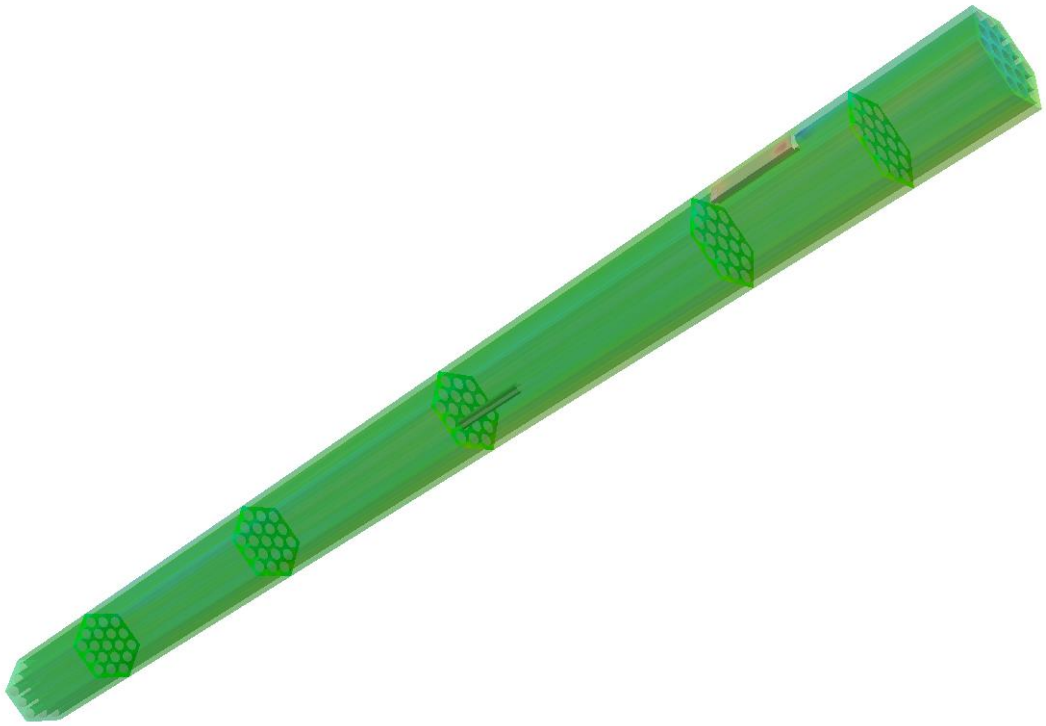

Figure 77 Velocity contour of the flow in coarse simulation

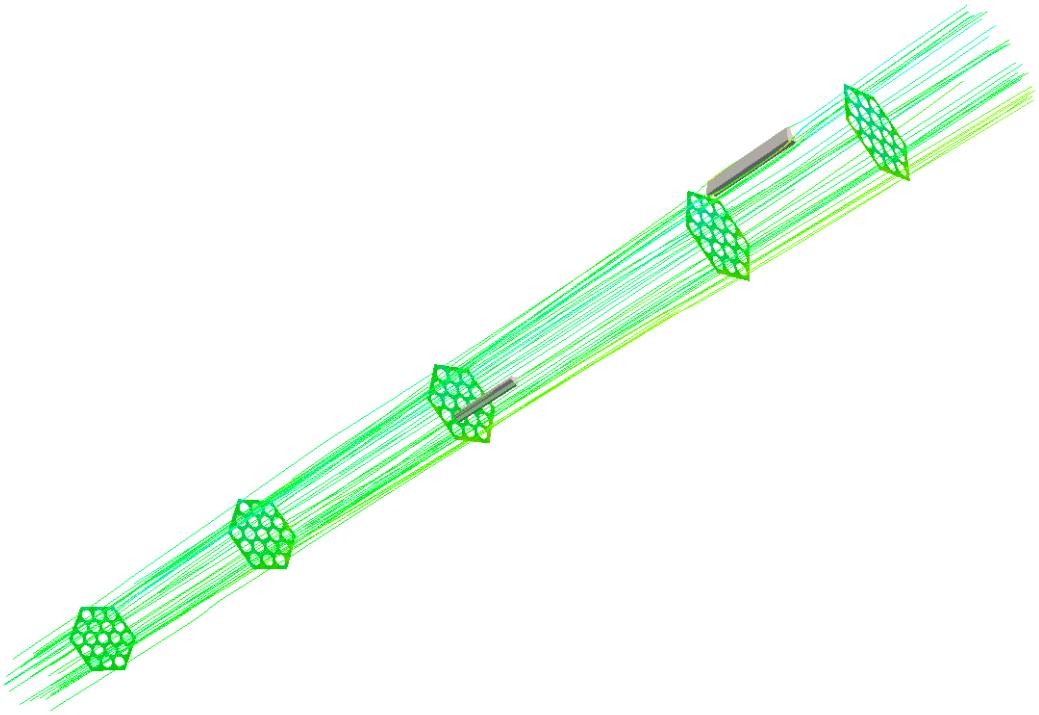

Figure 78 Streamline of the flow in coarse simulation

6.4.4 Comparison and discussion

Further comparison will be given near the upper and lower blockage parts, as way to evaluate the performance of the geometric-based flux correction and the physical-based flux correction. The pressure drop along the bundle will also be proceeded, which further compare the behaviors among the fine simulation, the coarse simulation with the geometric-based flux correction and the coarse simulation with the physical-based flux correction.

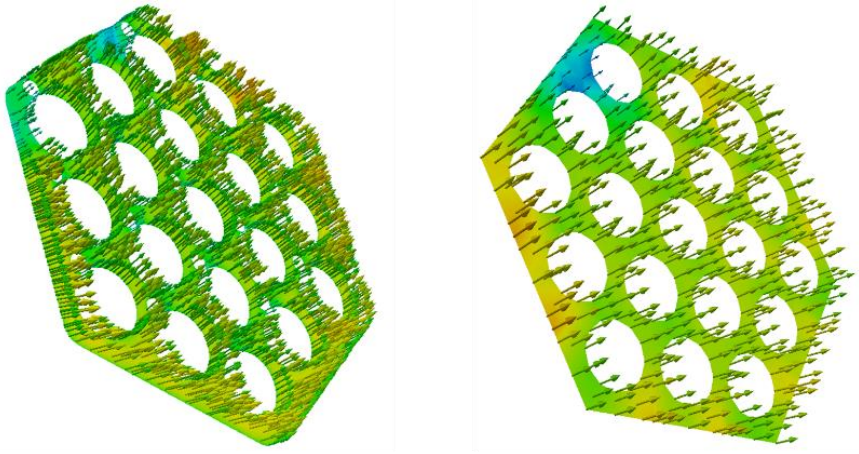

Figure 79 Comparison of the vector plot between the fine and coarse velocity field

By the comparison between the vector plot of fine simulation and coarse simulation shown in **Figure 79**, it can be observed that the coarse simulation has successfully caught the velocity distribution characteristics. The direction of the flow in the inner sub-channels is straight forward pointing to the vertical attitude. In the down part of the outline wall area, the flow deviates little bit from the vertical direction, which is suffering from the influence of the blockage at the lower location. Around the tail zone of upper blockage, both results show a low velocity area, owing to the obstructing effect of the upper blockage.

Furthermore, both the geometric-based flux correction and the physical-based correction are applied in the coarse simulation. To compare the performance, the velocity contour of flow field near the upper blockage and the lower blockage is provided.

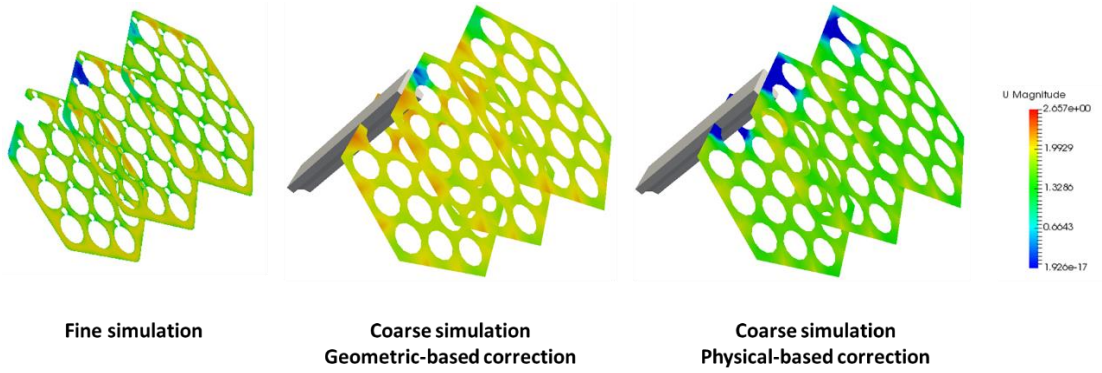

Figure 80 Comparison of the velocity fields at the upper blockage

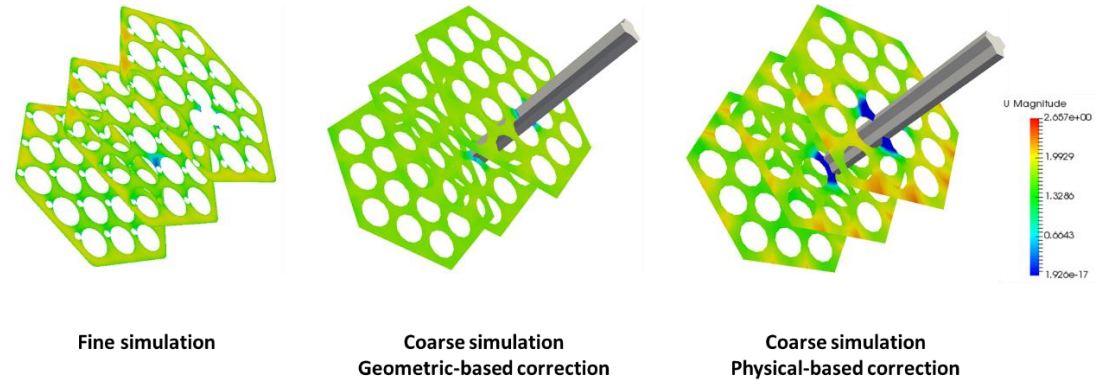

Figure 81 Comparison of the velocity fields at the lower blockage

As shown in **Figure 80** and **Figure 81**, both the geometric-based flux correction and the physical-based flux correction can be able to capture the velocity decreasing in the head zone and tail zone of the blockage. Compared with the fine simulation result, the geometric-based flux correction predicts a weaker decreasing effect of the velocity, while the physical-based flux correction performs a much stronger fixing on velocity decreasing around both the head-tail part and also the lateral part. The geometric-based approach only relies on the volume porosity to correct the surface permeability. Owing to the error on interpolation in coarse mesh cells and volume porosity mapping, there would be underestimation on the blocking effect. The physical-based approach tries to fix the flux by directly targeting on the difference between the fine and the coarse. As a result, the approach got a better prediction of the performance around the blockage area. However, owing to the difficulty on modeling the corrector factor exactly, there's certain degree of over-estimation on the velocity decreasing.

Based on the plot shown in **Figure 82**, it can be seen that the two coarse mesh simulations have successfully captured the overall pressure drop. The local pressure drop near the blockage shares a similar problem like in velocity distribution estimation. The Geometric-based simulation got a lower pressure drop compared with fine, while the physical-based simulation gives a better matching. This is because geometric-based flux correction only considers the influence of the blockage's effect, while neglecting the strong interruptive physical effect. Owing to the sudden narrowing down of the flow channel, a large velocity gradient can be generated. Therefore, a non-physical approach on modeling the surface permeability would lose certain degree of accuracy, as only geometric information is used. However, it can also be observed that the physical-based flux correction gives an overestimation of the global pressure drop. This is because the way by physically correcting the flux as shown in Section 6.3.4 could bring in certain degree of numerical correction on the smooth changing zone as well. Such an effect produces fake pressure drop, which at last promotes the global pressure drop.

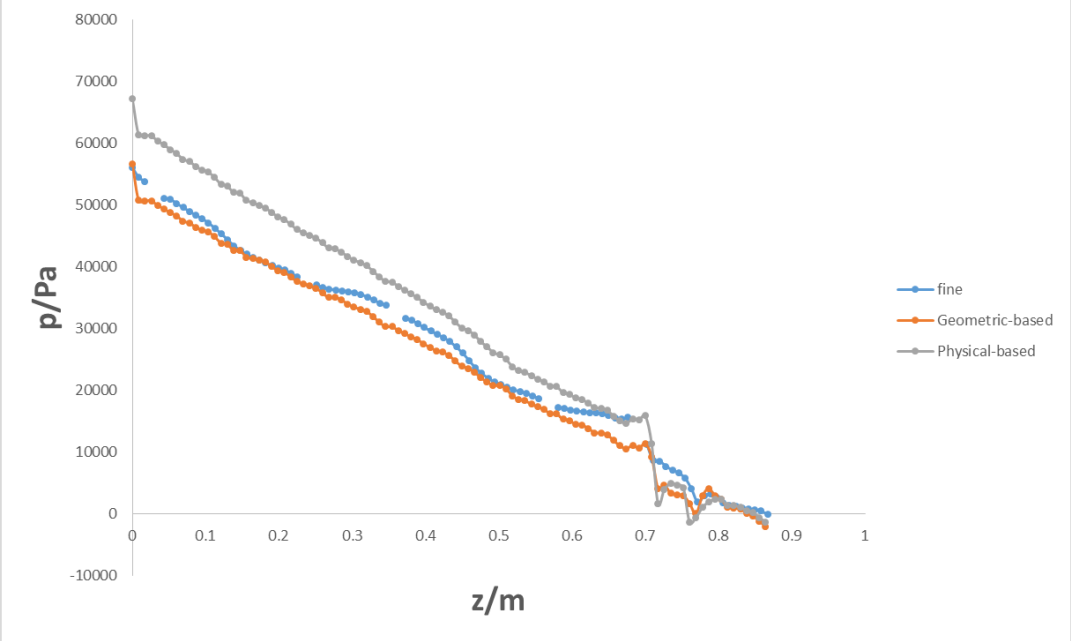

Figure 82 Comparison of the pressure drop plot

6.5 Conclusion and summary

In this chapter, the fast prediction solution, Coarse Grid CFD, has been introduced. Compared with the traditional CFD approach, Coarse Grid CFD is a data-driven method. By well taking advantage of the fine data, Coarse Grid CFD could model volume fraction, surface permeability and volumetric force. Under the implementation of Coarse Grid CFD, the simulation can be proceeded on a simplified geometric mesh with a high speed. In this chapter, a further method on flux correction, physical-based correction, has been set up. Compared with the traditional geometric-based flux correction, the new approach provides a better modeling on Coarse Grid CFD. At last, a validation of Coarse Grid CFD is done based on wired bundle flow case with a comparison between the two approaches. With Coarse Grid, engineers are freed from complicated structure meshing and longtime waiting during engineering design.

In the case of nuclear containment spray simulation, it has shown in the previous chapters that

complicated physical models, sophisticated mathematical treatment and limit on time and spatial discrete size are all the features of fine CFD simulation. Though better accuracy it could bring, the solution may only stay in prototype experimental facility study. However, if implementing Coarse Grid CFD on containment spray, the feature of 3D simulation can be maintained, while fast prediction efficiency is also guaranteed.

7. Summary and outlook

7.1 Summary

In this thesis, the numerical study upon the large-scale problems like nuclear containment spray is well studied. Traditionally, the study and design of the large-scale applications in nuclear industry always rely on experiment-based approach, which is economically not friendly. With the development of computer ability, lumped-parameter based system code becomes a new option for such problems. Though a marco-level or 1D-level numerical solution can be offered, the dropout of spatial information makes only global change of the concerning physical variables able to fetch. Under safety consideration, the facilities have to leave large margin of design, in order to maintain the safety redundancy. Therefore, 3D-based numerical simulation becomes a better option, which is able to offer a better support to specified nuclear engineering designs, with all the local details captured. However, the improper physical modeling could partly weaken the performance of CFD prediction on large-scale problems like containment spray. Moreover, the promotion of dimension in CFD-based numerical simulation triggers the booming of the total calculation amount. Therefore, the two issues are remaining to be improved in the nuclear engineering numerical study.

The study in this work are mainly proceeded through two directions: reliability and speed. The reliability study mainly focuses on setting up a better physical modeling of spray cooling process in nuclear containment, while the speed study mainly focuses on the acceleration of numerical prediction of containment spray process under severe accident. The work in this thesis can be briefly summarized as

Table 13 Summary of the work

	Details of work
OpenFOAM module development & extension	Stochastic Field Method Module development
	CGCFD algorithm realization with new flux correction modules
CFD modeling study	Eulerian approach on modeling spray cooling process
	Stochastic Field Method modeling on spray droplet dispersion and evaporation under turbulence
	CGCFD application on large-scale problem simulation with physics-based flux correction approach
Validation benchmarks	Validation of Eulerian spray cooling model based on THAI facility
	Validation of Stochastic Field Method modeling of turbulent effect upon spray cooling process based on Kieviet's dryer experiment facility
	Validation of CGCFD performance based on MYRRHA facility

Further conclusion from the above work will be discussed in the following two sections.

7.1.1 Summary of reliability promotion study

In the first part of the thesis, the topic of reliability promotion is well studied. To better model spray process, the models of mass, momentum, energy are widely reviewed and compared. The proper combination of models is derived for nuclear containment application. In addition, the turbulent influence upon spray cooling process is discussed in details. By Stochastic Field Method, the turbulent effect is further modelled.

Traditionally, the lumped-parameter based simulation is widely used on nuclear containment spray studies. The global-based approximation largely neglects the performance of the real droplet behavior. All the physical processes like evaporation have been roughly modelled as black-box rather than mechanism-based models. Furthermore, the interaction between spray droplets and turbulence is always not considered, which underestimates the additional droplet transport and cooling effect from the turbulence influence. Therefore, the three-dimensional CFD study with detailed physical modeling deserves further study.

In this work, the detailed physical modeling of the spray process is introduced and discussed. The three different kinds of way on modeling the discrete phase, Lagrangian approach, Mixture approach and Eulerian approach, are introduced. By well balancing the precision and calculation amount, Eulerian approach stays as the best candidate modeling approach and chosen as the method used in this work. Furthermore, the previous models on mass, momentum and energy exchange between gas phase and liquid phase have also been introduced, compared and studied. Meanwhile, the thermophysical modeling on spray evaporation has been reviewed as well. In addition, the influence of turbulence fluctuation upon droplet transfer in the large space has been studied as well. By importing the mathematical tool, stochastic differential equation, PDF family methods show the strong advantage on handling the non-linear mass and energy source terms of the spray droplets to the surrounding atmosphere. A detailed theoretical study and comparison of the three realizations of PDF methods are given as well. At last, the Stochastic Field Method is chosen on modeling the turbulent effect upon spray cooling process.

In the case study part, the validation of spray cooling physical models is given first, by a numerical simulation study based on THAI benchmark. With the comparison between simulation result and experiment data, it has been shown that the Eulerian approach of spray modeling provides an acceptable matching with the real process. To further validate the modeling of turbulent effect modeling upon spray droplet dispersion and atmosphere cooling, a second case study is proceeded based on a dryer case. With hot air keeping injecting into the inner space of the dryer, the evaporation cooling process is totally under turbulent condition. To realize the numerical study, the open-source package OpenFOAM is further extended with a Stochstic Field Method module. To study the behavior of Stochastic Field Method on modeling turbulent effect, two groups of numerical simulation with original Eulerian approach and stochastic field based Eulerian approach have been proceeded and compared with the experiment data. It has been shown that the Stochastic Field Method has given a reasonable prediction of the real process, while a better performance in comparison with original Eulerian approach.

With the effort of work in this part, several conclusions can be made:

- Eulerian approach is a reliable option for large-scale spray simulation like nuclear containment. The Eulerian approach can provide a prediction matching with the experiment, but with much less cost of calculation amount compared with particle-tracking-based

Lagrangian approach.

- Stochastic Field Method is an effective method on overcoming the non-closure problem in turbulence-particle interaction, which shows good performance on spray cooling under turbulence condition. The non-linearity in both dispersion from droplet transport and energy transfer from droplet evaporation can be better modelled, with Stochastic Field Method.

7.1.2 Summary of speed acceleration study

In the second part of the thesis, the topic of speed acceleration is well studied. To make use of the past simulation data, the Coarse Grid CFD methodology is introduced and discussed, which could offer a low-time-cost industrial solution for engineering design iteration.

Large amount of both experiment data and simulation data have been accumulated in the past two decades. How to well make use of the data storage becomes a new issue in the new century and also the core topic of Industry 4.0. In this work, a Coarse Grid CFD method has been introduced and further developed, which is a data-driven approach for nuclear engineering topics. Compared with traditional CFD simulation, Coarse Grid CFD overcomes the problems like large calculation amount, complex treatment and meshing difficulty though the usage of volume porosity, surface permeability and volumetric force. In this work, Coarse Grid CFD has been further modified by importing a physical-based flux correction approach. Compared with the traditional geometric-based way, the physical-based approach considers the real difference from data mapping between the fine and the coarse meshes. Furthermore, some technical issues on handling the complete solid cells and the way on modifying projection method to fit the governing equations of Coarse Grid CFD have also been discussed as well in this work.

In the case study part, the wired bundle fuel assemble benchmark MYRRHA has been used on validating the performance of Coarse Grid CFD approach with physical-based flux correction. In the MYRRHA case, some of the sub-channels of the flow have been blocked by preset blockages, in order to study the influence of channel blockage on the liquid metal flow. In the simulation part, the physical-based flux correction has been used on the coarse grid simulation of the sub-channel flow. According to the result, the Coarse Grid CFD approach with physical-based flux correction could provide a good matching with the fine simulation, but with a much lower time cost. In addition, the physical-based flux correction approach could give a better prediction of the velocity decrease and also the pressure drop increase near the blockage. As a data-driven method, Coarse Grid CFD deserves more study on combining with the modern data science and extending to more application areas in nuclear engineering.

With the effort of work in this part, several conclusions can be made:

- Coarse Grid CFD is a powerful tool on dealing with large-scale problems with repeated parts in geometry or working condition. It can maintain the three-dimensional characteristics of CFD approach, but be less costly on time and calculation resource.
- The new physical-based flux correction approach can provide a better prediction of the local parts with sharp gradient of change in physics, compared with traditional geometric-based approach.

7.2 Outlook

A comprehensive review of physical models and simulation approaches on nuclear containment spray has been provided. With the overall comparison and discussion, the proper choice of spray modeling is derived. Meanwhile, an innovative acceleration approach by Coarse Grid CFD has also been discussed in detail, with further modification by flux-based correction. In this section, an early study will be derived on how to well combine the two methods in the case of nuclear containment spray problem. Furthermore, the feasibility of implementing the popular machine learning approach on Coarse Grid CFD simulation will also be discussed.

Recently, with the progress of data science development [194], the data-driven technologies have been extended to practical applications like automatic driving, pedestrian recognition, disease diagnose, etc. Among all the data-driven approaches, machine learning stays as the most promising candidate method. One of the strong advantages of machine learning is the ability of self-evolution though the lesson from the past data, which is therefore treated as one of the most potential technical routine to realize artificial intelligence. The application of machine learning can also be found in nuclear industry [195], like reactor controlling, security monitoring and accident identification. Machine learning can be simply understood as an approach to fit a certain dataset into a non-linear co-relation expression through statistical methods. It is obvious that the machine learning approach is a good choice on extending data-driven methods. Therefore, the coupling of machine learning approach with Coarse Grid CFD is a powerful solution package, which deserves further study.

In this section, the dryer case shown in Chapter 5 will be re-studied by Coarse Grid CFD, together with machine learning approach, in order to discuss how to well use the old simulation data on fast prediction of the dryer spray cooling process. In this case, the machine learning approach will be used to learn the time development and spatial distribution of the fine simulation data, in order to build up a model on predicting the future time step physical fields. As shown in **Figure 83**, the machine learning approach will be used to study the flux corrector and volumetric force, in order to predict the physical variables like velocity, temperature and mass fraction at next time step.

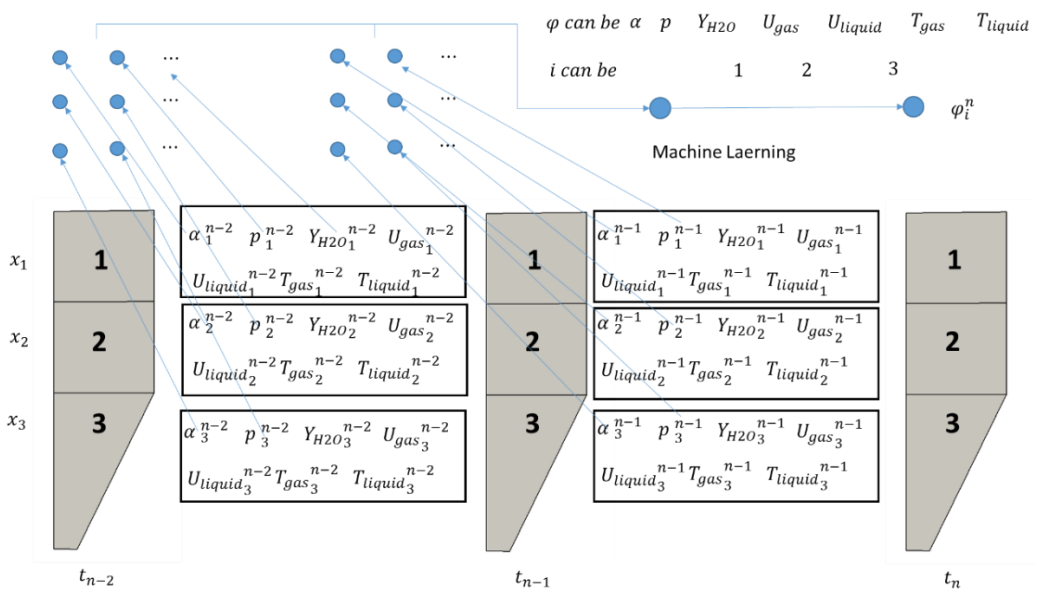

Figure 83 Application of machine learning on Coarse Grid CFD

A super tiny demo case will be tested first by a 3-cell super coarse 1-dimensional simulation of the dryer. Concerning the vertical temperature distribution is always the factor under safety analysis, the test case divides the calculation domain of the dryer into 3 cells along the vertical direction. Similar to the treatments discussed in Chapter 6, the local structures like ring shape inlet and the pipe outlet are all simplified as volume fraction in the coarse grid CFD simulation. Therefore, the geometry of the coarse case has been turned into a simple shape as shown in **Figure 84**. In the coarse case simulation, the first 300s are used as the data set for training models, while the later 80s are used on testing the performance of the model.

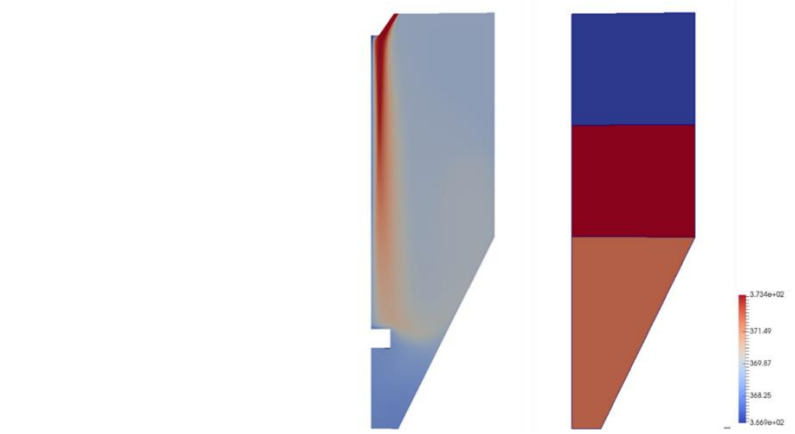

Figure 84 Temperature distribution of the fine case and the super coarse case

By the Coarse Grid CFD simulation, the plots of gas temperature change at location 1, x direction of velocity change at location 1 and gas temperature change at location 2 can be found in **Figure 85**, **Figure 86** and **Figure 87**.

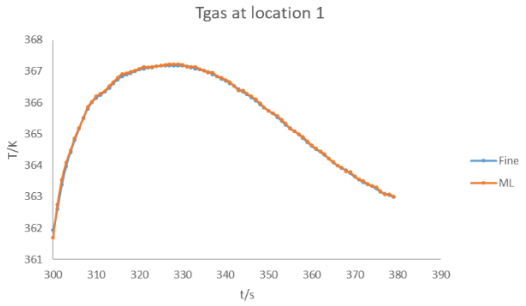

Figure 85 gas temperature change at location 1

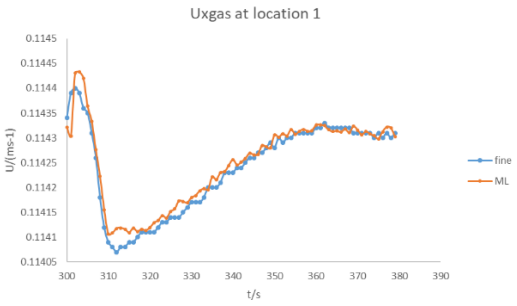

Figure 86 velocity x change at location 1

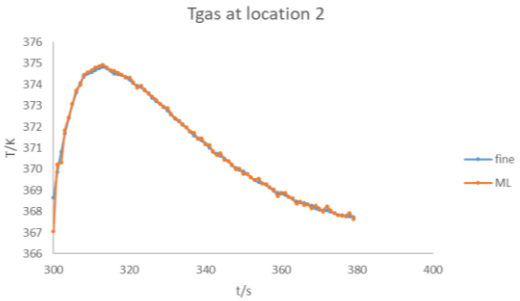

Figure 87 gas temperature change at location 2

As shown in the results, the Coarse Grid CFD simulation could give a good prediction, which got a well match with the fine simulation. When comes to the velocity prediction, there's obviously non-physical fluctuation at all time compared with the fine simulation. This is because the machine learning approach implements a pure statistical-based method on fitting the dataset, which would result in a prediction similar to the value change, but way different from the real physical process. However, it could still be seen that the overall trend has been successfully predicted by the Coarse Grid CFD simulation with machine learning approach, which means the method is able to basically work for the large-scale cases.

In practice, a 3-cell case simulation stays at similar level with lump parameter system codes. Though it could be used to provide fast prediction of the global physical value for engineering design, such a coarse case loses basic spatial information as a CFD simulation. Therefore, a further refined simulation with 72 cells will be given again on the dryer case. The mesh of the refined coarse case can be found in **Figure 88**.

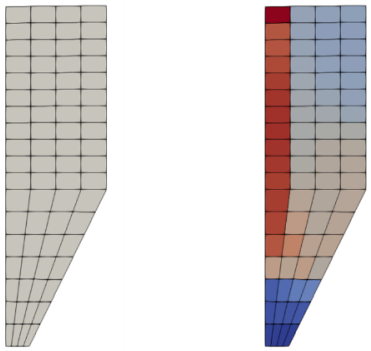

Figure 88 The refined coarse mesh and its temperature contour

Again, the first 300s are used as the training data set for machine learning, while the following 80s are used on validation of the model. As shown in **Figure 89** and **Figure 90**, the refined coarse case can be able to give a good matching on the temperature change at two chosen locations. The

non-physical oscillation is not very strong, owing to the smooth change of temperature in the large space of the vessel.

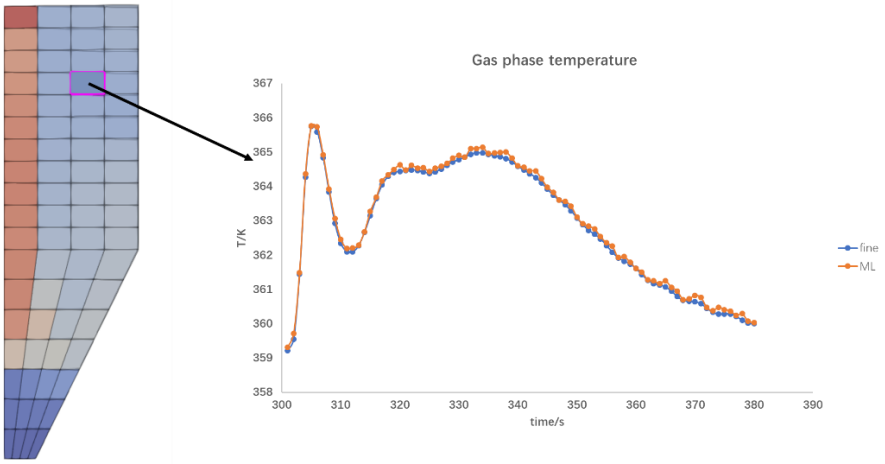

Figure 89 Gas phase temperature change at one chosen location

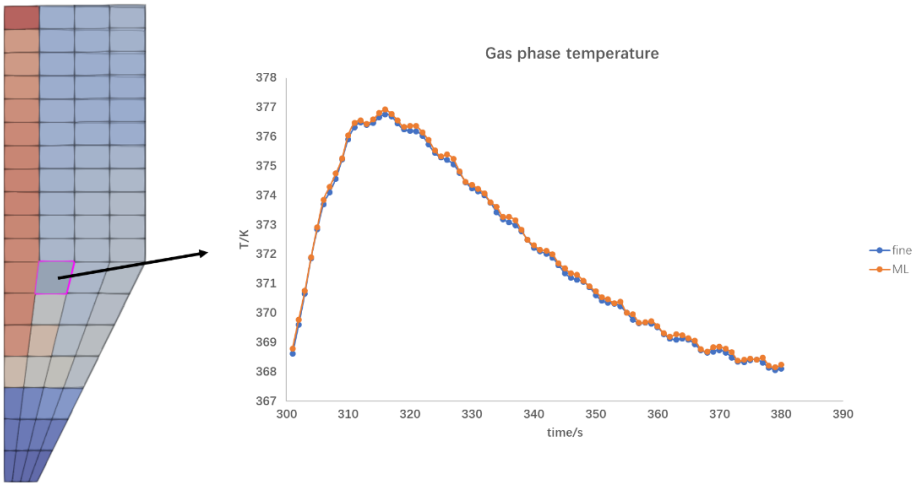

Figure 90 Gas temperature change at another chosen location

Meanwhile, the comparison of the flux at another chosen location in the fine simulation and refined coarse simulation can be found in **Figure 91**. As shown in the result, the basic trend of flux amount at the location can be successfully predicted in the coarse simulation compared with the fine simulation result. In this figure, certain level of non-physical oscillation can be observed in the plot, which results from the machine learning approach. In machine learning, a pure statistics-based “agent model”, which can fit the basic trend of the physical process, but way much easier to calculate in practice.

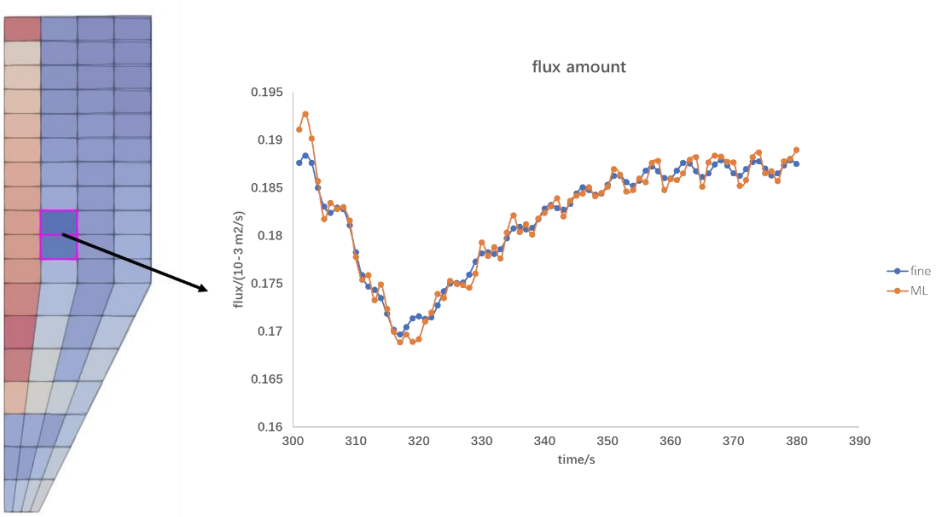

Figure 91 The comparison of flux in the fine simulation and corrected flux in the coarse simulation

By the coarse case study of the dryer spray in this section, it can be seen that the Coarse Grid CFD can be basically able to work for the large-scale spray problem simulation like the containment spray. In addition, it can also be seen that machine learning is a powerful tool on building up coarse model for large-scale industrial simulation, especially combined with data-driven methods like Coarse Grid CFD. The work shows that there still exists much space for the improvement in Coarse Grid CFD simulation on containment spray applications, which deserves further study in the future work.

Bibliography

[1] International Energy Agency. Energy and Climate Change: World Energy Outlook Special Report. International Energy Agency, 2015.

[2] IAEA, 2015a. Climate change and nuclear power 2015, international atomic energy agency. http://www-pub.iaea.org/MTCD/Publications/PDF/CCANP2015Web78834554.pdf (Accessed 25 January 2020)

[3] IAEA, 2017. The Database on Nuclear Power Reactors. https://www.iaea.org/pris/ (Accessed 25 January 2020)

[4] Ang, Beng Wah, W. L. Choong, and T. S. Ng. "Energy security: Definitions, dimensions and indexes." Renewable and Sustainable Energy Reviews 42 (2015): 1077-1093.

[5] MacElroy, JM Don. "Closing the carbon cycle through rational use of carbon-based fuels." Ambio 45.1 (2016): 5-14.

[6] Fawcett, Allen A., et al. "Can Paris pledges avert severe climate change?." Science 350.6265 (2015): 1168-1169.

[7] Adamantiades, Achilles, and Ioannis Kessides. "Nuclear power for sustainable development: current status and future prospects." Energy Policy 37.12 (2009): 5149-5166.

[8] Fathi, Nima, et al. "Efficiency enhancement of solar chimney power plant by use of waste heat from nuclear power plant." Journal of Cleaner Production 180 (2018): 407-416.

[9] Nowotny, Janusz, et al. "Towards sustainable energy. Generation of hydrogen fuel using nuclear energy." International Journal of Hydrogen Energy 41.30 (2016): 12812-12825.

[10] Suman, Siddharth. "Hybrid nuclear-renewable energy systems: a review." Journal of Cleaner Production 181 (2018): 166-177.

[11] IAEA. Objective and essential elements of a state's nuclear security regime. International Atomic Energy Agency, 2014.

[12] International Nuclear Safety Advisory Group. Defence in Depth in Nuclear Safety: INSAG-10: a Report. International Atomic Energy Agency, Vienna, 1996. https://www-pub.iaea.org/MTCD/publications/PDF/Pub1013e_web.pdf

[13] Müller-Ecker, Dieter. "WENRA and Its Expectations on the Safety of New NPP." INPRO Dialog Forum on Global Nuclear Energy Sustainability, Licensing and Safety Issues for Small-and Medium-sized Reactors (SMRs), Vienna. Vol. 29.

[14] Duarte, Juliana P., José de Jesús Rivero Oliva, and Paulo Fernando F. Frutuoso e Melo. "Generation IV Nuclear Systems: State of the Art and Current Trends with Emphasis on Safety and Security." Current Research in Nuclear Reactor Technology in Brazil and Worldwide (2013): 143.

[15] Kurokawa, Kiyoshi, et al. "The official report of the Fukushima nuclear accident independent investigation commission." The national diet of Japan (2012).

[16] TECPO, Fukushima Nuclear Accidents Investigation Report. http://www.tep-co.co.jp/en/press/corp-com/release/betu12_e/images/120620e0106.pdf (Accessed 25 January 2020)

[17] TECPO, The Development of and Lessons from the Fukushima Daiichi Nuclear Accident. http://www.tepco.co.jp/en/decommision/accident/images/outline01.pdf (Accessed 25 January 2020)

[18] Bull, Adrian. "The AP1000 Nuclear Power Plant-Global Experience and UK Prospects." presentation), Westinghouse UK (Nuclear Institute) (2011).
[19] https://sites.suffolk.edu/jstraka/2015/10/30/fukushima-daiichi-nuclear-disaster/ (Accessed 25 January 2020)
[20] https://nuclearstreet.com/nuclear-power-plants/w/nuclear_power_plants/containment-isolation (Accessed 25 January 2020)
[21] Row, T. H., L. F. Parsly, and H. E. Zittel. Design Considerations of Reactor Containment Spray Systems-Part I. No. ORNL-TM--2412 (Pt. 1). Oak Ridge National Lab., Tenn., 1969.
[22] Patterson, C.S.; Humphries, W.T. Design Considerations of Reactor Containment Spray Systems-Part II. Removal Of Iodine And Methyl Idodie From Air By Liquid Solutions. No. ORNL-TM-2412(Pt.2). Oak Ridge National Lab., Tenn., 1969.
[23] Griess, J. C., and A. L. Bacarella. Design Considerations of Reactor Containment Spray Systems-Part III. The Corrosion Of Materials In Spray Solutions. No. ORNL-TM--2412 (Pt. 3). Oak Ridge National Lab., Tenn., 1969.
[24] Parsly, L. F. Design Considerations of Reactor Containment Spray Systems-Part IV. Calculation Of Iodine-Water Partition Coefficients. No. ORNL-TM--2412 (Pt. 4). Oak Ridge National Lab., Tenn., 1970.
[25] Tanaka, Mitsugu. "Heat transfer of a spray droplet in a nuclear reactor containment." Nuclear Technology 47.2 (1980): 268-281.
[26] Chung, J. N., and P. S. Ayyaswamy. "The effect of internal circulation on the heat transfer of a nuclear reactor containment spray droplet." Nuclear Technology 35.3 (1977): 603-610.
[27] Griess, J. C., and A. L. Bacarella. "The corrosion of materials in reactor containment spray solutions." Nuclear Technology 10.4 (1971): 546-553.
[28] Nishio, Gunji, et al. "Containment spray Model for Predicting Radioiodine Removal in Light Water Reactors." Nuclear Technology 54.1 (1981): 68-86.
[29] Hashimoto, Kazuichiro, et al. "Iodine removal tests for BWR containment spray by large scale facility." Journal of Nuclear Science and Technology 18.4 (1981): 261-274.
[30] Nishio, Gunji, and Mitsugu Tanaka. "Calculation of Iodine Removal by Spray in LWRs Containment Vessels." Journal of Nuclear Science and Technology 16.11 (1979): 823-837.
[31] Nagasaka, H., and T. Kagawa. "Heat removal phenomena of nuclear reactor containment spray." Proc. 1st Int. Conf. Liquid Atomization and Spray Systems, Tokyo, p. 361 (1978).
[32] Tanaka, Mitsugu, et al. "Performance of containment sprays for light water reactors and evaluation of the heat transfer." Nuclear Technology 54.1 (1981): 54-67.
[33] Albiol, Thierry, et al. "SARNET: Severe accident research network of excellence." Progress in Nuclear Energy 52.1 (2010): 2-10.
[34] Sonnenkalb, Martin, and Gerhard Poss. "The international test programme in the THAI facility and its use for code validation." EUROSAFE Forum, Brussels, Belgium. 2009.
[35] Freitag, M. "Extension of the THAI test facility by installation of the second vessel–PAD." Technical Report 1501455-THAIPLUS-TR. Becker Technologies GmbH Eschborn, 2016.
[36] Kaltenbach, C., and E. Laurien. "CFD Simulation of aerosol particle removal by water spray in the model containment THAI." Journal of Aerosol Science 120 (2018): 62-81.
[37] Kaltenbach, C., and E. Laurien. "CFD simulation of spray cooling in the model containment THAI." Nuclear Engineering and Design 328 (2018): 359-371.
[38] Mansour, A., and E. Laurien. "Numerical error analysis for three-dimensional CFD

simulations in the two-room model containment THAI+: Grid convergence index, wall treatment error and scalability tests." Nuclear Engineering and Design 326 (2018): 220-233.
[39] https://www.irsn.fr/EN/Research/Scientific-tools/experimental-facilities-means/tosqan/Pages/TOSQAN-facility.aspx (Accessed 25 January 2020)
[40] Freitag, M., et al. "Simulation benchmark based on THAI-experiment on dissolution of a steam stratification by natural convection." Nuclear Engineering and Design 299 (2016): 37-45.
[41] Li, Yabing, et al. "Numerical investigation of natural convection inside the containment with recovering passive containment cooling system using GASFLOW-MPI." Annals of Nuclear Energy 114 (2018): 1-10.
[42] Freitag, M., et al. "Benchmark exercise TH-27 on natural convection with steam injection and condensation inside the extended THAI facility." Annals of Nuclear Energy 116 (2018): 90-104.
[43] Gupta, S., et al. "THAI test facility for experimental research on hydrogen and fission product behaviour in light water reactor containments." Nuclear Engineering and Design 294 (2015): 183-201.
[44] Funke, F., et al. "Iodine oxides in large-scale THAI tests." Nuclear Engineering and Design 245 (2012): 206-222.
[45] Porcheron, Emmanuel, et al. "Experimental investigation in the TOSQAN facility of heat and mass transfers in a spray for containment application." Nuclear Engineering and Design 237.15-17 (2007): 1862-1871.
[46] Mimouni, S., et al. "Modelling of sprays in containment applications with a CMFD code." Nuclear Engineering and Design 240.9 (2010): 2260-2270.
[47] Porcheron, Emmanuel, et al. "Experimental and numerical approaches of aerosol removal in spray conditions for containment application." Nuclear Engineering and Design 240.2 (2010): 336-343.
[48] Lemaitre, Pascal, and Emmanuel Porcheron. "Study of heat and mass transfers in a spray for containment application: Analysis of the influence of the spray mass flow rate." Nuclear Engineering and Design 239.3 (2009): 541-550.
[49] Malet, J., et al. "Achievements of spray activities in nuclear reactor containments during the last decade." Annals of Nuclear Energy 74 (2014): 134-142.
[50] Erkan, Nejdet, et al. "Experimental investigation of spray induced gas stratification break-up and mixing in two interconnected vessels." Nuclear Engineering and Design 241.9 (2011): 3935-3944.
[51] Kapulla, Ralf, Guillaume Mignot, and Domenico Paladino. "Large-Scale Containment Cooler Performance Experiments under Accident Conditions." Sci. Technol. Nucl. Install., 2012, 1–2, 1 (1996); https://doi.org/10.1155/2012/943197.
[52] Paladino, Domenico, et al. "A PANDA integral test on the effect of light gas on a Passive Containment Cooling System (PCCS)." Nuclear Engineering and Design 241.11 (2011): 4551-4561.
[53] Chatelard, P., et al. "Main modelling features of the ASTEC V2. 1 major version." Annals of Nuclear Energy 93 (2016): 83-93.
[54] Allelein, H-J., et al. "COCOSYS: status of development and validation of the German containment code system." Nuclear Engineering and Design 238.4 (2008): 872-889.

[55] Sandia National Laboratories, 2000. NUREG/CR-6119, Rev. 2, MELCOR Computer Code Manuals. In: Primer and User's Guide, Version 1.8.5, vol. 1.
[56] Yang, Jun, et al. "Counterpart experimental study of ISP-42 PANDA tests on PUMA facility." Nuclear Engineering and Design 258 (2013): 249-257.
[57] Kim, Jungwoo, Eunbum Jung, and Seongwon Kang. "Large eddy simulation of hydrogen dispersion from leakage in a nuclear containment model." International Journal of Hydrogen Energy 40.35 (2015): 11762-11770.
[58] Bandurski, Th, et al. "Influence of the distribution of noncondensibles on passive containment condenser performance in PANDA." Nuclear Engineering and Design 204.1-3 (2001): 285-298.
[59] Auban, O., R. Zboray, and D. Paladino. "Investigation of large-scale gas mixing and stratification phenomena related to LWR containment studies in the PANDA facility." Nuclear Engineering and Design 237.4 (2007): 409-419.
[60] Ritterath, Martin, et al. "New gas concentration measurement system for the PANDA containment test facility." Nuclear engineering and design 241.11 (2011): 4594-4603.
[61] Guelfi, Antoine, et al. "NEPTUNE: a new software platform for advanced nuclear thermal hydraulics." Nuclear Science and Engineering 156.3 (2007): 281-324.
[62] Foissac, Arnaud, et al. "Eulerian simulation of interacting PWR sprays including droplet collisions." Nuclear Technology 181.1 (2013): 133-143.
[63] Coste, P., et al. "Validation of the large interface method of NEPTUNE_CFD 1.0. 8 for pressurized thermal shock (PTS) applications." Nuclear Engineering and Design 253 (2012): 296-310.
[64] Mérigoux, N., et al. "Verification, validation and application of NEPTUNE_CFD to two-phase Pressurized Thermal Shocks." Nuclear Engineering and Design 312 (2017): 74-85.
[65] Laviéville, Jérôme, et al. "A generalized turbulent dispersion model for bubbly flow numerical simulation in neptune_cfd." Nuclear Engineering and Design 312 (2017): 284-293.
[66] Mimouni, S., et al. "Modelling and computation of cavitation and boiling bubbly flows with the NEPTUNE_CFD code." Nuclear Engineering and Design 238.3 (2008): 680-692.
[67] Prošek, Andrej, Boštjan Končar, and Matjaž Leskovar. "Uncertainty analysis of CFD benchmark case using optimal statistical estimator." Nuclear Engineering and Design 321 (2017): 132-143.
[68] Malet, J., et al. "Gas entrainment by one single French PWR spray, SARNET-2 spray benchmark." Nuclear Engineering and Design 282 (2015): 44-53.
[69] Ansys, C. F. X. "Theory guide." Ansys Inc (2015).
[70] Babic, Miroslav, and Ivo Kljenak. "CFD spray simulations for nuclear reactor safety applications with lagrangian approach for droplet modelling." in Proceeding of the International Conference Nuclear Energy for New Europe, p. 13, Portoroz, Slovenia, September 2007.
[71] Babić, Miroslav, Ivo Kljenak, and Borut Mavko. "Simulations of TOSQAN containment spray tests with combined Eulerian CFD and droplet-tracking modelling." Nuclear Engineering and Design 239.4 (2009): 708-721.
[72] Travis, J. R., et al. "GASFLOW: A computational fluid dynamics code for gases, aerosols, and combustion." Vol. I, Theory and Computational Model, Reports FZKA-5994, LA-13357-M (1998).

[73] Jain, Manish, et al. "Characterization of the full cone pressure swirl spray nozzles for the nuclear reactor containment spray system." Nuclear Engineering and Design 273 (2014): 131-142.
[74] Ding, Peng, et al. "The homogeneous and Lagrangian tracking approaches of the spray simulation in the containment." Annals of Nuclear Energy 101 (2017): 203-214.
[75] Ding, Peng, et al. "Numerical investigation on the performance of the combined passive and spray cooling system under nuclear severe accident." Annals of Nuclear Energy 105 (2017): 329-345.
[76] Li, Yabing, et al. "Numerical investigation of natural convection inside the containment with recovering passive containment cooling system using GASFLOW-MPI." Annals of Nuclear Energy 114 (2018): 1-10.
[77] Zhang, Han, et al. "Large eddy simulation of turbulent flow using the parallel computational fluid dynamics code GASFLOW-MPI." Nuclear Engineering and Technology 49.6 (2017): 1310-1317.
[78] Xiao, Jianjun, Jack Travis, and Maurizio Bottoni. "Status of dynamic water film model development in 3-D CFD code GASFLOW-MPI for analysis of passive containment cooling system." Annals of Nuclear Energy 108 (2017): 99-112.
[79] Ma, Zhenhui, et al. "Study on the hydrogen risk in venturi scrubber filter of filtered containment venting system under PWR severe accident." Nuclear Engineering and Design 327 (2018): 61-69.
[80] Jain, Manish, et al. "An experimental study on the depressurization of the containment by water spray in a small scale facility." Annals of Nuclear Energy 112 (2018): 208-224.
[81] Malet, J., O. Degrees du Lou, and T. Gelain. "Water evaporation over sump surface in nuclear containment studies: CFD and LP codes validation on TOSQAN tests." Nuclear Engineering and Design 263 (2013): 395-405.
[82] Povilaitis, Mantas, Egidijus Urbonavičius, and Sigitas Rimkevičius. "Validation of special nodalisation features for lumped-parameter injection modelling based on MISTRA facility tests from ISP-47 and SARNET." Nuclear Engineering and Design 278 (2014): 86-96.
[83] Ravva, Srinivasa Rao, et al. "CFD code benchmark against the air/helium tests performed in the MISTRA facility." Annals of Nuclear Energy 69 (2014): 37-43.
[84] Abe, Satoshi, et al. "Stratification breakup by a diffuse buoyant jet: The MISTRA HM1-1 and 1-1bis experiments and their CFD analysis." Nuclear Engineering and Design 331 (2018): 162-175.
[85] Hoyes, J. R., and M. J. Ivings. "CFD modelling of hydrogen stratification in enclosures: Model validation and application to PAR performance." Nuclear Engineering and Design 310 (2016): 142-153.
[86] Povilaitis, Mantas, et al. "Sensitivity and uncertainty analysis of atmosphere stratification modelling in MISTRA using lumped-parameter code COCOSYS." Nuclear Engineering and Design 265 (2013): 108-119.
[87] Povilaitis, M., E. Urbonavičius, and S. Rimkevičius. "Modeling of atmosphere stratification in containments of nuclear power plants using lumped-parameter code." Nuclear Engineering and Design 241.8 (2011): 3111-3120.
[88] Malet, J., and R. Laissac. "CFD calculations of stratification build-up tests of light gas in a closed vessel under controlled boundary conditions." Computers & Fluids 107 (2015):

224-241.
[89] Malet, J., et al. "Code-experiment comparison on wall condensation tests in the presence of non-condensable gases—Numerical calculations for containment studies." Nuclear Engineering and Design 253 (2012): 98-113.
[90] Kljenak, Ivo, et al. "Modeling of containment atmosphere mixing and stratification experiment using a CFD approach." Nuclear Engineering and Design 236.14-16 (2006): 1682-1692.
[91] Filippov, A., et al. "CMFD simulation of ERCOSAM PANDA spray tests PE1 and PE2." Nuclear Engineering and Design 299 (2016): 81-94.
[92] Kim, Jongtae, et al. "Spray effect on the behavior of hydrogen during severe accidents by a loss-of-coolant in the APR1400 containment." International communications in heat and mass transfer 33.10 (2006): 1207-1216.
[93] Kudriakov, S., et al. "The TONUS CFD code for hydrogen risk analysis: Physical models, numerical schemes and validation matrix." Nuclear Engineering and Design 238.3 (2008): 551-565.
[94] Xiao, Jianjun, et al. "Three-dimensional all-speed CFD code for safety analysis of nuclear reactor containment: Status of GASFLOW parallelization, model development, validation and application." Nuclear Engineering and Design 301 (2016): 290-310.
[95] Houkema, M., et al. "Validation of the CFX4 CFD code for containment thermal-hydraulics." Nuclear Engineering and Design 238.3 (2008): 590-599.
[96] Jasak, Hrvoje. "OpenFOAM: open source CFD in research and industry." International Journal of Naval Architecture and Ocean Engineering 1.2 (2009): 89-94.
[97] Ishigaki, Masahiro, et al. "Influence of mesh non-orthogonality on numerical simulation of buoyant jet flows." Nuclear Engineering and Design 314 (2017): 326-337.
[98] Patel, G., V. Tanskanen, and R. Kyrki-Rajamäki. "Numerical modelling of low-Reynolds number direct contact condensation in a suppression pool test facility." Annals of Nuclear Energy 71 (2014): 376-387.
[99] Corzo, Santiago F., et al. "Thermal hydraulics simulation of the RD-14M steam generator facility." Annals of Nuclear Energy 105 (2017): 282-301.
[100] Wu, Hsingtzu. "A tightly coupled scheme for neutronics and thermal–hydraulics using open-source software." Annals of Nuclear Energy 87 (2016): 16-22.
[101] Alali, Abdullah, et al. "Numerical investigations on the coupling of the one-group interfacial area transport equation and subcooled boiling models for nuclear safety applications." Annals of Nuclear Energy 120 (2018): 155-168.
[102] Sugrue, Rosemary, et al. "Assessment of a simplified set of momentum closure relations for low volume fraction regimes in STAR-CCM+ and OpenFOAM." Annals of Nuclear Energy 110 (2017): 79-87.
[103] Hasslberger, Josef, et al. "Three-dimensional CFD analysis of hydrogen-air-steam explosions in APR1400 containment." Nuclear Engineering and Design 320 (2017): 386-399.
[104] Harlow, Francis H., and J. Eddie Welch. "Numerical calculation of time-dependent viscous incompressible flow of fluid with free surface." The physics of fluids 8.12 (1965): 2182-2189.
[105] Migdal, David, and V. D. Agosta. "A source flow model for continuum gas-particle flow." Journal of Applied Mechanics 34 (1967): 860.

[106] Tsuji, Yutaka, Toshihiro Kawaguchi, and Toshitsugu Tanaka. "Discrete particle simulation of two-dimensional fluidized bed." Powder technology 77.1 (1993): 79-87.
[107] Bokhove, Onno, and Marcel Oliver. "Parcel Eulerian–Lagrangian fluid dynamics of rotating geophysical flows." Proceedings of the Royal Society A: mathematical, physical and engineering sciences 462.2073 (2006): 2575-2592.
[108] Nobile, Fabio, and Luca Formaggia. "A stability analysis for the arbitrary lagrangian: Eulerian formulation with finite elements." East-West Journal of Numerical Mathematics 7.EPFL-ARTICLE-176278 (1999): 105-132.
[109] Tong, L. S., and Y. S. Tang. Boiling Heat Transfer And Two-Phase Flow. Boca Raton, Florida, U.S.A. CRC Press, 1997.
[110] Ishii, Mamoru, and Takashi Hibiki. Thermo-fluid dynamics of two-phase flow. Berlin. Springer Science & Business Media, 2010.
[111] Pope, S. B. Turbulent Flows. Cambridge, England. Cambridge University Press, 2000.
[112] Reynolds, Osborne. "XXIX. An experimental investigation of the circumstances which determine whether the motion of water shall he direct or sinuous, and of the law of resistance in parallel channels." Philosophical Transactions of the Royal Society of London 174 (1883): 935-982.
[113] Faulkner, Bill, and Roslyn Russell. "Turbulence, chaos and complexity in tourism systems: a research direction for the new millennium." In Tourism in the 21st Century: Lessons from Experience, Edited by: Faulkner, B., Moscardo, G. and Laws, E. 328–349. London: Continuum. 2000.
[114] Benzi, Roberto, et al. "On the multifractal nature of fully developed turbulence and chaotic systems." Journal of Physics A: Mathematical and General 17.18 (1984): 3521.
[115] Ikeda, K., H. Daido, and O. Akimoto. "Optical turbulence: chaotic behavior of transmitted light from a ring cavity." Physical Review Letters 45.9 (1980): 709.
[116] https://www.quora.com/Fluid-Dynamics-What-is-the-difference-between-chaotic-flow-and-turbulent-flow (Accessed 25 January 2020)
[117] Richardson, Lewis Fry. Weather prediction by numerical process. Cambridge, England. Cambridge University Press, 2007.
[118] Kolmogorov, Andrey Nikolaevich. "The local structure of turbulence in incompressible viscous fluid for very large Reynolds numbers." Cr Acad. Sci. URSS 30 (1941): 301-305.
[119] Tikhomirov, V. M. "On the degeneration of isotropic turbulence in an incompressible viscous fluid." Selected Works of AN Kolmogorov. Springer, Dordrecht, 1991. 319-323.
[120] Eggels, J. G. M., et al. "Fully developed turbulent pipe flow: a comparison between direct numerical simulation and experiment." Journal of Fluid Mechanics 268 (1994): 175-210.
[121] Sagaut, Pierre. Large eddy simulation for incompressible flows: an introduction. Berlin. Springer Science & Business Media, 2006.
[122] Leonard, A. "Energy cascade in large-eddy simulations of turbulent fluid flows." Adv. Geophys. A 18.A (1974): 237-248.
[123] Smagorinsky, Joseph. "General circulation experiments with the primitive equations: I. The basic experiment." Monthly weather review 91.3 (1963): 99-164.
[124] Germano, Massimo, et al. "A dynamic subgrid-scale eddy viscosity model." Physics of Fluids A: Fluid Dynamics 3.7 (1991): 1760-1765.
[125] Zhang, Han, et al. "Large eddy simulations of the all-speed turbulent jet flow using 3-D

CFD code GASFLOW-MPI." Nuclear Engineering and Design 328 (2018): 134-144.
[126] Kim, Jungwoo, Eunbum Jung, and Seongwon Kang. "Large eddy simulation of hydrogen dispersion from leakage in a nuclear containment model." International Journal of Hydrogen Energy 40.35 (2015): 11762-11770.
[127] Jones, W. P., and Brian Edward Launder. "The prediction of laminarization with a two-equation model of turbulence." International journal of heat and mass transfer 15.2 (1972): 301-314.
[128] Bradshaw, P. "Possible origin of Prandt's mixing-length theory." Nature 249.5453 (1974): 135.
[129] Wilcox, David C. Turbulence modeling for CFD. Vol. 2. La Canada, CA: DCW industries, 1998.
[130] Spalart, Philippe, and Steven Allmaras. "A one-equation turbulence model for aerodynamic flows." 30th aerospace sciences meeting and exhibit. Reno, NV, U.S.A. (1992): 439.
[131] Wilcox, David. "A half century historical review of the k-omega model." 29th Aerospace Sciences Meeting. Reno, NV, U.S.A. 1991.
[132] Pope, Stephen B. "PDF methods for turbulent reactive flows." Progress in energy and combustion science 11.2 (1985): 119-192.
[133] Gardiner, Crispin W. "Handbook of stochastic methods for physics, chemistry and the natural sciences." Applied Optics 25 (1986): 3145.
[134] Xu, Guanglei, et al. "Turbulent mixing simulation via a quantum algorithm." AIAA Journal 56.2 (2018): 687-699.
[135] Brennen, Christopher Earls, and Christopher E. Brennen. Fundamentals of multiphase flow. Cambridge, England. Cambridge University Press, 2005.
[136] Frossling, Nils. "Uber die Verdunstung Fallernder Tropfen." Gerlands Beitr. Geophys. 52 (1938): 170-216.
[137] Schiller, Links. "A drag coefficient correlation." Zeit. Ver. Deutsch. Ing. 77 (1933): 318-320.
[138] White, F. M. "Viscous Fluid Flow, McGraw-Hill, New York, 1991."
[139] Ishii, Mamoru, and Novak Zuber. "Drag coefficient and relative velocity in bubbly, droplet or particulate flows." AIChE Journal 25.5 (1979): 843-855.
[140] J. D. Valle, Micrometrics, Pitman Publishing Co., New York, 1948
[141] Moore, D. W. "The boundary layer on a spherical gas bubble." Journal of Fluid Mechanics 16.2 (1963): 161-176.
[142] Ranz, W. E., and W. R_ Marshall. "Evaporation from drops." Chem. Eng. Prog 48.3 (1952): 141-146.
[143] Buck, Arden L. "New equations for computing vapor pressure and enhancement factor." Journal of applied meteorology 20.12 (1981): 1527-1532.
[144] McBride, Bonnie J. Coefficients for calculating thermodynamic and transport properties of individual species. Vol. 4513. NASA Langley Research Center, 1993.
[145] Chorin, Alexandre Joel. "The numerical solution of the Navier-Stokes equations for an incompressible fluid." Bulletin of the American Mathematical Society 73.6 (1967): 928-931.
[146] Taira, Kunihiko, and Tim Colonius. "The immersed boundary method: a projection approach." Journal of Computational Physics 225.2 (2007): 2118-2137.
[147] Crank, John, and Phyllis Nicolson. "A practical method for numerical evaluation of solutions of partial differential equations of the heat-conduction type." Mathematical

Proceedings of the Cambridge Philosophical Society. Cambridge, UK, Cambridge University Press, 1947. 43(1): 50-67.

[148] Butcher, John Charles. Numerical methods for ordinary differential equations. Hoboken, New Jersey. John Wiley & Sons, 2016.

[149] Patankar, Suhas V., and D. Brian Spalding. "A Calculation of Procedure for Heat, Mass and Momentum Transfer in Three-dimensional Parabolic Flows." Int. J. Heat Mass Transfer 15 (1972): 1787-1806.

[150] Issa, Raad I. "Solution of the implicitly discretised fluid flow equations by operator-splitting." Journal of computational physics 62.1 (1986): 40-65.

[151] Patankar, Suhas. Numerical heat transfer and fluid flow. CRC press, 1980.

[152] Rhie, C. M., and W. Li Chow. "Numerical study of the turbulent flow past an airfoil with trailing edge separation." AIAA journal 21.11 (1983): 1525-1532.

[153] Jasak, H. "Error Analysis and Estimation for the Finite Volume Method with Applications to Fluid Flows." PhD. Thesis, Imperial College, University of London (1996).

[154] Anderson, John David, and J. Wendt. Computational fluid dynamics. New York: McGraw-Hill, 1995.

[155] Ferziger, Joel H., and Milovan Peric. Computational methods for fluid dynamics. Berlin: Springer, 2002

[156] Godunov, Sergei Konstantinovich. "A difference method for numerical calculation of discontinuous solutions of the equations of hydrodynamics." Matematicheskii Sbornik 89.3 (1959): 271-306.

[157] Roe, Philip L. "Approximate Riemann solvers, parameter vectors, and difference schemes." Journal of computational physics 43.2 (1981): 357-372.

[158] Merkle, Charles. "Time-accurate unsteady incompressible flow algorithms based on artificial compressibility." AIAA Paper 97-l 137, 1987 (unpublished).

[159] Chen, Z. J., and A. J. Przekwas. "A coupled pressure-based computational method for incompressible/compressible flows." Journal of Computational Physics 229.24 (2010): 9150-9165.

[160] Xiao, Cheng-Nian, Fabian Denner, and Berend GM van Wachem. "Fully-coupled pressure-based finite-volume framework for the simulation of fluid flows at all speeds in complex geometries." Journal of Computational Physics 346 (2017): 91-130.

[161] Oboukhov, A. M. "Structure of the temperature field in turbulent flows." Isv. Geogr. Geophys. Ser. 13 (1949): 58-69.

[162] Corrsin, Stanley. "On the spectrum of isotropic temperature fluctuations in an isotropic turbulence." Journal of Applied Physics 22.4 (1951): 469-473.

[163] Drivas, Theodore D., and Gregory L. Eyink. "A Lagrangian fluctuation–dissipation relation for scalar turbulence. Part I. Flows with no bounding walls." Journal of Fluid Mechanics 829 (2017): 153-189.

[164] Falkovich, G., K. Gawędzki, and Massimo Vergassola. "Particles and fields in fluid turbulence." Reviews of modern Physics 73.4 (2001): 913.

[165] Kupiainen, A. "Nondeterministic dynamics and turbulent transport." Annales Henri Poincaré. Vol. 4. No. 2. Basel, Switzerland. Birkhäuser-Verlag, 2003.

[166] Gawedzki, K. "Soluble models of turbulent transport." Non-equilibrium statistical mechanics and turbulence 355 (2008): 44-107.

[167] Hunt, Julian CR. "Lewis Fry Richardson and his contributions to mathematics, meteorology, and models of conflict." Annual Review of Fluid Mechanics 30.1 (1998): 13-36.

[168] Hulburt, Ho M., and Stanley Katz. "Some problems in particle technology: A statistical mechanical formulation." Chemical Engineering Science 19.8 (1964): 555-574.

[169] McGraw, Robert. "Description of aerosol dynamics by the quadrature method of moments." Aerosol Science and Technology 27.2 (1997): 255-265.

[170] Marchisio, Daniele L., and Rodney O. Fox. "Solution of population balance equations using the direct quadrature method of moments." Journal of Aerosol Science 36.1 (2005): 43-73.

[171] Valiño, Luis. "A field Monte Carlo formulation for calculating the probability density function of a single scalar in a turbulent flow." Flow, turbulence and combustion 60.2 (1998): 157-172.

[172] Bird, R. Byron, Edwin N. Lightfoot, and E. Warren Stewart. Transport phenomenon. Hoboken, New Jersey. Wiley, 2007.

[173] Bini, M., and W. P. Jones. "Large eddy simulation of an evaporating acetone spray." International Journal of Heat and Fluid Flow 30.3 (2009): 471-480.

[174] Malet, J., E. Porcheron, and J. Vendel. "OECD International Standard Problem ISP-47 on containment thermal-hydraulics—Conclusions of the TOSQAN part." Nuclear Engineering and Design 240.10 (2010): 3209-3220.

[175] Schwarz, S., et al. "Benchmark on hydrogen distribution in a containment based on the OECD-NEA THAI HM-2 experiment." Nuclear Technology 175.3 (2011): 594-603.

[176] Xiao, Jianjun, and John R. Travis. "How critical is turbulence modeling in gas distribution simulations of large-scale complex nuclear reactor containment?." Annals of nuclear energy 56 (2013): 227-242.

[177] Huang, Lin Jie, and P. S. Ayyaswamy. "Heat transfer of a nuclear reactor containment spray drop." Nuclear Engineering and Design 101.2 (1987): 137-148.

[178] Kieviet, Frank, and Piet JAM Kerkhof. "Measurements of particle residence time distributions in a co-current spray dryer." Drying Technology 13.5-7 (1995): 1241-1248.

[179] Fletcher, D. F., et al. "What is important in the simulation of spray dryer performance and how do current CFD models perform?." Applied Mathematical Modelling 30.11 (2006): 1281-1292.

[180] Kieviet, Frank Geert. Modelling quality in spray drying. PhD. Thesis, Laboratory of Separation Processes and Transport Phenomena, Department of Chemical Engineering, Eindhoven University of Technology, 1997.

[181] Class, Andreas G., Mathias O. Viellieber, and Steffen R. Himmel. "Coarse Grid CFD for underresolved simulation." APS 63 (2010): QA-010.

[182] Viellieber, Mathias, and Andreas G. Class. "Anisotropic porosity formulation of the Coarse-Grid-CFD (CGCFD)." 2012 20th International Conference on Nuclear Engineering and the ASME 2012 Power Conference. American Society of Mechanical Engineers, 2012, 44984: 473-483.

[183] Viellieber, Mathias, Philipp Dietrich, and Andreas Class. "Investigation of a wire wrapped fuel assembly with the Anisotropic Coarse-Grid-CFD (AP-CGCFD)." Atw. Internationale Zeitschrift fuer Kernenergie 59.10 (2013): 573-575.

[184] Viellieber, Mathias, Philipp Dietrich, and Andreas G. Class. "Coarse-Grid-CFD for a Wire Wrapped Fuel Assembly." PAMM 13.1 (2013): 317-318.

[185] Viellieber, Mathias, and Andreas Class. "Coarse-Grid-CFD for the Thermal Hydraulic Investigation of Rod-Bundles." PAMM 15.1 (2015): 497-498.

[186] Viellieber, M., and A. Class. "Investigating reactor components with the coarse-grid-methodology." 16th International Topical Meeting on Nuclear Reactor Thermalhydraulics, Chicago, USA. 2015 , 16: 2788-2801.

[187] Viellieber, Mathias, and Andreas G. Class. "Reducing numerical costs for core wide nuclear reactor CFD simulations by the Coarse-Grid-CFD." APS (2013): R28-010.

[188] Class, Andreas G., Fujiang Yu, and Thomas Jordan. "An engineering closure for heavily under-resolved coarse-grid CFD in large applications." APS (2016): KP1-135.

[189] Fujiang Yu, Class, Andreas G., Jianjun Xiao and Thomas Jordan. Coarse grid CFD methodology: flux corrections for individual mesh cells and application to rod bundles. SE 17th International Topical Meeting on Nuclear Reactor Thermal Hydraulics, Xi'an, Shaanxi, China, Sept. 3-8, 2017. Paper No. 21717

[190] Hanna, Botros N., et al. "Coarse-Grid Computational Fluid Dynamic (CG-CFD) Error Prediction using Machine Learning." arXiv preprint arXiv:1710.09105 (2017).

[191] Chang, Chih-Wei, and Nam T. Dinh. "Classification of machine learning frameworks for data-driven thermal fluid models." International Journal of Thermal Sciences 135 (2019): 559-579.

[192] Kim, Byungsoo, et al. "Deep Fluids: A Generative Network for Parameterized Fluid Simulations." arXiv preprint arXiv:1806.02071 (2018).

[193] Batta, A.; Class, A.; Pacio, J. "Numerical analysis of a LBE-cooled blocked 19-pin hexagonal wire wrapped rod bundle experiment carried out at KIT-KALLA within EC-FP7 project MAXSIMA," 17th International Topical Meeting on Nuclear Reactor Thermal Hydraulics, Xi'an, Shaanxi, China, Sept. 3-8, (2017). Paper No. 20532

[194] Murphy, Kevin P. Machine learning: a probabilistic perspective. Cambridge, Massachusetts. MIT press, 2012.

[195] Kim, Song Hyun, et al. "Feasibility study on application of an artificial neural network for automatic design of a reactor core at the Kyoto University Critical Assembly." Progress in Nuclear Energy 119 (2020): 103183.

[196] Ling, Yongsheng, et al. "Nuclear accident source term estimation using Kernel Principal Component Analysis, Particle Swarm Optimization, and Backpropagation Neural Networks." Annals of Nuclear Energy 136 (2020): 107031.

[197] An, Ye Ji, et al. "Critical flow prediction using simplified cascade fuzzy neural networks." Annals of Nuclear Energy 136 (2020): 107047.

[198] Pei, Cao, et al. "An artificial neural network based neutron field reconstruction method for reactor." Annals of Nuclear Energy 138 (2020): 107195.